UNIVERSITEIT VAN PRETORIA
UNIVERSITY OF PRETORIA
YUNIBESITHI YA PRETORIA

Development of a tunable vibration isolator utilising a smart actuator

by

Johan Marthinus Cronjé

submitted in partial fulfilment of the requirements for the degree

M.Eng (Mech)

in the Faculty of Engineering

University of Pretoria

Pretoria

December 2002

Development of a tunable vibration isolator utilising a smart actuator

By

Johan Marthinus Cronjé

Supervisors	:	Prof. P.S. Heyns, Prof. N. J. Theron, Dr. P. Loveday
Department	:	Mechanical and Aeronautical Engineering
Degree	:	M. Eng

Summary

Vibrating machinery like rock drills and compactors are becoming more prominent in modern industry. The vibrations of these machines can damage surrounding structures and foundations and be harmful to their operators. Hand arm vibration syndrome is one example of serious injuries suffered by operators of these machines.

Due to the fact that these machines need to vibrate, vibration absorbers that minimise the vibrations of the machines cannot be used. In such cases vibration isolators are necessary to isolate the vibration between the vibrating machine and other bodies like the handle or foundations. A tuned vibration isolator is a type of isolator that is able to isolate a certain frequency very effectively. These isolators can retain low mass and high stiffness compared to traditional isolators and can obtain complete isolation at the isolation frequency if no damping is present. The liquid inertia vibration eliminator (LIVE) is such a tuned vibration isolator that makes use of hydraulic amplification, which result in a very compact design.

A LIVE isolator was designed incorporating the variable stiffness spring and a variable damping mechanism. Equations for the damped natural and isolation frequency of the LIVE isolator were also derived. The reason for changing the stiffness was to be able to adjust the isolation frequency of the isolator to coincide with the excitation frequency that resulted in a more effective isolator. The variable

stiffness spring consisted of two leaf springs mounted on top of each other and separated at the centre to stiffen the whole spring assembly. The leaf springs were separated by a wax actuator that was controlled with a closed loop displacement control system to form a smart actuator. A stiffness change of 2.7 times the original stiffness was obtained by separating the springs.

The variable damping mechanism was to be able to control the amount of amplification of noise at the natural frequency. An experimental isolator was built and tested and resulted in a tunable vibration isolator. The isolation frequency of the isolator could be shifted from 22.8 Hz to 36.2 Hz and a transmissibility of 10% was achieved over that whole range. The variable damping mechanism increased the viscous damping ratio from 0.001 to 0.033.

A control system was designed and implemented that tuned the isolator automatically to the excitation conditions. It incorporated an optimisation algorithm to determine the optimum settings and then kept the isolator at that setting until the excitation conditions change. The whole process was then repeated.

A tunable vibration isolator was therefore successfully developed that can be used to isolate tonal vibrations very effectively. The isolation frequency and damping of the isolator can be changed while in operation and a transmissibility of 10% can be achieved at the isolation frequency.

Keywords: Vibration isolator, LIVE, tuned, variable stiffness spring, wax actuator, smart actuator, transmissibility, isolation frequency, variable damping, control.

Ontwikkeling van 'n verstelbare vibrasie isoleerder deur 'n slim aktueerder te gebruik

deur

Johan Marthinus Cronjé

Studieleiers	:	Prof. P.S. Heyns, Prof. N. J. Theron, Dr. P. Loveday
Departement	:	Meganiese en Lugvaartkundige Ingenieurswese
Graad	:	M. Ing

Opsomming

Vibrerende masjiene soos rotsbore en kompakteerders is besig om al hoe meer prominent in die moderne industrie te word. Die masjiene se vibrasies kan ernstige skade veroorsaak aan omliggende strukture, fondasies en operateurs. Hand-arm vibrasie sindroom is 'n voorbeeld van hoe ernstig die beserings aan operateurs is.

Omdat hierdie masjiene moet vibreer, kan vibrasie absorbeerders wat die masjien se vibrasies minimeer nie gebruik word nie. Vibrasie isoleerders wat die vibrasies van die masjien isoleer van omringende liggame soos die handvatsel of fondasie is nodig. Gestemde vibrasie isoleerders is 'n tipe vibrasie isoleerder wat vibrasie baie effektief by 'n spesifieke frekwensie isoleer. Hierdie isoleerders behaal goeie isolasie met hoë styfheid en lae massa in vergelyking met normale isoleerders en kan 100% isolasie behaal indien geen demping teenwoordig is nie. Die LIVE (liquid inertia vibration eliminator) is so 'n isoleerder wat van hidrouliese versterking gebruik maak wat die isoleerder baie kompak maak.

Om die isoleerder so effektief as moontlik te maak, moet dit moontlik wees om die isolasiefrekwensie van die isoleerder te kan rondskuif om saam met die opwekkingsfrekwensie te val. Dit is moontlik gemaak deur 'n veranderbare styfheid veer te ontwikkel wat uit twee bladvere bestaan wat bo-op mekaar pas en dan in die middel uitmekaar gedruk word om die globale styfheid van die veersamestelling te

verander. Die vere is deur middel van 'n was aktueerder uitmekaar gedruk wat deur 'n geslote lus verplasings beheerstelsel beheer is om 'n slim aktueerder te vorm. 'n Styfheidsverandering van 2.7 keer is behaal deur die vere uitmekaar te druk.

'n LIVE isoleerder is ontwerp wat die veranderbare styfheid veer inkorporeer asook 'n veranderbare demping meganisme. Die veranderbare demping is om die amplitude van versterking van geraas by die natuurlike frekwensie van die isoleerder te kan beheer. 'n Eksperimentele isoleerder is gebou en getoets. Die isolasiefrekwensie van die isoleerder kan van 22.8 Hz tot 36.2 Hz geskuif word en 'n transmissibiliteit van 10% is behaal oor die hele span. Die viskeuse dempingsverhouding kan verander word van 0.001 tot 0.033.

'n Beheerstelsel is ook ontwerp en geïmplementeer wat die isoleerder outomaties verstel om optimal vir die opwekkingstoestande to werk. Die beheerstelsel inkorporeer 'n optimeringsalgoritme wat die optimale verstellings bepaal en dan die isoleerder by daardie waardes hou tot die opwekkingstoestande verander. Die hele siklus word dan van voor af herhaal.

'n Suksesvolle verstelbare vibrasie isoleerder is dus ontwikkel wat gebruik kan word om vibrasies effektief te isoleer. Die isolasiefrekwensie en demping van die isoleerder kan verstel word en 'n transmissibiliteit van 10% kan by die isolasiefrekwensie behaal word.

Sleutelwoorde: Vibrasie isoleerder, LIVE, gestemde isoleerder, veranderbare styfheid veer, was aktueerder, slim aktueerder, transmissibiliteit, isolasiefrekwensie, veranderbare demping, beheer.

Acknowledgements

I would like to thank:

- Prof. P.S. Heyns, Prof. N.J. Theron and Dr. P. Loveday for their guidance, help and support
- Frans Windell for his help with the experimental work
- Marietjie Calder for her help in the administrative and financial department
- Jeremy Wallace and Dr. Philip Loveday at the CSIR for the financial support for the project.

Table of contents

Nomenclature

Symbol	Meaning	SI Units
A	Amplitude	m
A_a	Tuning port area	m^2
A_b	Reservoir area	m^2
c	Viscous damping coefficient	N.s/m
c_c	Critical damping coefficient	N.s/m
d_a	Tuning port diameter	m
d_b	Reservoir diameter	m
E	Modulus of elasticity	Pa
F	Force amplitude	N
F_0	Force transmitted to ground	N
F_i	Applied force	N
F_t	Transmitted force	N
F_p	Force due to pressure difference	N
f	Frequency	Hz
$f(t)$	Force as a function of time	N
$f_i(t)$	Applied force as a function of time	N
G_a	Ratio of undamped natural frequency to isolation frequency	
$G(s)$	Transfer function of system	
h	Hysteresis damping constant	N/m
I	Moment of inertia	
I	Current	A
k	Stiffness	N/m
l	Tuning port length	m
m	Mass	kg
m_b	Absorber mass	kg
P	Pressure	Pa
P	Power	W
r,R	Arm length	m
t	Time	s

T_r	Complex transmissibility	
V	Potential difference	V
X,x	Displacement	m
$x(t)$	Displacement	m
$\dot{x}(t)$	Velocity	m/s
$\ddot{x}(t)$	Acceleration	m/s^2
$Y(s)$	Response of system in Laplace domain	m
$Y(t)$	Response of system in time domain	m
δ_{st}	Static deflection	m
ϕ	Phase angle	rad
η	Loss factor	
τ	Time constant	s
ω	Circular frequency	rad/s
ω_a	Undamped isolation frequency	rad/s
ω_n	Undamped natural frequency	rad/s
ω_{ad}	Damped isolation frequency	rad/s
ω_{nd}	Damped natural frequency	rad/s
ζ	Damping ratio	

Abbreviations

DAVI	Dynamic anti-resonant vibration isolator
FEM	Finite element method
FFT	Fast Fourier transform
IFFT	Inverse fast Fourier transform
IRIS	Improved rotor isolation system
ISO	International standards organisation
LIVE	Liquid inertia vibration eliminator
LVDT	Linearly variable differential transformer
SMA	Shape memory alloy
RMS	Root mean square

CHAPTER 1

Introduction and literature review

1.1 Introduction

Oscillating machines have become an integral part of modern industry. These machines use mechanisms such as rotating imbalances or pneumatic devices to excite the machine at a particular frequency. Rock-drills, compactors and jackhammers are examples of oscillating machines that are presently used in the industry and are depicted in Figure 1. 1. Because oscillatory motion is vital to the performance of these machines, it is not sensible to attempt to minimize the vibration of these machines with vibration absorbers. On the other hand, these vibrations can cause extensive noise and damage to structures, foundations and humans if proper vibration isolation is not achieved in the linkages between the machine and the surrounding area.

Figure 1. 1 Examples of vibrating machines used in industry today

Operators exposed to vibration when handling portable hand-held vibrating tools can, if exposed for long periods of time, (usually measured in years) be at risk of injuries collectively known as Hand-Arm Vibration Syndrome (HAVS). Raynaud's Phenomena or Vibration White Finger, (VWF) is one example of an HAVS injury, which was described as early as the 1890s. (Raw, 1999)

There are many ways to achieve the isolation of vibrations. Most of these use a soft spring and mass that together have a very low natural frequency. Such isolators lead to large displacements and are usually not suitable for machines that are controlled by an operator. With such large displacements operators are unable to accurately control

the machines. There are however a class of isolators that were developed by the helicopter industry to isolate the fuselage from the main rotor's vibration. Examples of such isolators are the IRIS (Improved Rotor Isolation System) (Desjardins & Hooper, 1976 & Desjardins & Hooper, 1980), DAVI (Dynamic Antiresonant Vibration Isolator) (Braun, 1980 & Rita et al., 1976) and LIVE (Liquid Inertia Vibration Eliminator) (Halwes, 1981 and Halwes & Simmons, 1980) systems. These devices are able to achieve good isolation with high stiffness and low mass penalty.

A major problem with the implementation of such isolators on oscillating machines is the fact that the isolator is tuned for a specific isolation frequency and that other frequencies can be amplified. Although oscillating machines usually have a primary excitation frequency, this frequency may easily change by as much as 10% during operation. Furthermore, the vibration at other frequencies can change due to operating conditions such as the hardness of rock. Therefore the isolator has to be able to adapt to these changes in the excitation frequency and noise levels.

1.2 Vibration control for vibrating machines

Vibration on vibrating machines can be reduced in the following ways (Rao, 1995):

1. By controlling the natural frequencies of the system and avoiding resonance under external excitation.
2. By preventing excessive response of the system, even at resonance by introducing a damping or energy-dissipating mechanism.
3. By reducing the transmission of the excitation forces from one part of the machine to another, by the use of vibration isolators.
4. By reducing the response of the system, by the addition of an auxiliary mass neutraliser or vibration absorber.

A more practical explanation of the above is:

1. Make sure that the machine is not excited at its natural frequency.
2. Put enough damping in the system to minimise response at the natural frequency.
3. Install a vibration isolator between the machine and another body.

4. Install a vibration absorber on the machine to minimise the vibration of the machine.

A vibration isolator is the device that we are interested in and will be described in detail in the following section. Although vibration absorbers are not suitable for the purposes of this study, they will also be studied to further explain some basic principles that are also present in vibration isolators.

1.2.1 Vibration absorbers

The basic principle of a vibration absorber is to minimise the response of a machine at a specific frequency. This is usually achieved by adding a secondary mass with a spring to the system. There are three main types of vibration absorbers. All three will be discussed in the following paragraphs.

1.2.1.1 Classic vibration absorber

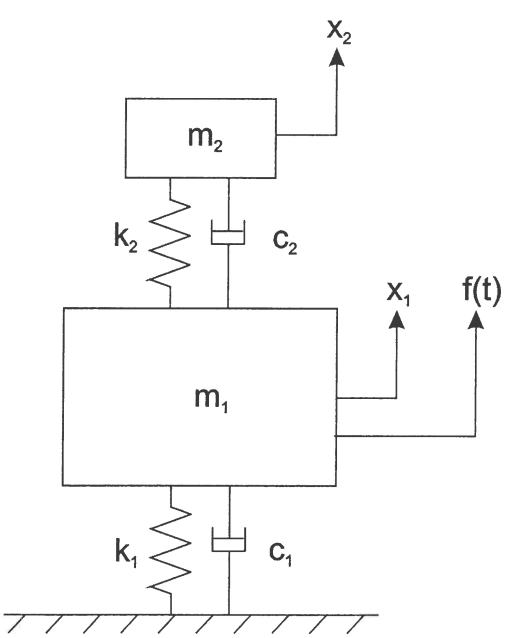

Figure 1. 2 Classic vibration absorber

The classic vibration absorber was patented by Frahm in 1911 (Sun et al., 1994). A vibration absorber consists of a primary system to which a secondary mass is added as shown in Figure 1. 2. The objective of the absorber is to minimise the motion of the primary mass. This is achieved by tuning the natural frequency of the absorber to coincide with the excitation frequency. The result is a two-degree of freedom system with zero response at the tuned frequency if no damping is present. Sometimes the excitation frequency and the natural frequency of the primary system can be the same. In this special case the use of an absorber is very useful as can be seen Figure 1. 3. The use of an absorber is however not limited to this special case and can be used on most structures by tuning the absorber to the excitation frequency.

The equation of the response of the primary mass before and after the addition of an absorber are as follows:

Without absorber:

$$\frac{X_1}{\delta_{st}} = \frac{1}{1-\left(\frac{\omega}{\omega_1}\right)^2} \tag{1.1}$$

With absorber: (Rao, 1995)

$$\frac{X_1}{\delta_{st}} = \frac{1-\left(\frac{\omega}{\omega_2}\right)^2}{\left[1+\frac{k_2}{k_1}-\left(\frac{\omega}{\omega_1}\right)^2\right]\left[1-\left(\frac{\omega}{\omega_2}\right)^2\right]-\frac{k_2}{k_1}} \tag{1.2}$$

With:

X	-	Displacement
δ_{st}	-	Static deflection, displacement due to gravitation
$k_1.k_2$	-	Spring stiffness
m_1,m_2	-	Mass
ω_1, ω_2	-	Circular frequency

Figure 1. 3 gives the response of the primary system before and after the addition of an undamped absorber with a mass ratio of 1/20.

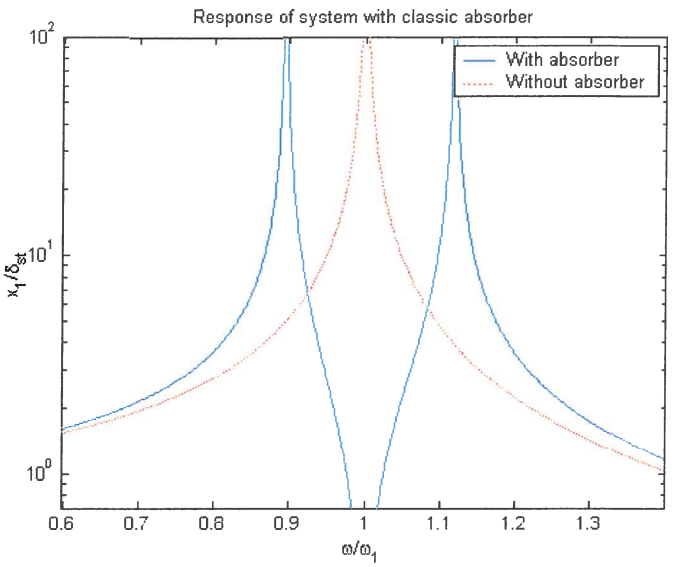

Figure 1. 3 **Response of system with and without an absorber**

1.2.1.2 Semi-active vibration absorbers

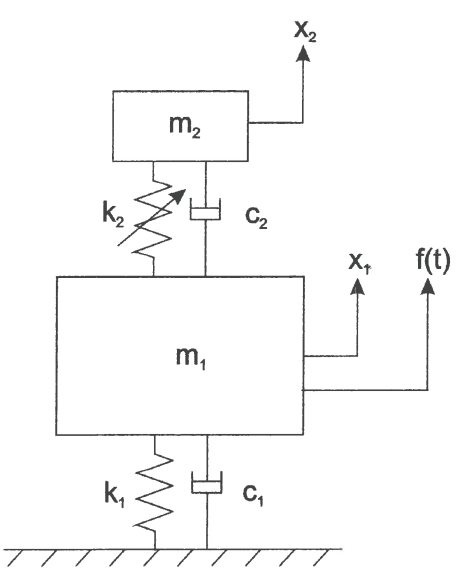

Figure 1. 4 **Semi-active vibration absorber**

The difference between classic and semi-active vibration absorbers is that where a classic vibration absorber is tuned to a specific frequency, a semi-active vibration absorber can be tuned to different frequencies while in operation. There are many published mechanisms to accomplish this. Viscoelastic materials are often used as the spring element in such a device (Ketema, 1998) and modification to the viscoeleastic material by means of temperature change (Fosdick & Ketema, 1998) result in a semi-active vibration absorber. The most common way of achieving a semi-active absorber is by using a variable stiffness spring as shown in Figure 1. 4. As the stiffness of the spring varies, the natural frequency of the absorber changes and therefore the tuned frequency varies. Different ways to change the stiffness have been implemented based on shape memory alloys (Williams et al., 1999 & Williams et al., 2000), Terfenol-D (Flatau et al., 1998) or by changing the tension in strings (Onoda et al., 1992). Electromechanical systems have also been used (Nagem et al., 1997) to change the stiffness (Tentor &Wicks, 2000) and the damping (Seto & Yamanouch, 1978). The advantage of these absorbers over a classic absorber is that if the primary machine's operating or excitation frequency changes while in operation, the absorber can adapt to such a change and ensure that the minimum response of the primary system is obtained at all times.

Figure 1. 5 show how changing the stiffness of the absorber spring can alter the response of the system. The dotted line is the response of the original system without an absorber.

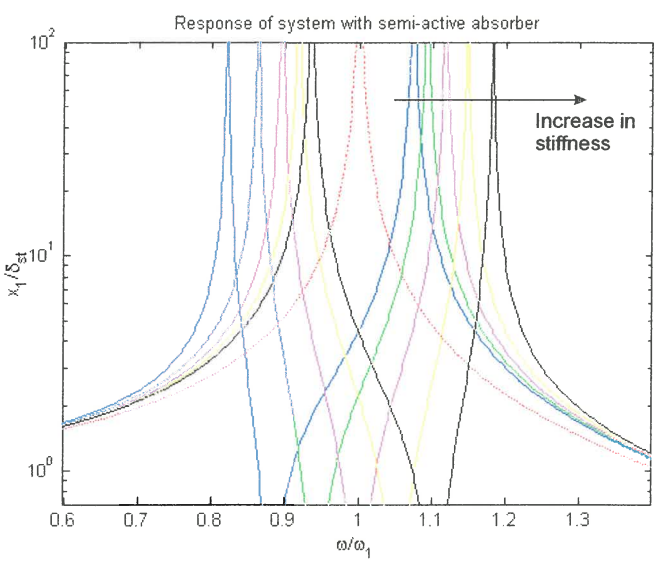

Figure 1. 5 Response of a semi-active absorber

When a very small mass ratio is used, the use of a semi-active absorber can become crucial because of the small bandwidth of the absorber. With a classic absorber, a small change in excitation frequency can excite a resonance of the system causing serious problems. In such a case a semi-active vibration absorber would be the best option to prevent this from happening.

1.2.1.3 Active vibration absorbers

Where the classic and semi-active vibration absorbers are basically the same mechanism with the one having a variable stiffness spring instead of a normal spring, the active vibration absorber works on a totally different principle. The purpose of the absorber is still the same namely to minimise the response of the primary system, but in this case some type of actuator together with a control system is used to accomplish this.

The control system will sense the response of the primary system with accelerometers or other sensors and will drive the actuator in such a way to minimise that response. The advantage of this type of absorber is that a wide band absorber is achieved, which is effective not only at one frequency, but over a whole frequency band.

It must be noted that there are a lot of differences between the three types of absorbers. Table 1. 1 gives an indication of the differences between the different absorbers.

It can be seen that the active vibration absorbers come at a substantial cost and are only used when it is really needed. Usually classic or semi-active absorbers will be used because of their low cost.

Table 1. 1 Differences between different types of absorbers

Criteria	Classic	Semi-active	Active
Complexity	Low	Medium	Very High
Cost	Low	Medium	Very High
Energy input	None	Low	High
Effectiveness	Low (very small band)	Medium (small band)	High (wide band)

1.2.2 Vibration Isolators

The main difference between a vibration absorber and a vibration isolator is that where a vibration absorber minimises the response of the primary system, a vibration isolator minimises the vibration transmitted from the primary system to another body. Therefore the primary system's response is not altered substantially, but a device is installed between the primary system and a surrounding body that does not transmit the vibrations or forces at certain frequencies.

Again, there are a few different types of isolators that will be discussed in detail.

1.2.2.1 Vibration isolator

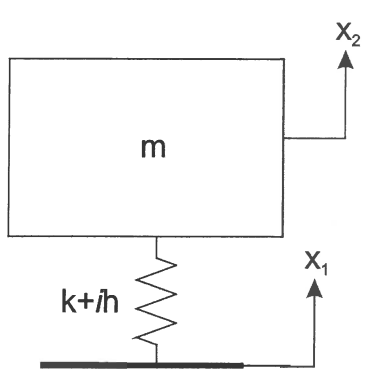

Figure 1. 6 Vibration isolator

The normal passive vibration isolator is simply a spring with low stiffness as shown in Figure 1. 6. Engine mounts are common examples of such isolators (Maw, 1991). The primary system is connected to the ground or to another body with a soft spring. This gives it a very low natural frequency with isolation above $\sqrt{2}$ times the natural frequency.

The response of a mass on a spring with structural damping under an external excitation force is given by:

$$\frac{X}{F_i} = \frac{1}{k - \omega^2 m + ih} \tag{1.3}$$

With:

F_i - Applied force

h - Hysteresis damping constant

The following substitutions can be made:

$$\omega_n = \sqrt{\frac{k}{m}}$$
$$h = k\eta \tag{1.4}$$

With:

η - Loss factor

The following equation can be derived for the response of the primary system:

$$\frac{X}{F_i} = \frac{1}{k\left(1 - \left(\frac{\omega}{\omega_n}\right)^2 + i\eta\right)} \tag{1.5}$$

To get the force transmissibility, the force transmitted to the base must be calculated. The only force transmitted to the base is through the spring with structural damping. The following equation gives the force transmitted to the base due to a displacement of the primary mass:

$$F_T = k(1 + i\eta)X \tag{1.6}$$

By eliminating X in the last two equations the force transmissibility of a vibration isolator is obtained as follows:

$$\frac{F_T}{F_i} = \frac{1+i\eta}{1-\left(\frac{\omega}{\omega_n}\right)^2+i\eta} \tag{1.7}$$

When this is plotted for different loss factors, the graphs in Figure 1. 7 are obtained.

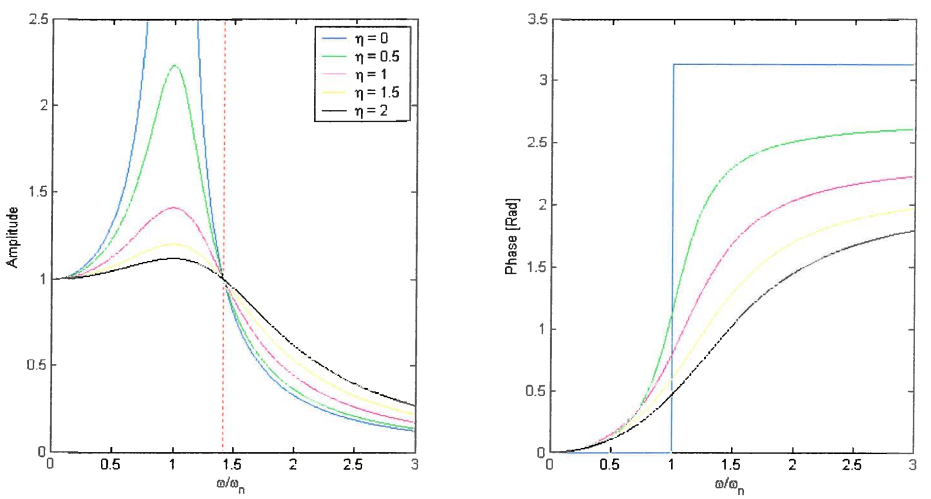

Figure 1. 7 Force transmission response of a vibration isolator

It can be seen that the transmissibility becomes less than one at frequencies above $\sqrt{2}$ times the natural frequency (dotted line). Therefore the isolator is effective above that frequency.

A major disadvantage of this type of isolator is the fact that such a soft spring must be used to make the natural frequency as low as possible. The practical implications of such a soft spring are very large displacements that are usually not permissible. It is furthermore not that easy to make such a soft spring with high lateral stiffness. Usually natural rubber is used to make engine mountings while steel springs are used in vibrating screens. When a very low natural frequency is needed, air springs are usually used because of the very low stiffness that can be obtained.

1.2.2.2 Tuned vibration isolator

The tuned vibration isolator was developed in the helicopter industry in the mid 1960s and employed in the 1970s to isolate the main rotor from the rest of the helicopter. These isolators are anti-resonant vibration isolators that are tuned to a specific frequency that is called the isolation frequency. The major advantages of these isolators over normal isolators are that stiffer springs and smaller masses can be used to achieve better isolation than is possible with normal isolators.

The first two types of isolators were the IRIS (Desjardins & Hooper, 1976 & Desjardins & Hooper, 1980) and the DAVI (Braun, 1980 & Rita et al., 1976 & Flannelly, 1966). The working principle is depicted in Figure 1. 8.

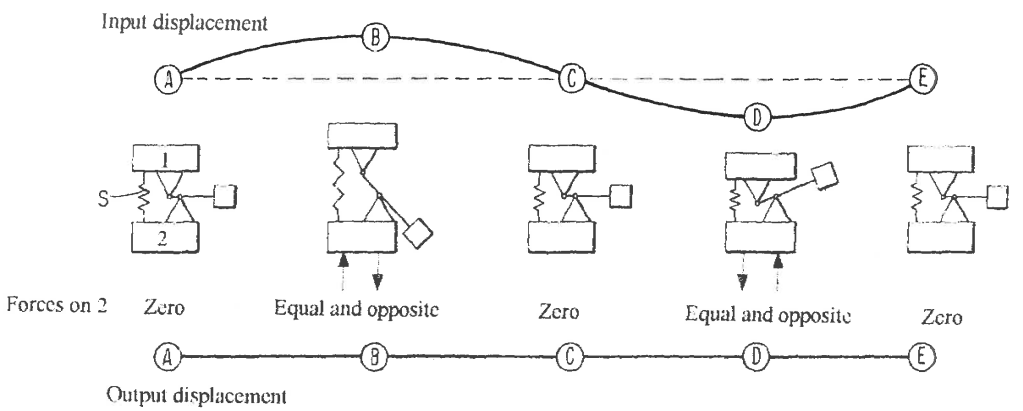

Figure 1. 8 Explanation of force cancellation (Desjardins & Hooper, 1976)

It can be seen that the small mass's motion is amplified with a lever and that the inertia of the mass cancels out the force transmitted through the spring to the base. Therefore the transmitted force is zero at the tuned frequency if no damping is present.

Figure 1. 9 give a schematic model of such an isolator.

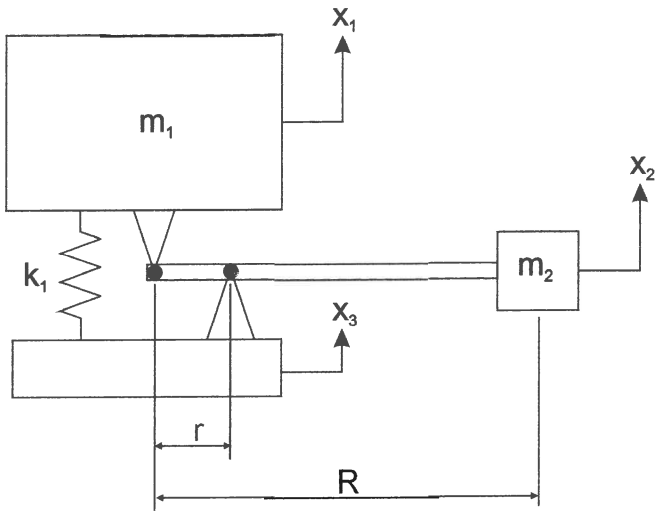

Figure 1. 9 Tuned vibration isolator

The transmissibility of the isolator is given by (Flannelly, 1966):

$$T = \frac{k_1 - \omega^2\left[\frac{I}{r^2} + m_2\frac{R}{r}\left(\frac{R}{r} - 1\right)\right]}{k_1 - \omega^2\left[m_1 + \frac{I}{r^2} + m_2\left(\frac{R}{r} - 1\right)^2\right]} \tag{1.8}$$

and the isolation frequency by:

$$\omega_a = \sqrt{\frac{k_1}{\frac{I}{r^2} + m_2\frac{R}{r}\left(\frac{R}{r} - 1\right)}} \tag{1.9}$$

With:

I	-	Moment of inertia about centre of gravity of m_2
r, R	-	Lever length
ω_a	-	Isolation frequency

A more practical version of the IRIS isolator is given in Figure 1. 10 that was used for floor isolation.

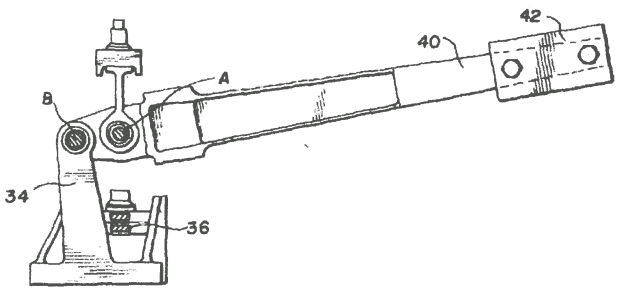

Component description	
A	Airframe pivot
B	Floor pivot
34	Anchor pad
36	Spring
40	Arm
42	Weight

Figure 1. 10 IRIS for helicopter passenger floor isolator (Desjardins & Hooper, 1980)

The transmissibility graph is given in Figure 1. 11. The natural or resonance frequency and the isolation frequency are the prominent features on the graph. The position, form and amplitude of these peaks are influenced by various parameters of the isolator and system.

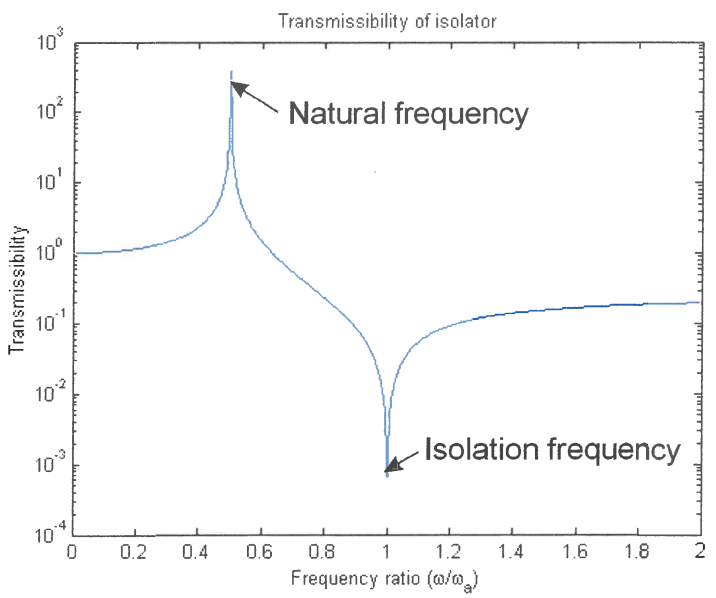

Figure 1. 11 Response of tuned vibration isolator for a typical system

These tuned vibration isolators can now be compared to the normal vibration isolators. For the comparison, systems with the same natural frequency and same amount of damping were used and the result can be seen in Figure 1. 12.

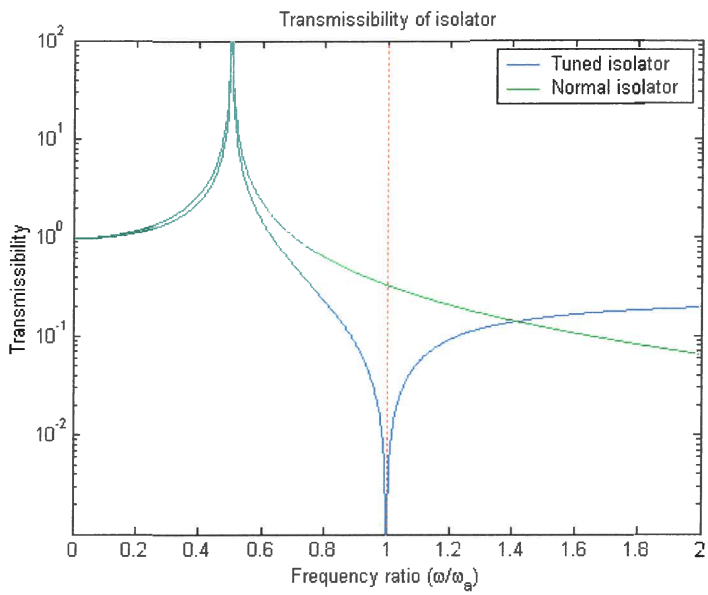

Figure 1. 12 Comparison between a tuned and normal vibration isolator

From the graph it can be seen that at the isolation frequency the normal isolator can only achieve a transmissibility of 0.33 compared to the theoretical 0 of the tuned isolator. It is only at frequencies above a frequency ratio of $\sqrt{2}$ that the normal isolator performs better than the tuned isolator.

All the tuned vibration isolators use this principle, but use different ways to amplify the motion of the small mass. One very popular way to increase the effective mass was with hydraulic amplification. Figure 1. 13 show an isolator design based on this principle.

The concept of hydraulic amplification resulted in the design of the LIVE (Halwes, 1981 & Halwes & Simmons, 1980) system. This tuned vibration isolator is depicted in Figure 1. 14.

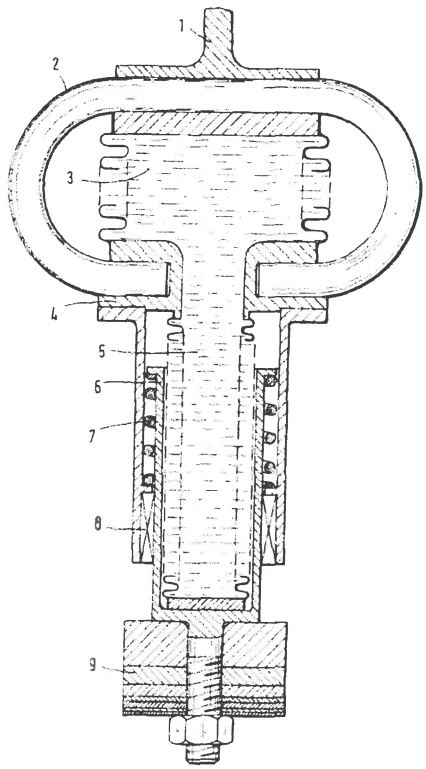

Description of elements	
1	Input force attachment
2	Glass fibre spring
3	Primary fluid chamber
4	Support
5	Secondary fluid chamber
6	Bushing
7	Spring
8	Bearing
9	Inertia mass

Figure 1. 13 MBB vibration absorber (Braun, 1980)

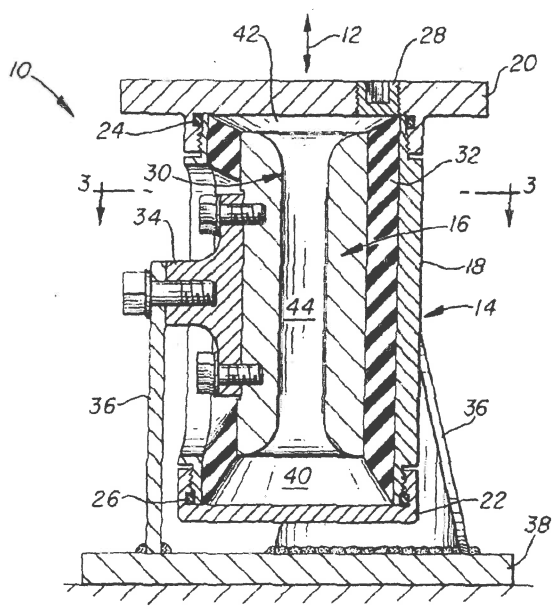

Component description	
10	Vibration isolator
12	Force direction
14	Outer housing
16	Inner housing
18	Central section
20	End section
30	Tuning cylinder
32	Elastomeric spring
38	Plate
40	Chamber
42	Chamber
44	Passage

Figure 1. 14 LIVE system internal design (Halwes et al., 1980)

It used hydraulic amplification and the fluid in the port as the small mass. This makes the design very compact and simple and is why it was also used on helicopters for the main rotor isolation. This type of tuned vibration isolator was selected to be used in this study. The theory will be derived in the next chapter.

Hydraulic engine mountings are another common form of isolators. In principle, they are the same as the LIVE isolator, except that very high damping is used to get wide band isolation (Flower, 1985 & Yu et al., 2000).

1.2.2.3 Semi-active vibration isolators

The same difference between passive and semi-active vibration absorbers exists between passive and semi-active vibration isolators namely that the spring is replaced by a variable stiffness spring to be able to change the natural frequency. It is not logical to use a semi-active vibration isolator as the lower the stiffness, the better the isolation at higher frequencies.

Here follows an example why semi-active vibration isolators are used in practise. While the machine is running at operating speed, the lowest stiffness gives the lowest transmission of forces to the ground. The problem comes in when the machine is shut down or started from standstill. Because the natural frequency is at a low frequency, the machine has to go through this natural frequency to reach its operating frequency. If the machine cannot accelerate through this natural frequency fast enough, it can cause serious problems. With very large machines it will cost too much to install a larger motor to increase the acceleration of the machine and therefore a semi-active vibration isolator offers an advantage. Instead of accelerating the machine through the natural frequency at high speed, the natural frequency is shifted past the excitation frequency at high speed. This can provide a more cost effective solution to the problem than to install a larger motor. Another option can also be to increase the damping in the system for the time which the machine is going through the natural frequency.

With tuned vibration isolators, the objective of the semi-active tuned vibration isolator is not to move the natural frequency of the isolator, as was the case with absorbers and normal isolators, but to move the isolation or anti-resonant frequency of the isolator. This can be achieved in a number of ways.

In the IRIS and DAVI systems, it can be achieved by changing parameters like the stiffness or arm length. In the LIVE isolator there are basically three parameters that can be changed to alter the isolation frequency:

1. Stiffness: By changing the stiffness, the natural and isolation frequencies are changed (Hodgson & Duclos, 1991).
2. Port length: The port length can be modified by using a sleeve inside the port and pushing it out (Smith & Stamps, 1995).
3. Port diameter: It is also possible to change the port diameter (Smith & Stamps, 1998). Figure 1. 15 illustrate concepts on how the last two possibilities can be achieved.

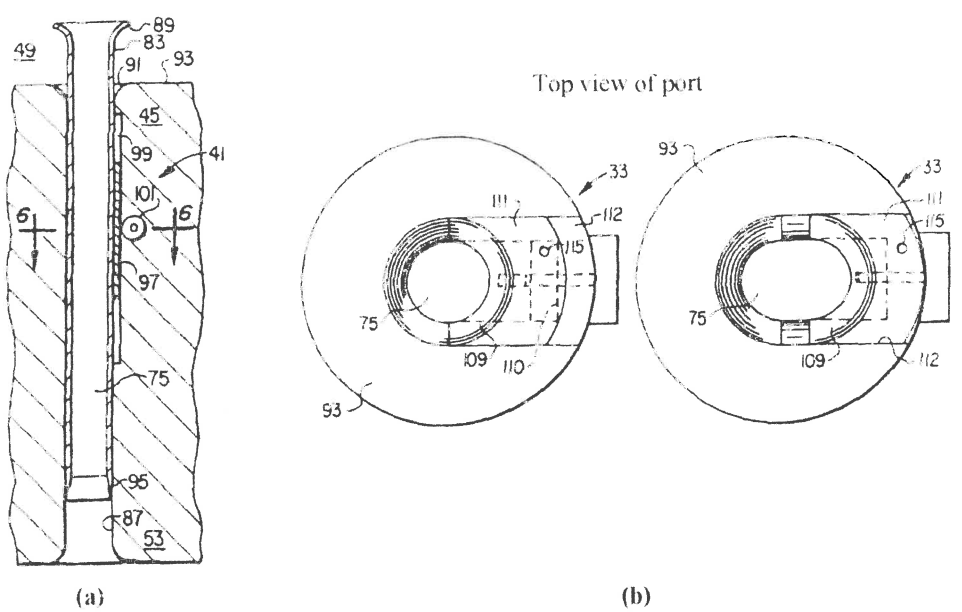

Figure 1. 15 Adjustable (a) port length and (b) area (Smith & Stamps, 1998)

Other more complex methods were also proposed (McKeown et al., 1995), but these concepts will not be dealt with in detail.

1.2.2.4 Active vibration isolator

This type of isolator is basically the same as an active vibration absorber, except that the objective in this case will be to minimise the forces transmitted to an external body. Therefore the response of the external body will be minimised and not the primary body as was the case with the absorber.

At the control side of the isolator, there will usually be a feedforward and a feedback loop. The feedforward loop will sense the vibration of the primary mass so that the actuator can react to that before the external body is influenced by it. The feedback loop senses the external body's vibration and the control system tries to minimise that.

The same table that was given for vibration absorbers is applicable to vibration isolators so that normal engine mountings are by far the most widely used type of isolator and active vibration isolators very rare because of their cost.

1.3 Smart Materials

Smart materials are a group of materials that have the ability to react to changes in environmental conditions like temperature, force and magnetic field. These materials are quite new and are not used widely in the industry. Normally one of the material properties change due to environmental conditions. This has the tendency to let the materials look "smart" or intelligent.

1.3.1 Piezoelectric material

The most common smart material is the piezoelectric material. This material has the ability to change the electric field over its poles when force is applied to it. This

ability works in the opposite way as well so that if an electric voltage is supplied over its poles, the material will expand and will work like an actuator. This material is used extensively for accelerometers, sonar and high frequency actuation. A very important property of piezoelectric actuators is that their displacement is extremely small (usually smaller than 5 micron) but that they can operate at extremely high frequencies. This makes them ideal for applications like accelerometers or sonar transducers. A lot of effort has been put into the development of high displacement piezoelectric actuators. The most common way to achieve larger displacements is to put the actuators in stacks (Hooker, 1997). The advantage of stacks is that the force is not sacrificed to achieve large displacements.

Another interesting way to achieve large displacements was the use of inchworms (Herakovic, 1998). These actuators consist of 3 piezo actuators that work together to move like a worm. This enables the actuator to move long distances. Figure 1. 16 illustrates the working principle.

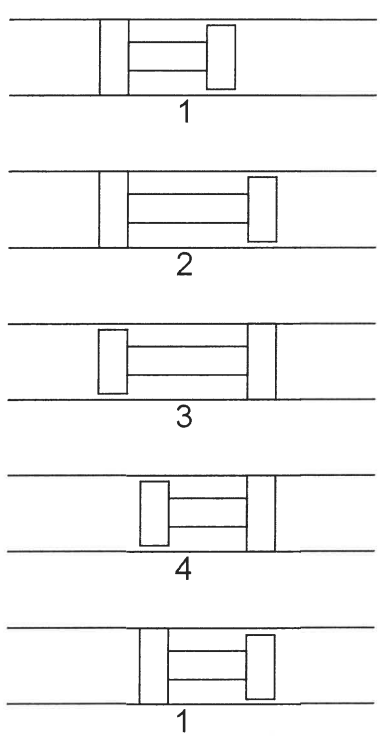

Figure 1. 16 Working principle of an inchworm

Hybrid actuators were developed (Janker, 1998) to improve the displacement of piezo or other small displacement actuators. It consists of a displacement

amplification device to improve displacement of the actuator, but at the cost of force. Such an actuator is illustrated schematically in Figure 1. 17.

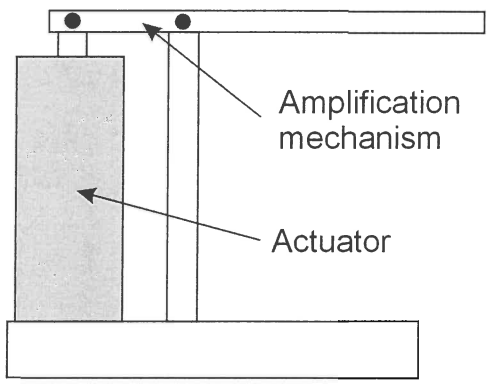

Figure 1. 17 Displacement amplification hybrid actuator

Another interesting mechanism is a locking mechanism to enable a low force actuator to withstand large forces when stationary (Chen, 1999).

It can be seen that piezoelectric actuators are very well suited for high frequency applications and not where large displacements at low frequencies are needed.

1.3.2 Shape memory alloys

Another very common smart material is shape memory alloys (SMA). This material changes its molecular grouping from austenite to martensite above certain temperatures and that results in a change in Young's modulus (Stalmans & Van Humbeeck, 1995 & Duerig et al., 1990). The shape memory effect was first observed in 1932 (Hodgson et al., 1999). If a SMA is deformed when cold, it will return to its original form when heated above its transition temperature (Lin, 1996). This is where the name shape memory alloy comes from, because it seems as if the metal remembered its original form. The forces applied by the metals to return to their

original form can be quite significant and allow the SMAs to be used as actuators (Baz et al., 1990 & Meghdari et al., 1993).

Many models have been developed to predict the behaviour of Nitinol, the most common shape memory alloy (Ford et al., 1995, Witting & Cozzarelli, 1994, Bo & Lagoudas, 1994 & Monkman, 2000). The damping of Nitinol has also been characterised (Lin et al., 1993) and many springs have been developed to act as variable stiffness springs due to the material change of the shape memory alloys (Liang & Rogers, 1993). In vibrations, shape memory alloy has been used for altering stiffness in systems (Segalman et al., 1993) or to form part of the system to induce changes (Feng & Li, 1996).

These materials can usually only produce large displacement or large force, and not both. Their availability is also a problem and can usually only be bought in very thin wires that is not always the format needed.

1.3.3 Other materials

Another useful smart material is magnetorheological (MR) elastomers. This is basically an elastomer like natural rubber, but with approximately 30% of very fine iron powder mixed into it (Davis, 1999 & Jolly et al., 1996a & Jolly et al., 1996b & Ginder et al., 2000 & Ginder et al., 1999). The rubber is cured in a magnetic field and this leads to an elastomer that changes stiffness in the presence of a magnetic field. One practical problem with this material is the magnitude of the magnetic field that is required for the change. It is normally not possible to produce such a magnetic field over a large distance, so the physical size of the elastomer must be very small, which limits practical applications.

Wax actuators are another type of compact actuator. The most common example of this is the thermostat of most cars. It consists of a sealed copper cup filled with a type of wax (that expands significantly when heated) and a shaft. When the wax expands

it pushes the shaft outwards and acts as an actuator. Problems with these actuators are the heating and especially the cooling of it and also the control of its displacement. In contrast to traditional smart materials, these actuators can produce very large forces and displacements making them very useful. Forces of up to 500N and displacements of 10mm are common with these actuators.

1.4 Variable stiffness springs

Although little has been published about this subject, there are a few attempts at developing variable stiffness springs documented in the literature. The most impressive of these is a spring which can change stiffness by 45 times by separating two beams of a compound leaf spring (Walsh & Lamancusa, 1992). The application of the spring was a semi-active vibration absorber. The mass-spring system that they used is depicted in Figure 1. 18.

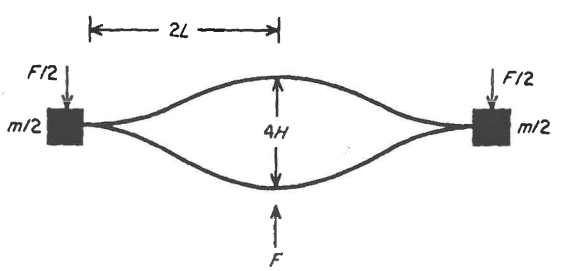

Figure 1. 18 Variable stiffness absorber (Walsh & Lamancusa, 1992)

Although other authors do not see this as practically applicable (Brennan, 2000), it shows that the concept has certain possibilities. The concept was therefore developed further and Figure 1. 19 show different possibilities to create such a semi-active absorber with the use of beams or leaf springs.

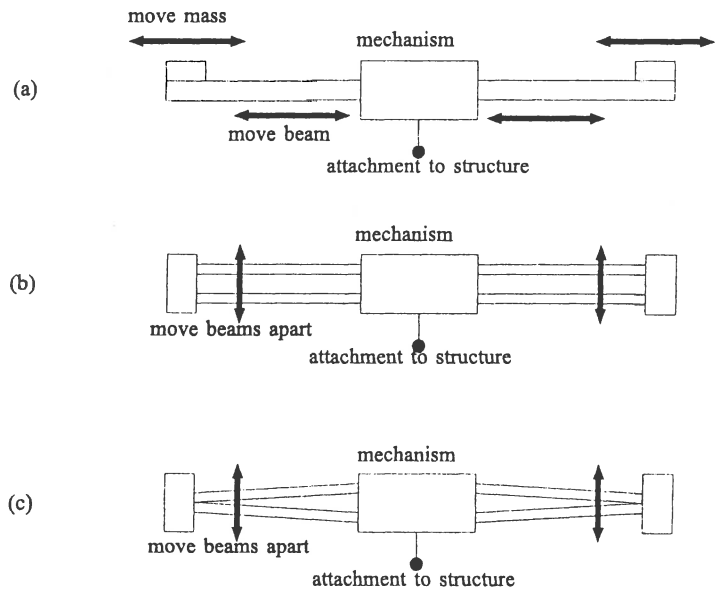

Figure 1. 19 Different ways of configuring a beam as a semi-active vibration absorber (Brennan, 2000)

Another concept is a mass suspended between two air springs of which the stiffness can be changed by altering the pressure inside the air springs (Longbottom & Rider, 1987). This concept has the ability to achieve very low stiffness due to the use of air springs. This concept was later improved with a simple method of automatically adjusting the stiffness (Brennan et al., 1996).

Changing the number of active coils in a coil spring is also a way of making a variable stiffness spring (Franchek et al., 1995) and also the heating of a temperature dependant viscoelastic element (Smith, 1991). Another concept is to change the angle at which the coil springs are orientated to change the effective stiffness as depicted in Figure 1. 20 (Ribakov & Gluck, 1998).

Electro magnetism can be used to influence the stiffness of a spring. Figure 1. 21 show such a variable stiffness spring that has primary coil springs that is de-stiffened by an electro-magnetic negative stiffness (Von Flotow et al., 1994).

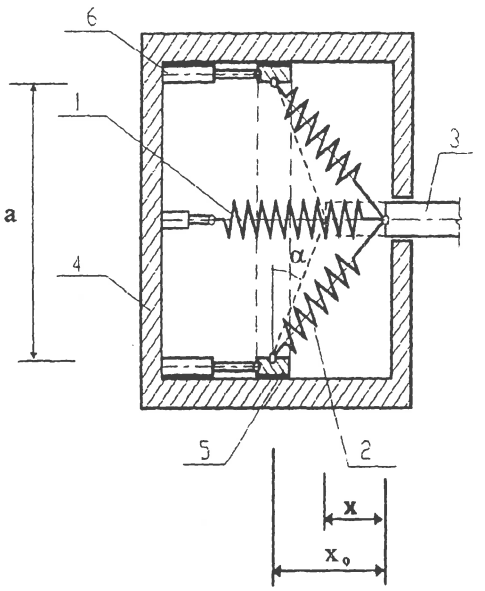

Figure 1. 20 **Variable stiffness coils spring assembly (Ribakov & Gluck, 1998)**

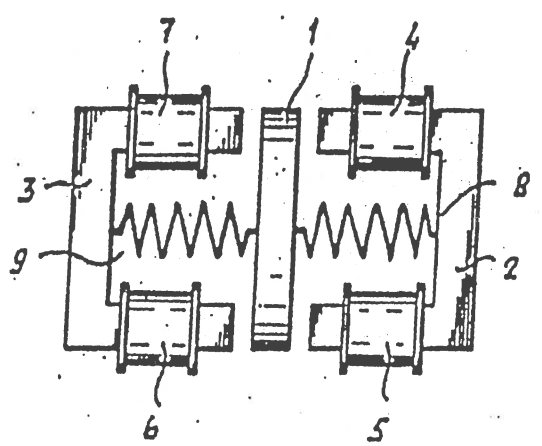

Figure 1. 21 **Electro-magnetic variable stiffness spring (Von Flotow et al., 1994)**

As mentioned in the previous section, shape memory alloys have the ability to change their Young's modulus when heated. Therefore a variable stiffness spring can be made if such shape memory alloy wire is turned into a coil spring. Figure 1. 22 shows a concept of a variable stiffness spring that utilizes shape memory alloy coil springs to achieve the variation in stiffness (Siler & Demoret, 1996).

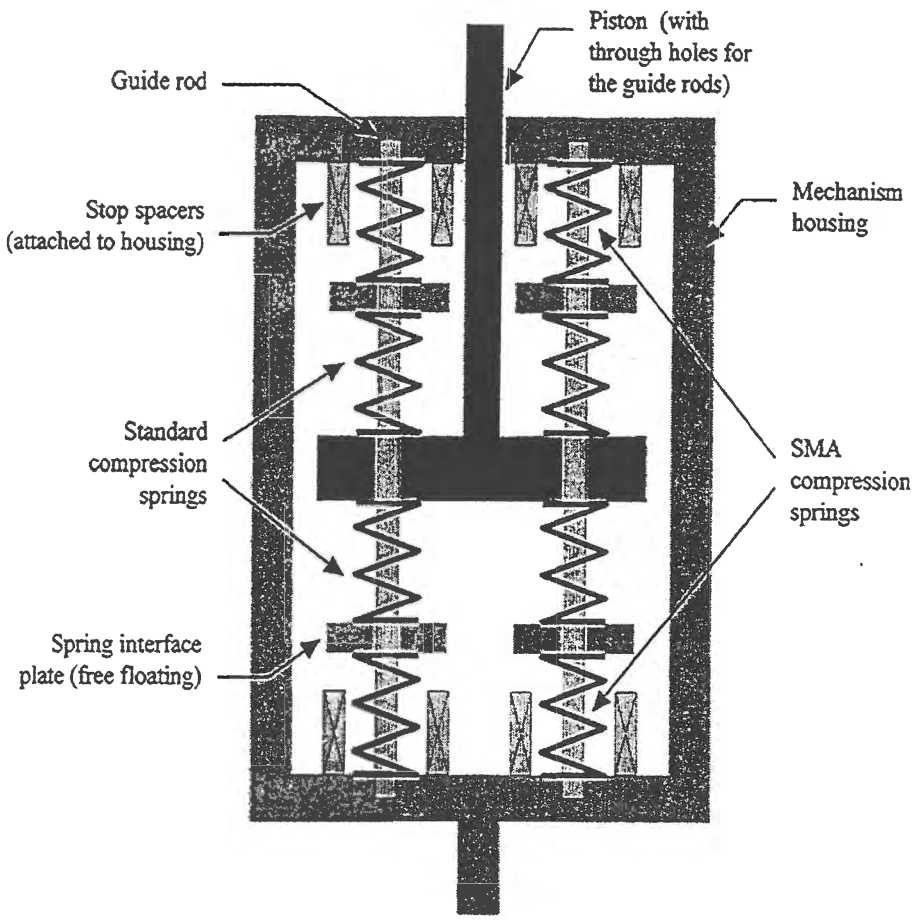

Figure 1. 22 Shape memory alloy variable stiffness spring (Siler & Demoret, 1996)

One last interesting concept used packs of cylindrical panels to create a variable stiffness spring (Mashinostroehiya, 1987). Most of these devices were developed for vibration absorbers and were designed appropriately. In vibration isolators the requirements for the stiffness element is different concerning lateral stiffness, damping and stroke and therefore it is necessary to develop a new variable stiffness spring for application in vibration isolators.

1.5 Objectives

The LIVE concept gives the possibility of a very compact and practical isolator. The hydraulic amplification mechanism makes it possible to modify parameters of the isolator to create a semi-active tuned vibration isolator. Smart materials are a new

class of materials that is not used in many applications up to now. These materials are seen as materials with a lot of potential for actuators and sensors, but more suitable applications are needed to develop these materials. The aim of this study is to develop a tunable LIVE isolator by changing the stiffness and damping of the isolator. The change in stiffness shifts the isolation frequency of the isolator, while the variable damping control the amplification at the natural frequency. This will be dealt with in more detail in Chapter 2.

The specific objectives of the study are to:

- Develop a variable stiffness spring that can be incorporated in a LIVE isolator to change the isolation frequency of the isolator. It is preferable to make use of smart materials to obtain the change in stiffness.
- Design and build a tunable LIVE isolator, incorporating the variable stiffness spring and a variable damping mechanism.
- Characterise the isolator and determine the effectiveness of the stiffness and damping changes.
- Develop a control system to demonstrate that it is practically possible to tune the isolator automatically to the excitation conditions.

1.6 Conclusions

This chapter gave an overview of the background of absorbers, isolators, smart materials and variable stiffness springs. The differences between absorbers and isolators were addressed as well as all the different types of absorbers and isolators. A literature study on smart materials was done and the relevant concepts were mentioned and explained. Variable stiffness springs were also addressed with a detailed literature study. Explanations of the different concepts encountered were provided. The objectives for the project were listed.

CHAPTER 2

Mathematical model of isolator

2.1 Introduction

It is important to derive a mathematical model of the isolator before the design phase to be able to predict the performance of the isolator. In this chapter a one-dimensional model of the isolator will be derived to obtain equations for the natural and isolation frequency as well as the transmissibility of the isolator.

The derivations in sections 2.2.1 to 2.2.5 have been done by Du Plooy, 1999 and are given because of the relevance to this work. The derivation was done for an isolator that was attached to the ground on the one side and to a vibrating machine on the other. The transmissibility equation obtained is still applicable if both ends are free to move (acceleration transmissibility), as long as the direction is kept the same. If the direction is turned around, the equations change slightly. Therefore the derivation of the equation for this case is done in section 2.2.7. The derivation of the damped isolation and natural frequency in section 2.2.6 has not been published previously and was done as part of this study.

2.2 Mathematical 1-DOF model of isolator:

2.2.1 Equations of motion

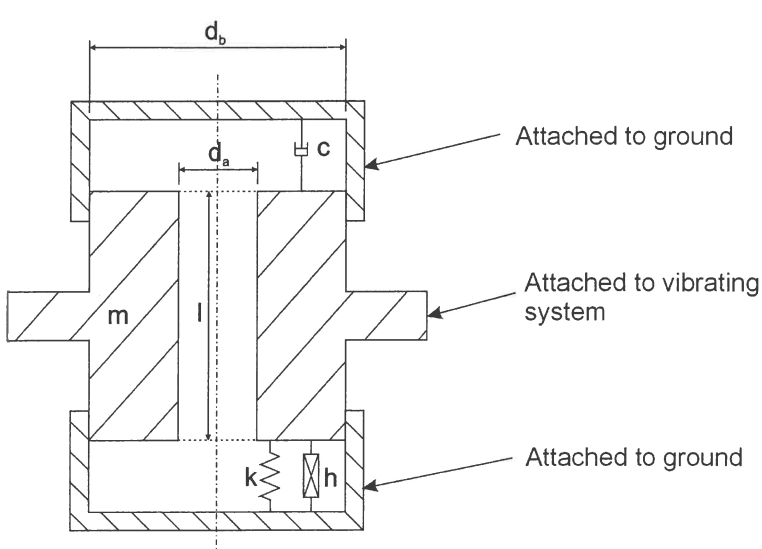

Figure 2. 1 Definition of LIVE system geometry

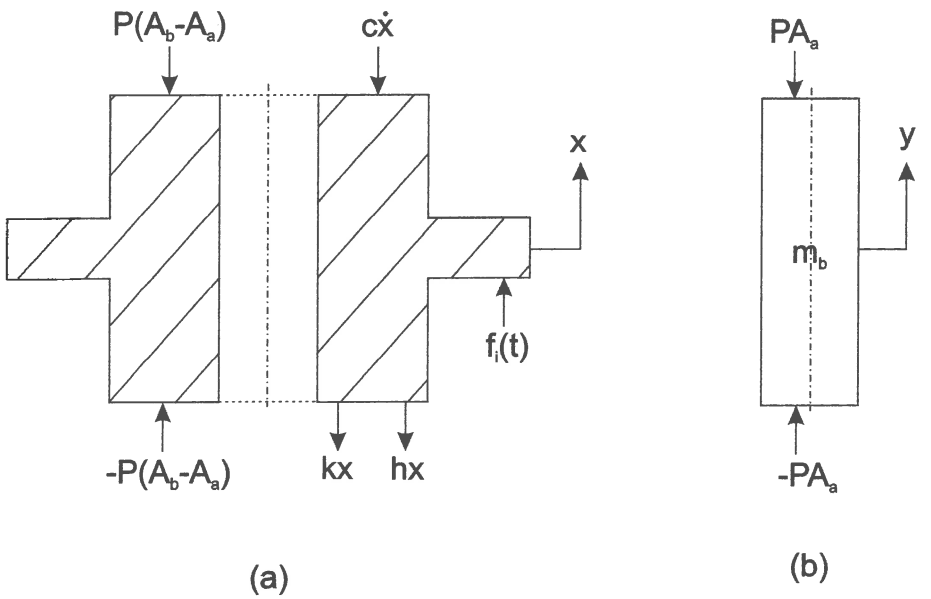

Figure 2. 2 Forces acting on (a) isolator assembly and (b) liquid column in port

In the figure above, the following abbreviations are used:

m	-	System mass
m_b	-	Absorber mass
k	-	Stiffness of spring
h	-	Structural damping of spring
c	-	Viscous damping of fluid
l	-	Length of the port
d_a	-	Diameter of the port
d_b	-	Diameter of the reservoir
x	-	Displacement of the port
y	-	Displacement of liquid in port

The relationship between $\dot{x}$ and $\dot{y}$ can be found by applying mass conservation and finding the continuity equation:

$$\dot{y}A_a = -\dot{x}(A_b - A_a)$$
$$\dot{y} = \left(1 - \frac{A_b}{A_a}\right)\dot{x} \tag{2.1}$$

The force balance on the system mass (m) is:

$$m\ddot{x} = -c\dot{x} - kx - ihx - 2P\left(A_b - A_a\right) + f_i\left(t\right) \tag{2.2}$$

The force balance on the absorber mass ($m_b = \rho l A_a$) is:

$$m_b\ddot{y} = -2PA_a \tag{2.3}$$

Substituting the acceleration in equation (2.3) with the conservation of mass found in equation (2.1) gives the equation for the peak pressure:

$$P = -\frac{m_b}{2A_a^2}\left(A_a - A_b\right)\ddot{x} \tag{2.4}$$

Substituting this peak pressure and $h = k\eta$ into equation (2.2) give the following single degree-of-freedom equation of motion for the system:

$$\left[m + m_b\left(1 - \frac{A_b}{A_a}\right)^2\right]\ddot{x} + c\dot{x} + k\left(1 + i\eta\right)x = f_i\left(t\right) \tag{2.5}$$

On inspection it can be seen that this equation is basically the same as a normal single DOF mass, spring and damper system except that the total mass here is a summation of the system mass (m) and the absorber mass (m_b) amplified by the area ratio. The implication of this is that it can be handled as a simple mass, spring and damper system, except that the mass used in the equations must always be the combined mass of the isolator.

From this insight, the undamped natural frequency can be written directly as follow:

$$\omega_n = \sqrt{\frac{k}{m + m_b\left(1 - \frac{A_b}{A_a}\right)^2}} \tag{2.6}$$

2.2.2 Frequency response function

Equation (2.5) can be transformed to the frequency domain by substituting the harmonic response and its derivatives, which result from harmonic excitation:

$$\begin{aligned} x(t) &= Xe^{i\omega t} \\ \dot{x}(t) &= i\omega Xe^{i\omega t} \\ \ddot{x}(t) &= -\omega^2 Xe^{i\omega t} \\ f_i(t) &= F_i e^{i\omega t} \end{aligned} \tag{2.7}$$

By making the substitutions, the following equation for the dynamic stiffness of the isolator can be found:

$$\frac{F_i}{X} = k(1+i\eta) + i\omega c - \omega^2 \left[m + m_b \left(1 - \frac{A_b}{A_a} \right)^2 \right] \tag{2.8}$$

This is graphically represented in Figure 2. 3:

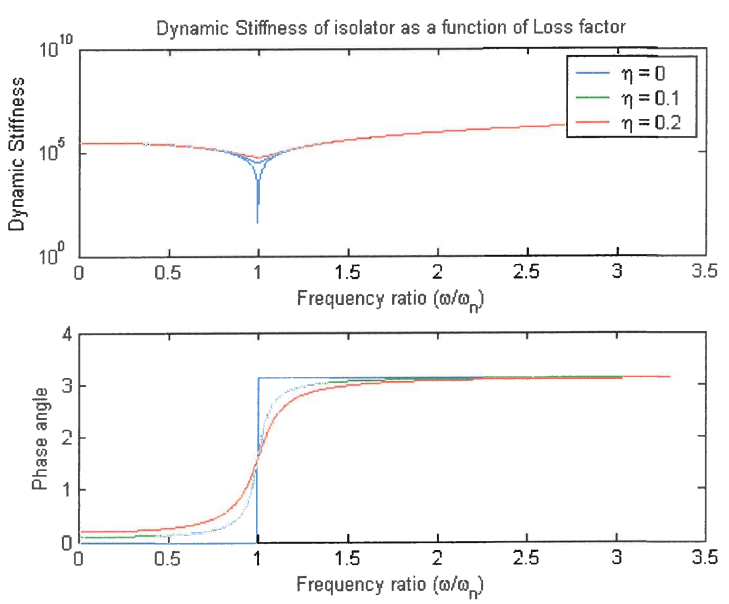

Figure 2. 3 Dynamic stiffness of isolator as function of loss factor (*c*=0)

2.2.3 Transmissibility

The transmissibility is defined as the force amplitude ratio of the force transmitted to the ground (F_0) and the applied force (F_i).

The applied force can be derived from the dynamic stiffness equation (2.8):

$$F_i = \left\{ k(1+i\eta) + i\omega c - \omega^2 \left[m + m_b \left(1 - \frac{A_b}{A_a} \right)^2 \right] \right\} X \tag{2.9}$$

The force transmitted to the ground is a combination of the force due to the pressure difference, spring and damping.

The force resulting from the pressure difference in the reservoirs is:

$$F_p = 2PA_b \tag{2.10}$$

Substituting the peak pressure found in equation (2.4) into equation (2.10) gives the force due to the pressure difference:

$$F_p = m_b \left(1 - \frac{A_b}{A_a} \right) \frac{A_b}{A_a} \omega^2 X \tag{2.11}$$

Combining this with the spring and damper forces give the reaction force on the ground:

$$F_0 = \left[k(1+i\eta) + i\omega c + \omega^2 m_b \left(1 - \frac{A_b}{A_a} \right) \frac{A_b}{A_a} \right] X \tag{2.12}$$

The transmissibility is given by eliminating X in equations (2.9) and (2.12):

$$\frac{F_0}{F_i} = \frac{k(1+i\eta) + i\omega c + \omega^2 m_b \left(1 - \frac{A_b}{A_a} \right) \frac{A_b}{A_a}}{k(1+i\eta) + i\omega c - \omega^2 \left[m + m_b \left(1 - \frac{A_b}{A_a} \right)^2 \right]} \tag{2.13}$$

The objective of the isolator is to minimize the force transmitted to the ground and therefore minimizing the transmissibility.

2.2.4 Undamped natural and isolation frequency

The undamped natural frequency of the isolator has already been determined previously in equation (2.6) as:

$$\omega_n = \sqrt{\frac{k}{m + m_b\left(1 - \frac{A_b}{A_a}\right)^2}} \tag{2.14}$$

At the undamped isolation frequency, the transmissibility will be equal to zero and therefore the undamped transmitted force (F_0) must also be equal to zero:

$$k + \omega_a^{\,2} m_b\left(1 - \frac{A_b}{A_a}\right)\frac{A_b}{A_a} = 0 \tag{2.15}$$

where ω_a is the undamped isolation frequency.

By rearranging equation (2.15) the following equation for the undamped isolation frequency is obtained:

$$\omega_a = \sqrt{\frac{-k}{m_b\left(1 - \frac{A_b}{A_a}\right)\frac{A_b}{A_a}}} \tag{2.16}$$

In the literature this frequency is often called the anti-resonant frequency. Since anti-resonance for an undamped system is defined as a point of no response to excitation (Maia *et al.*, 1998) and since the isolator discussed here does not aim to do that, the term isolation frequency will be used.

It is important to note that this frequency is independent of the system mass. This is an extremely attractive property since a changing system mass, as may be the case for many machines, will not effect the isolation frequency. Because of real materials and fluids, the damping will never be zero and therefore it must be ensured that the lowest possible damping is achieved to obtain the best possible isolation at the isolation frequency.

With the undamped natural and isolation frequency known, the frequency ratio can now be defined as follows:

$$G_a = \frac{\omega_n}{\omega_a} = \sqrt{\frac{m_b\left(\frac{A_b}{A_a}-1\right)\frac{A_b}{A_a}}{m+m_b\left(\frac{A_b}{A_a}-1\right)^2}} \tag{2.17}$$

There is a correlation between the frequency ratio and the amount of isolation that can be achieved. Figure 2. 4 illustrate this by giving the minimum transmissibility that can be achieved for a specific frequency ratio.

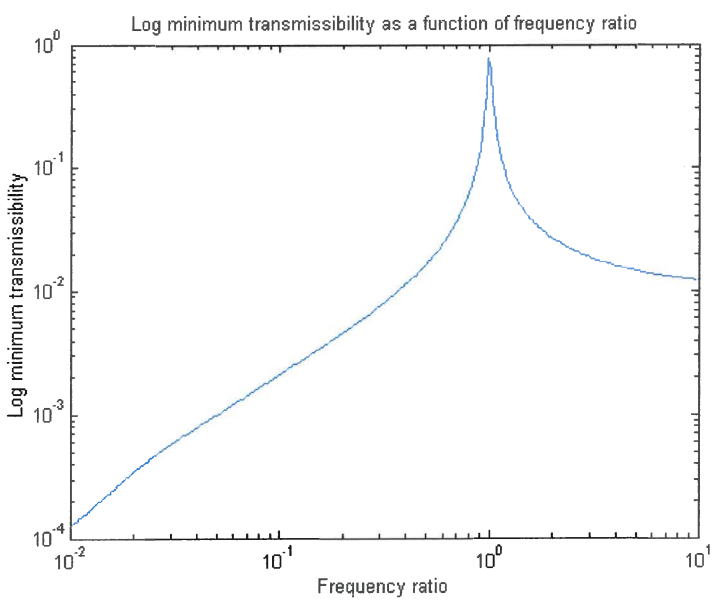

Figure 2. 4 Log minimum transmissibility as a function of frequency ratio

It can be seen that a low frequency ratio results in a low transmissibility.

2.2.5 Non-dimensional transmissibility

It is always a good practice to use non-dimensional equations. To derive a non-dimensional transmissibility equation, the following substitutions must be made together with the undamped natural and isolation frequencies:

$$\zeta = \frac{c}{2\left[m + m_b\left(1 - \frac{A_b}{A_a}\right)^2\right]\omega_n} \tag{2.18}$$

$$\eta = \frac{h}{k} \tag{2.19}$$

The non-dimensional transmissibility (T_r) is the given by:

$$T_r = \frac{1 - \left(\frac{\omega}{\omega_a}\right)^2 + i\left(2\zeta\frac{\omega}{\omega_n} + \eta\right)}{1 - \left(\frac{\omega}{\omega_n}\right)^2 + i\left(2\zeta\frac{\omega}{\omega_n} + \eta\right)} \tag{2.20}$$

The absolute transmissibility is:

$$|T_r| = \left\{\frac{\left[1 - \left(\frac{\omega}{\omega_a}\right)^2\right]^2 + \left[2\zeta\frac{\omega}{\omega_n} + \eta\right]^2}{\left[1 - \left(\frac{\omega}{\omega_n}\right)^2\right]^2 + \left[2\zeta\frac{\omega}{\omega_n} + \eta\right]^2}\right\}^{\frac{1}{2}} \tag{2.21}$$

The phase angle is:

$$\phi = \tan^{-1}\left\{\frac{2\zeta\frac{\omega}{\omega_n} + \eta}{1 - \left(\frac{\omega}{\omega_a}\right)^2}\right\} - \tan^{-1}\left\{\frac{2\zeta\frac{\omega}{\omega_n} + \eta}{1 - \left(\frac{\omega}{\omega_n}\right)^2}\right\} \tag{2.22}$$

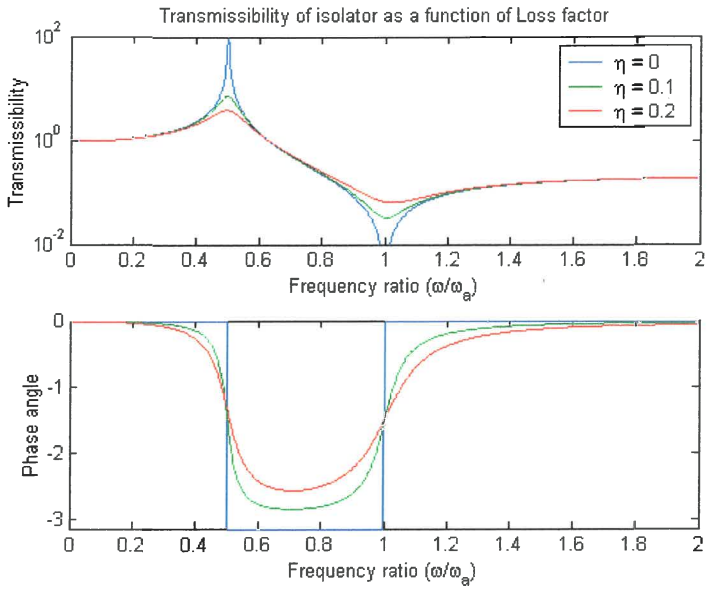

Figure 2. 5 Transmissibility of isolator as function of loss factor (ζ=0)

2.2.6 Damped natural and isolation frequency

There will always be damping in a system. Furthermore, it is the aim of the project to develop a variable stiffness and damping isolator that will have quite a large amount of damping present when set to maximum damping. Therefore it is necessary to determine the equations for the damped natural and isolation frequency.

For this derivation, structural damping will be neglected. The reason for this is that the derivation is not possible with the structural damping included and that it is a fair assumption to combine all damping in the system into one viscous damping constant.

To determine the natural and isolation frequency, the derivative with respect to frequency, of the absolute value of the transmissibility, must be set equal to zero. The frequency values at which this will be true are the natural and isolation frequency. In essence, the frequency of maximum transmissibility is determined and not the damped natural frequency. Because a single degree of freedom system is considered, it is a fair assumption that the frequency of maximum transmissibility and the damped natural frequency will be the same or very close to each other. Therefore the term

damped natural frequency will be used to be consistent with the undamped natural frequency used in previous sections.

The transmissibility without structural damping is:

$$|T_r| = \left\{ \frac{\left[1-\left(\frac{\omega}{\omega_a}\right)^2\right]^2 + \left[2\zeta\frac{\omega}{\omega_n}\right]^2}{\left[1-\left(\frac{\omega}{\omega_n}\right)^2\right]^2 + \left[2\zeta\frac{\omega}{\omega_n}\right]^2} \right\}^{\frac{1}{2}} \tag{2.23}$$

Setting its derivative equal to zero gives:

$$\frac{\partial}{\partial\omega}\left\{ \frac{\left[1-\left(\frac{\omega}{\omega_a}\right)^2\right]^2 + \left[2\zeta\frac{\omega}{\omega_n}\right]^2}{\left[1-\left(\frac{\omega}{\omega_n}\right)^2\right]^2 + \left[2\zeta\frac{\omega}{\omega_n}\right]^2} \right\}^{\frac{1}{2}} = 0 \tag{2.24}$$

$$\frac{\frac{1}{2}\left\{ \frac{\frac{-4\left[1-\left(\frac{\omega}{\omega_a}\right)^2\right]\omega}{\omega_a^2} + \frac{4\left(2\zeta\frac{\omega}{\omega_n}\right)\zeta}{\omega_n}}{\left[1-\left(\frac{\omega}{\omega_n}\right)^2\right]^2 + \left(2\zeta\frac{\omega}{\omega_n}\right)^2} - \frac{\left\{\left[1-\left(\frac{\omega}{\omega_a}\right)^2\right]^2 + \left(2\zeta\frac{\omega}{\omega_n}\right)^2\right\}\left\{ \frac{-4\left[1-\left(\frac{\omega}{\omega_n}\right)^2\right]\omega}{\omega_n^2} + \frac{4\left(2\zeta\frac{\omega}{\omega_n}\right)\zeta}{\omega_n} \right\}}{\left[1-\left(\frac{\omega}{\omega_n}\right)^2\right]^2 + \left(2\zeta\frac{\omega}{\omega_n}\right)^2} \right\}}{\left\{ \frac{\left[1-\left(\frac{\omega}{\omega_a}\right)^2\right]^2 + \left[2\zeta\frac{\omega}{\omega_n}\right]^2}{\left[1-\left(\frac{\omega}{\omega_n}\right)^2\right]^2 + \left[2\zeta\frac{\omega}{\omega_n}\right]^2} \right\}^{\frac{1}{2}}} = 0 \tag{2.25}$$

Solving this equation gives five roots of which one is zero, two are negative frequencies ($-\omega_{nd}$, $-\omega_{ad}$) and the other two give the damped natural and isolation frequencies that look as follow:

Damped natural and isolation frequency:

$$\omega_{n_d}, \omega_{a_d} = \omega_n \sqrt{\frac{-1-\left(\frac{\omega_a}{\omega_n}\right)^2 \pm \sqrt{\left(1-\left(\frac{\omega_a}{\omega_n}\right)^2\right)^2 + 8\left(\frac{\omega_a}{\omega_n}\right)^2 \zeta^2 \left(1+\left(\frac{\omega_a}{\omega_n}\right)^2\right)}}{4\zeta^2\left(1+\left(\frac{\omega_a}{\omega_n}\right)^2 - \frac{1}{2\zeta^2}\right)}} \quad (2.26)$$

It is important to note that the inverse of the frequency ratio features a few times in this equation. The importance of this is that this damped natural and isolation frequency is dependent on the system mass, because the frequency ratio is dependent on it as well as the undamped natural frequency that stands in front of the equation.

2.2.7 Acceleration transmissibility

The force transmissibility was derived in the previous sections. This is applicable as long as one side of the isolator is attached to the ground. If the isolator is implemented between a handle and a vibrating machine, the force transmissibility is no longer applicable. An acceleration or displacement transmissibility is then representative of the system. The force transmissibility is the same as the acceleration transmissibility due to Newton's second law. The difference is that the outside part is no longer attached to ground, but is also moving. If the isolator is used in this way, say for example for isolation of a handle from a machine, the heavier outside part is attached to the handle and the inner part to the vibrating machine. This will result in better isolation due to the heavier mass on the handle. This orientation causes the transmissibility to change slightly and the derivation for the case depicted in Figure 2. 6 will follow.

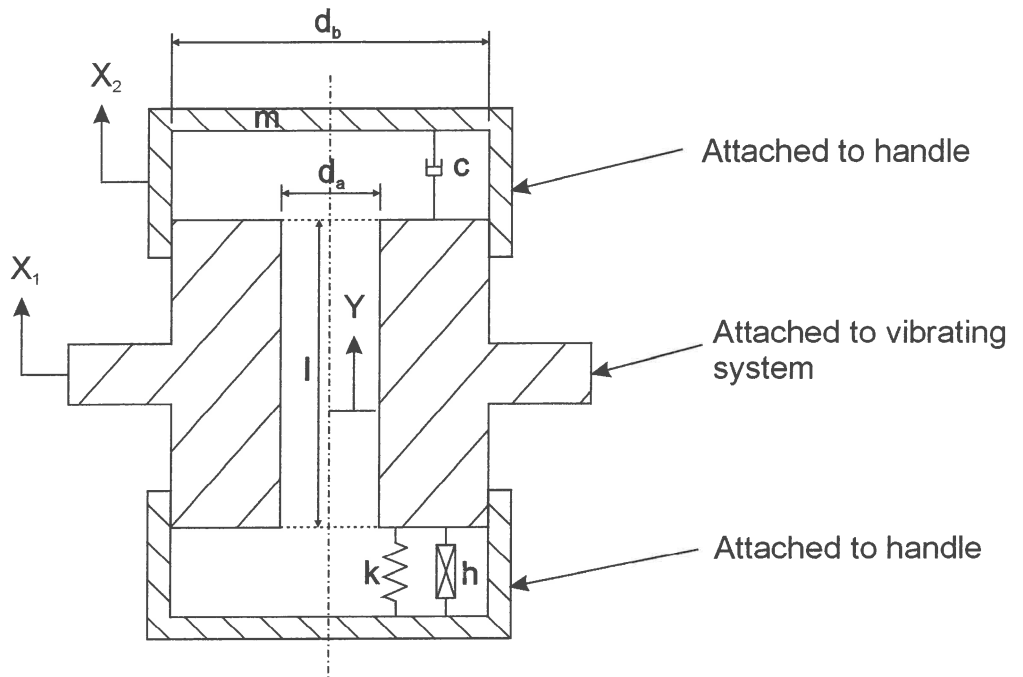

Figure 2. 6 LIVE system implemented on handle

In the above system the displacement X_1 will be given a prescribed displacement. The continuity equation becomes:

$$\dot{y}A_a = -\dot{x}_1(A_b - A_a) + \dot{x}_2 A_b$$
$$\dot{y} = \left(1 - \frac{A_b}{A_a}\right)\dot{x}_1 + \frac{A_b}{A_a}\dot{x}_2 \tag{2.27}$$

The force balance on the system mass (m) is:

$$m\ddot{x}_2 = -c(\dot{x}_1 - \dot{x}_2) - k(x_1 - x_2) - ih(x_1 - x_2) + 2P(A_b) \tag{2.28}$$

The force balance on the absorber mass ($m_b = \rho l A_a$) is:

$$m_b\ddot{y} = -2PA_a \tag{2.29}$$

Substituting the acceleration in equation (2.29) with the conservation of mass found in equation (2.27) gives the equation for the peak pressure:

$$P = -\frac{m_b}{2A_a}\left[\left(1-\frac{A_b}{A_a}\right)\ddot{x}_1 + \frac{A_b}{A_a}\ddot{x}_2\right] \tag{2.30}$$

Substituting this peak pressure and $h = k\eta$ into equation (2.28) and transforming it to the frequency domain give the following motion for the system:

$$k(1+i\eta)(X_1 - X_2) + i\omega c(X_1 - X_2) + \omega^2 m X_2 + \omega^2 m_b \frac{A_b}{A_a}\left[\left(1-\frac{A_b}{A_a}\right)X_1 + \frac{A_b}{A_a}X_2\right] = 0 \tag{2.31}$$

Rewriting of the equation gives the transmissibility directly as:

$$\frac{X_2}{X_1} = \frac{k(1+i\eta) + i\omega c + \omega^2 m_b\left(1-\frac{A_b}{A_a}\right)\frac{A_b}{A_a}}{k(1+i\eta) + i\omega c - \omega^2\left[m + m_b\left(\frac{A_b}{A_a}\right)^2\right]} \tag{2.32}$$

This is then the displacement or acceleration transmissibility for the isolator for a forced response of the inner part. For this case the undamped natural frequency becomes:

$$\omega_n = \sqrt{\frac{k}{m + m_b\left(\frac{A_b}{A_a}\right)^2}} \tag{2.33}$$

The undamped isolation frequency stay unchanged.

2.3 Reasons for changing stiffness and damping

In this study, it was decided to develop a tunable vibration isolator by means of changing the stiffness and damping of the isolator. At this stage it is necessary to

explain why the stiffness and damping of the isolator will be changed and what the effect of the changes will be.

Tuned vibration absorbers were developed for tonal (single frequency) excitation. For the isolator to perform optimal, the tonal excitation frequency and the isolation frequency of the isolator must coincide exactly. This is not as easy as it sounds even if the excitation frequency is constant. To design and build such a LIVE isolator where the practical and designed isolation frequency is exactly the same, is almost impossible. Therefore it is usually necessary in practice to be able to shift the isolation frequency after the isolator has been installed to tune the isolator to exactly the excitation frequency.

If such isolators are implemented on machines where the excitation frequency is not constant, the problem becomes even greater and that is the situation for which this isolator is designed. In practice, machines seldom operate at exactly the same frequency throughout their lifetime. Some machines can change over the years, but others can have constant change over minutes as operating conditions change. In such a case, it is necessary to be able to continuously change the isolation frequency of the isolator while in operation to achieve maximum isolation. Imagine what would happen if the excitation frequency decreases to the extent that it coincides with the natural frequency of the isolator! Therefore it is necessary to be able to change the isolation frequency of the isolator.

As stated in the previous chapter, the isolation frequency of a LIVE isolator can be changed in three ways:

- Change of the stiffness of the isolator
- Change of the port length of the isolator
- Change of the port diameter of the isolator.

The last two options have practical difficulties and have already been patented. Therefore it was decided to use the change of the isolator's stiffness to change the isolation frequency of the isolator. Another advantage of changing the stiffness rather

than the port length and port diameter, is the amount of isolation achieved. Changing the port diameter and length results in a change in the absorber's mass (the mass of the fluid in the port), which causes the amount of isolation achieved to change. The stiffness is the only parameter that will not change the absorber mass and that will result in a constant amount of isolation.

Figure 2. 7 shows how the transmissibility graphs change as the stiffness is changed.

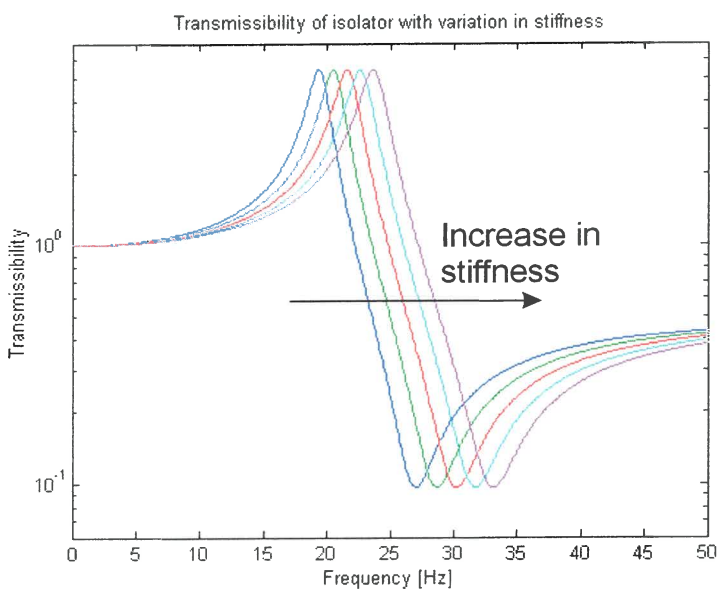

Figure 2. 7 Transmissibility of isolator with variation in stiffness

It can be seen how the isolation frequency increases as the stiffness is increased. The natural frequency also increases with the increase in stiffness. It is therefore clear that the change in stiffness enables the isolator to adapt to a change in excitation frequency.

The reason for changing the damping is that tonal excitation is not encountered in practice. Noise is always present on real machines and differs in amplitude and frequency. Usually a noise floor will be present: a constant amplitude noise over the whole frequency range.

When the transmissibility of a tuned vibration isolator is considered, it is noted that there is a region below the isolation frequency, where the vibrations are amplified and that maximum amplification occurs at the natural frequency. For pure tonal excitation the natural frequency will not have any influence, but the moment a noise floor is present, the noise at the natural frequency will be amplified. If the amplitude of the noise is very small, the effect will be very small, but as the noise levels increase, the amplification of the noise can have a significant influence. The factor that has to be considered is the ratio between the amplitude of excitation at the isolation frequency and at the natural frequency of the isolator. As this ratio decreases, a point will be reached where the noise at the natural frequency will be amplified more than the excitation frequency is decreased by the isolator. Therefore the result will be that one would have been better off without the isolator.

Increasing the damping in the isolator can reduce the response to noise at the natural frequency of the isolator. Figure 2. 8 show the effect of an increase in viscous damping on the transmissibility graph of the isolator.

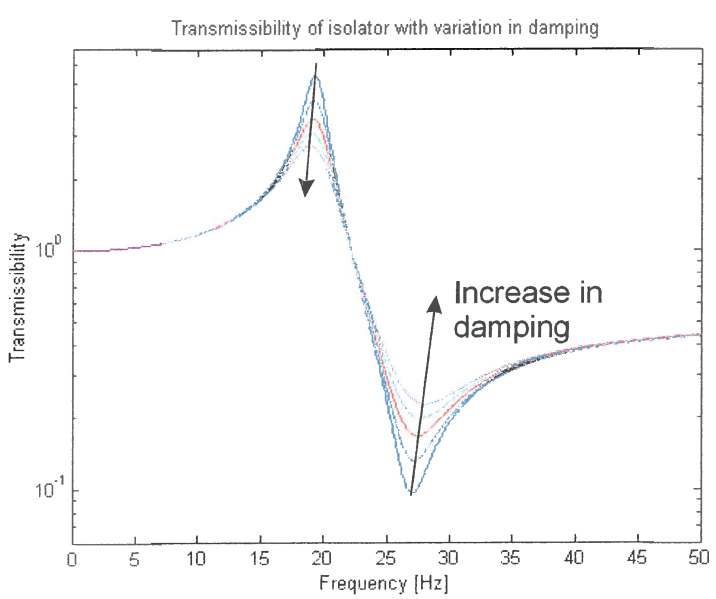

Figure 2. 8 Transmissibility of isolator with variation in damping

As the damping increases, the amplitude of the natural frequency decreases, but at the same time the amplitude at the isolation frequency also increases. For a certain level of noise, there will be an amount of damping that would give the least transmission of vibration over the whole frequency range that would not necessarily be the least damping. Therefore it is also necessary to be able to change the damping of the isolator to be able to obtain best isolation at all times under all excitation conditions.

2.4 Conclusion

In this chapter a one-degree of freedom model was formulated for the LIVE isolator. Equations for the undamped natural frequency and isolation frequency were derived as well as an equation for the transmissibility of the isolator that was also non-dimensionalised. The last equations derived were that of the damped natural frequency and isolation frequency. The last part of the chapter addressed the issue around the reasons for changing the stiffness and damping of the isolator. It was explained how the stiffness change the isolation frequency of the isolator and how the change in damping helps with control of noise amplification.

CHAPTER 3

Design of a variable stiffness spring

3.1 Introduction

In this chapter the design of the variable stiffness spring will be addressed. The design starts with the concept phase where some concepts will be addressed individually and followed by the detailed design of the selected concept.

The objective of this chapter is to design, build and test a variable stiffness spring with low damping and to use smart materials to obtain the stiffness change. The reason for the low damping is due to the fact that it is foreseen to change the damping of the isolator. To be able to give the isolator a reasonable damping change, it is necessary that the primary damping of the spring is not too high.

A usable variable stiffness spring would typically require a change in stiffness of at least 40% (the maximum stiffness must be 1.4 times the minimum stiffness), but a larger stiffness change is preferable. The structural damping constant of the spring must be lower than 0.15. A last factor that must be considered is the response time of the stiffness change. If it takes too long for the spring to change its stiffness, the spring would be impractical. Furthermore it is foreseen to implement an optimisation algorithm at the end to control the spring. A response time of minutes or hours would cause the optimisation to take too long to be of any practical value. Therefore a response time below 30 seconds was chosen as goal, but a faster response time - one less than 10 seconds would be preferable.

3.2 Concepts

Three concepts were investigated. In each case the concept was tested with an experiment to validate the theory. Each concept will be addressed separately.

3.2.1 Magnetorheological elastomer

Magnetorheological materials are materials that react to a magnetic field. These materials are relatively new and were patented in 1992 by the Lord Corporation (Carlson & Weiss, 1992) who are still about the only company specialising in these materials. The common form of this class of materials is magnetorheological fluid, which is commonly used in adaptive dampers (Dyke et al., 1996). The viscosity of a magnetorheological fluid changes in a magnetic field making this fluid ideal for adaptive dampers.

Magnetorheological elastomers are elastomeric materials which stiffness changes under the influence of a magnetic field. The Lord Corporation did the first development of a theoretical model of this material in 1996 (Jolly et al., 1996a; Jolly et al., 1996b) and was followed by the Ford Motor Company in 1999 (Ginder et al., 1999; Ginder et al., 2000) who developed a variable stiffness suspension bushing for their cars.

In its basic form, a magnetorheological elastomer is a normal elastomer like natural rubber or polyurethane that has a certain amount of magnetic iron particles in it. It was shown that a volume fraction of 0.27 yields the best results. These particles are mixed into the elastomer prior to curing. The elastomer is then cured in the presence of a magnetic field of 0.5 Tesla. This causes the iron particles to line up in chains inside the elastomer. During curing these particles is then locked into the elastomer matrix. When the cured elastomer is deformed, these particles move out of the chains. If this happens while the elastomer is in the presence of a magnetic field, the magnetic field restricts the particles from moving out of the chains and causes the modulus of the elastomer to increase. Jolly et al. achieved an increase of up to 39%. The damping of the elastomer also decreased as the modulus increased.

Complex theoretical models were developed that used the magnetic force between two adjacent particles to calculate modulus change. FEM models were also used to predict the modulus changes in the material.

Magnetorheological elastomers seemed to be a viable concept out of the literature study. The next step was to do an experimental test to investigate whether the effect could be reproduced. Polyurethane was used as the elastomer for the tests. Rubber has less damping than polyurethane and made it more suitable for the tests, but polyurethane is much easier to produce than natural rubber. If the tests with polyurethane were successful, the final spring could be made from rubber for lower damping.

The initial design of the spring was taken from the design of the suspension bushing developed by Ford Motor Company depicted in Figure 3. 1.

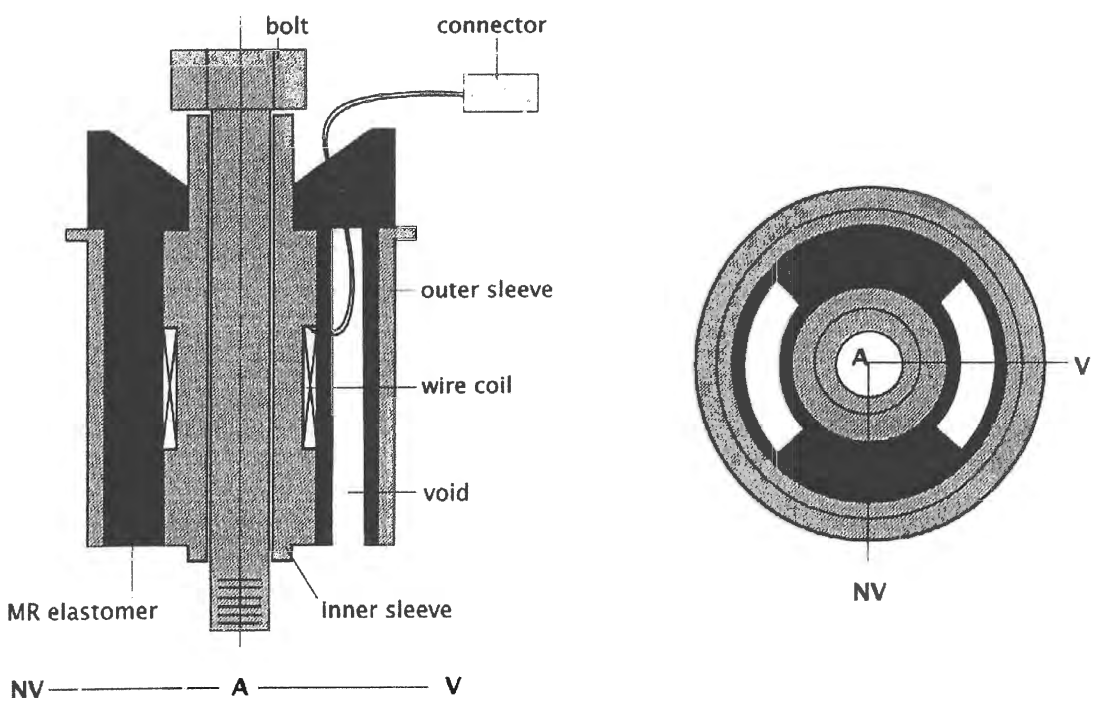

Figure 3. 1 Variable stiffness suspension bushing using MR elastomer (Ginder et al., 2000)

The bushing had an outside and inside metal sleeve to conduct the magnetic field and an electric coil around the inside sleeve to generate the magnetic field. A similar spring was designed, but on a larger scale due to the fact that a large spring was needed for the isolator and not a tiny spring like the bushing. The design is given in Figure 3. 2.

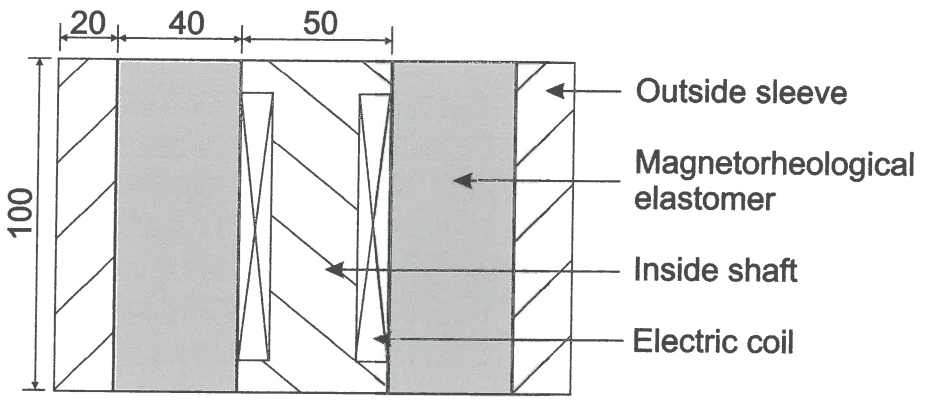

Figure 3. 2 **Design of MR elastomer spring**

The spring was manufactured and tested in a servo-hydraulic actuator by fixing the outside sleeve and moving the inside shaft axially at a constant frequency and amplitude. The experimental spring is depicted in Figure 3. 3.

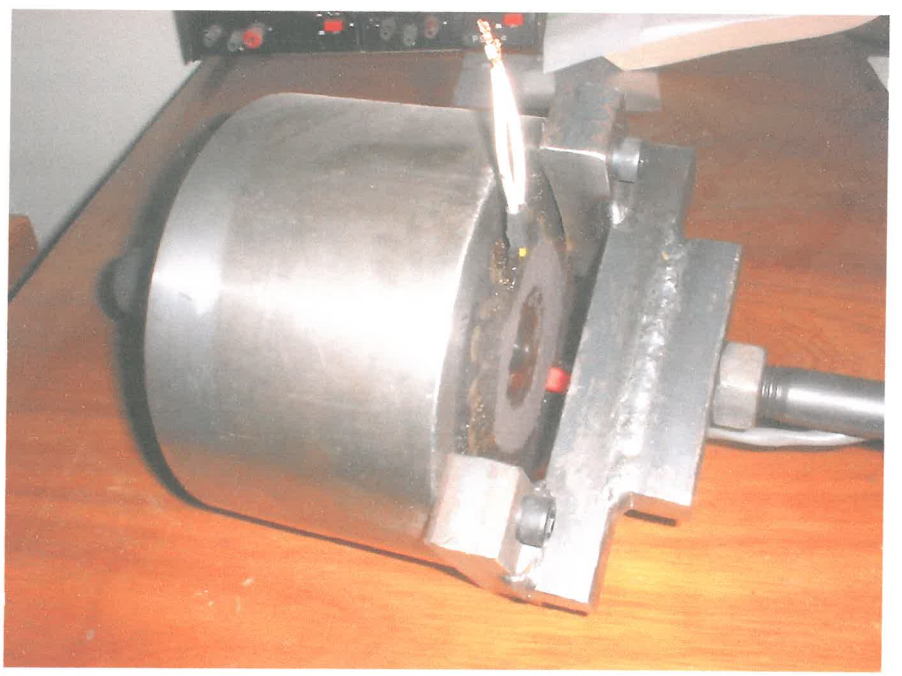

Figure 3. 3 **Experimental MR elastomer spring**

The results in Figure 3. 4 were obtained for an excitation frequency of 16 Hz and different currents through the coil.

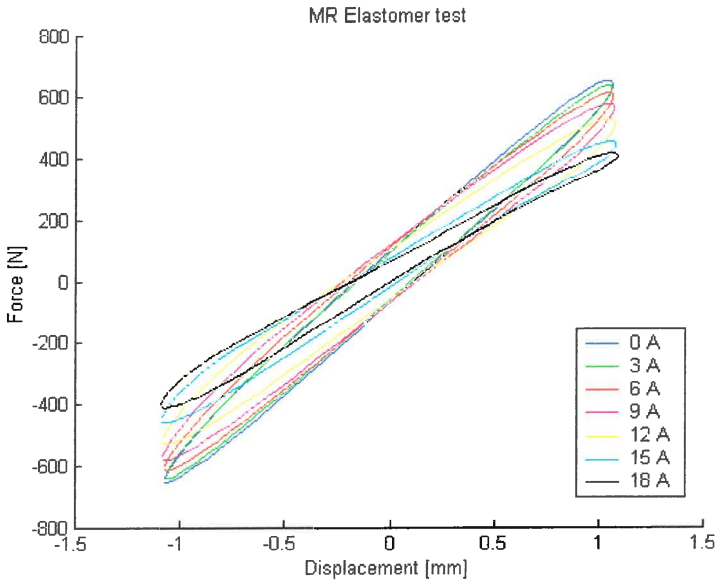

Figure 3. 4 **Hysteresis loops from MR elastomer spring for different currents**

The method used to determine the stiffness and damping from the experimental results can be seen in Appendix A. The corresponding stiffness and damping values are plotted in Figure 3. 5.

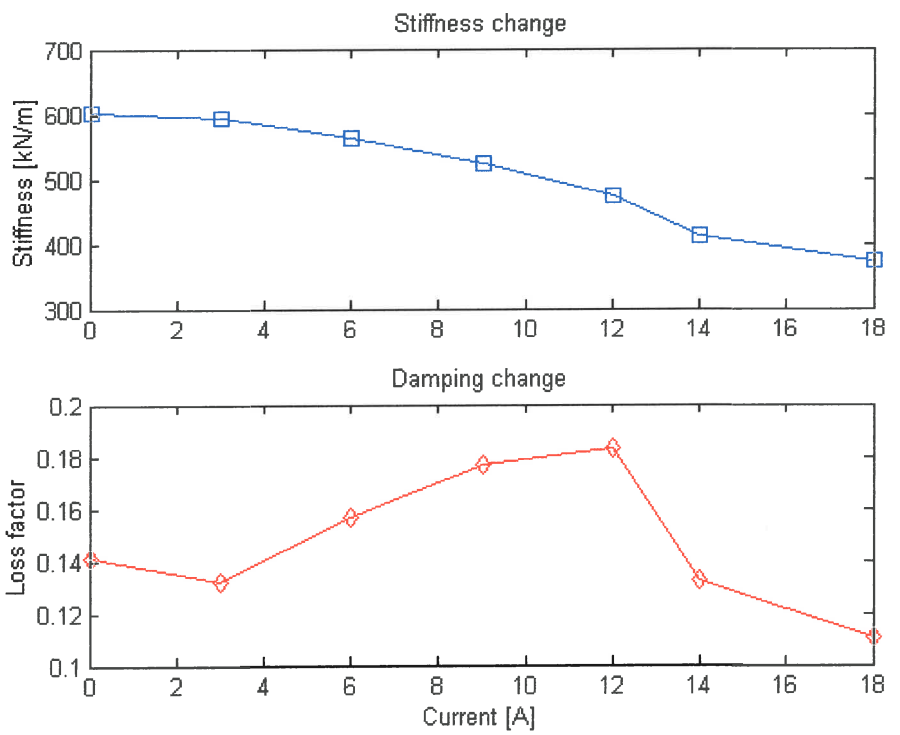

Figure 3. 5 **Stiffness and damping as function of current**

The resulting stiffness change was 60% and the damping was almost in the required range. One problem was that the stiffness of the elastomer decreased as the current or the magnetic field was increased. This is exactly the opposite of what was predicted from the literature study and theory. Another problem was that the polyurethane and the inside shaft did not bond properly and had some amount of slip. Although satisfied with the amount of stiffness change, the discrepancy with the theory resulted in a second test that included a few modifications.

The first modification was that grooves were made in the inside shaft so that the polyurethane will attach better to the shaft. Secondly a magnetic sensor was installed in the polyurethane to be able to measure the magnetic field inside the rubber. The last modification was that a significantly larger coil was inserted around the shaft to decrease the current that was needed for the tests.

The same test was done on the second spring, but the test was repeated directly after each other to test for consistency. The results are given in Figure 3. 6.

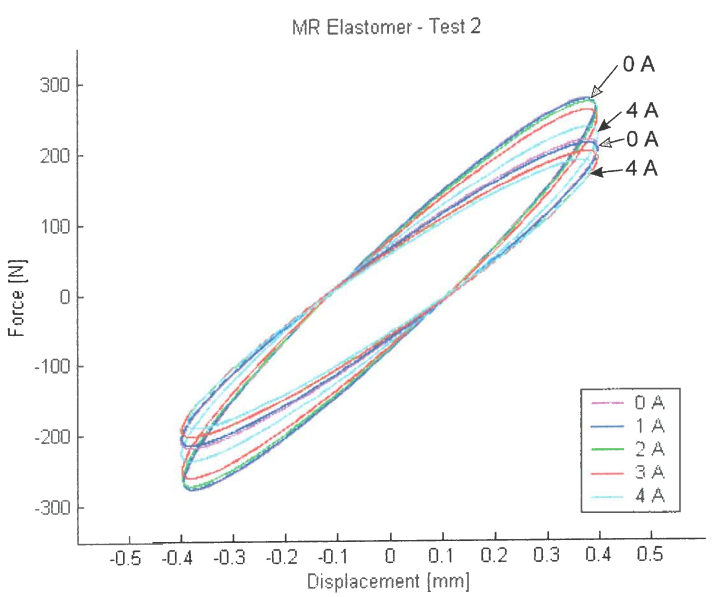

Figure 3. 6 Hysteresis loops for second experimental test

The stiffness again decreased as the current was increased as in the first test. An interesting observation was that when the test was repeated the second time, the

stiffness was lower than the first time. Even the stiffness of the 0A test was lower than the 4A test of the first run. It was concluded that the stiffness change was not due to the magnetorheological effect, but due to an increase in temperature of the polyurethane. Due to the large currents that were sent through the coil that was situated inside the polyurethane, the coil heated up and heated the polyurethane. That is the reason why the stiffness in the second test was lower than in the first test.

Further tests did not result in any indication of the magnetorheological stiffening of the spring. One main reason for this was the magnitude of the magnetic field. The magnetic sensor installed in the polyurethane indicated that the magnetic field in the polyurethane was not even 1% of the desired value. To be able to create a magnetic field of 0.5 – 1 Tesla in an elastomer, even in a very small specimen, without heating the elastomer will require an external magnetic source (electromagnet) or a very small and well-designed specimen. This concept was just not viable on the scale that was needed for this project.

3.2.2 Heating of elastomer

Although the results from the first concept did not show the magnetorheological effect, it showed that a reasonable stiffness change could be obtained by heating the polyurethane. Therefore a logical second concept was to investigate the heating of an elastomer as a variable stiffness spring.

The biggest problem foreseen with this concept was response time. To heat and especially cool a solid piece of polyurethane is not an easy task. Although forced convection is the obvious way to approach such a problem, it was not preferable in this case due to the complexity that comes with it. Natural convection was the first choice in this case and the design tried to increase the response time without using forced convection.

Basically the same design of the spring was used as in the magnetorheological elastomer. The changes made were an inside sleeve instead of the solid shaft and

much thinner steel parts to conduct heat faster. A soft polyurethane was used as the elastomer for this spring. A heating coil was moulded inside the polyurethane together with a thermocouple to be able to measure the temperature of the polyurethane. The design is depicted in Figure 3. 7.

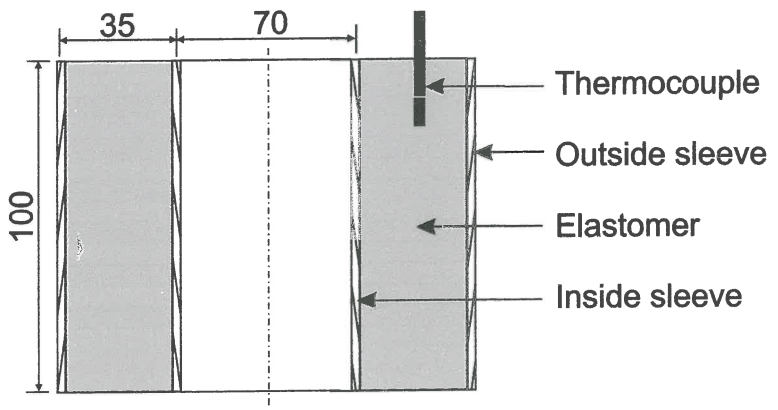

Figure 3. 7 **Design of elastomeric spring**

The temperature was controlled with a 0 – 200 °C temperature controller using a Pt 100 thermocouple. The response of the spring was measured at 5 °C intervals from 30 °C to 80 °C. The response was measured at different frequencies to be able to see the frequency effect to stiffness and damping. Figure 3. 8 show the results.

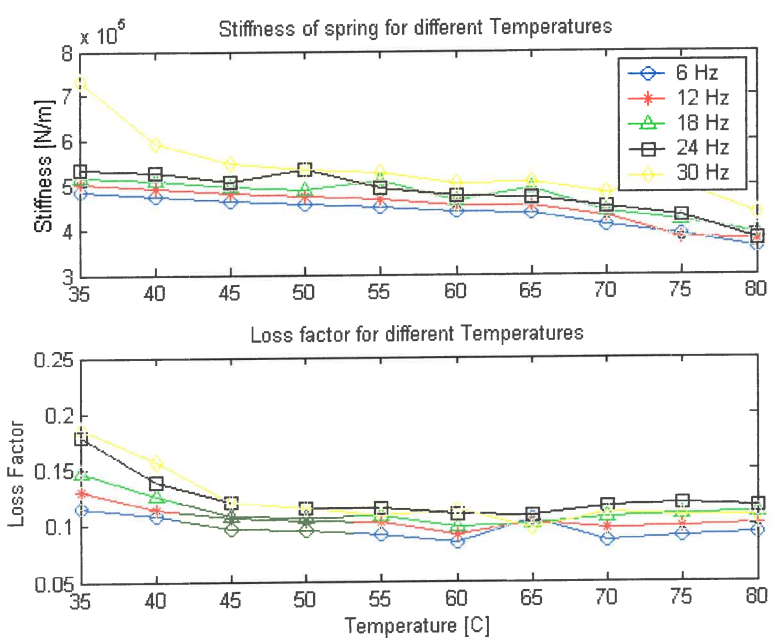

Figure 3. 8 **Stiffness and damping as a function of temperature**

The decrease in stiffness and damping with an increase in temperature can clearly be seen. The discrepancies in the linearity of the graphs were due to a faulty servo-hydraulic controller and should not be taken into account. Overall the graphs indicate a quite linear decrease in stiffness with an increase in temperature. Furthermore it can be seen that the higher frequencies resulted in higher stiffness and damping.

Although the damping was in an acceptable range, the stiffness change of 34 % was not quite sufficient for the application. Furthermore, the response time was definitely too long to even be considered as an option. This concept was discarded due to these reasons.

3.2.3 Compound leaf spring

The third concept originated out of a publication (Walsh & Lamancusa, 1992) that claimed to have achieved a stiffness change of 6200% (62 times) of which 4500% (45 times) was linear with respect to the separation of the leaf springs. Walsh & Lamancusa used very thin leaf springs to get a very low minimum stiffness that is probably the reason for the impressive figures. This result has been regarded by other authors (Brennan, 2000) as impractical and not possible to implement on a practical problem. It is possibly the case, but it shows that the concept has quite a lot of potential. Even if only 10% of the reported stiffness change can be achieved, it will still be a very significant stiffness change in the application of a LIVE isolator. Another very attractive property of this concept is the fact that steel springs are used instead of elastomeric springs that were the case in the previous two concepts. Steel springs are known to have a very low loss factor and therefore it would be possible to decrease the damping of the spring significantly.

The first test was a basic experiment with two straight leaf springs separated with a lead screw. The experiment is depicted in Figure 3. 9.

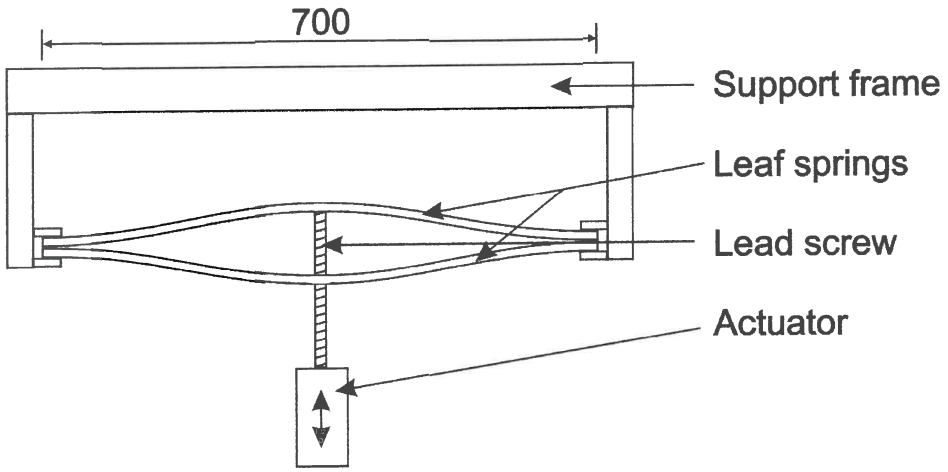

Figure 3. 9 Compound leaf spring design

This was a quite big spring and not suitable for implementation on an isolator. This test was therefore only a preliminary test to validate the concept and to see what stiffness change is practically possible for this concept.

The results are given in Figure 3. 10.

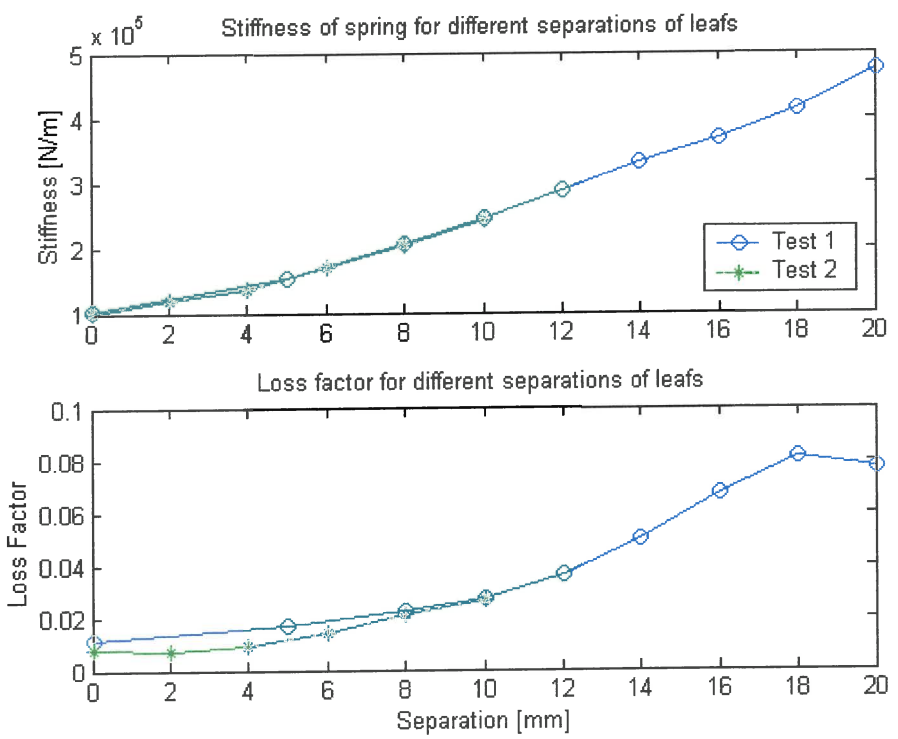

Figure 3. 10 Stiffness and damping as a function of separation

Two prominent features of the results are the reasonable stiffness change (4.5 times) and the very low damping of the spring. Both these two observations were expected beforehand and therefore the test was successful in proving the concept and giving some estimated figures regarding stiffness change and loss factor. From the graphs it can be seen that two test runs were performed and that the result were basically the same. This proves the repeatability of the tests.

Finite element modelling provides a method of analysing structures without setting up an experimental test. Therefore it would be ideal to have an accurate finite element model of the springs to be able to calculate the stiffness for different designs and configurations. A FEM model was built of one of the springs that were used in the test to compare with the experimental results.

The finite element package from MSC software was used and included MSC Patran and MSC Marc, a pre-processor and a non-linear solver. The leaf spring was meshed with brick elements and deformed in the way the spring deformed during the test by clamping the ends of the spring and displacing the centre. The reaction forces were extracted and the stiffness calculated at different displacements.

Two simulations were done. The first modelled the ends to be clamped in all directions except in the x direction (horizontally in-line with the spring). The second simulation modelled the ends clamped in all directions. The reason for this is that the boundary condition will have a significant influence on the stiffness and that in the practical test, the ends were not completely fixed and not completely free, so it was suspected to be somewhere in between. The results are given in Figure 3. 11.

The method of obtaining separation force from the force on a single spring is described in Appendix B.

As expected the experimental results were between the results from the two simulations. One interesting observation is the amount of difference in stiffness change between the clamped and free simulations. This is important to understand for future design of such springs and need to be explained.

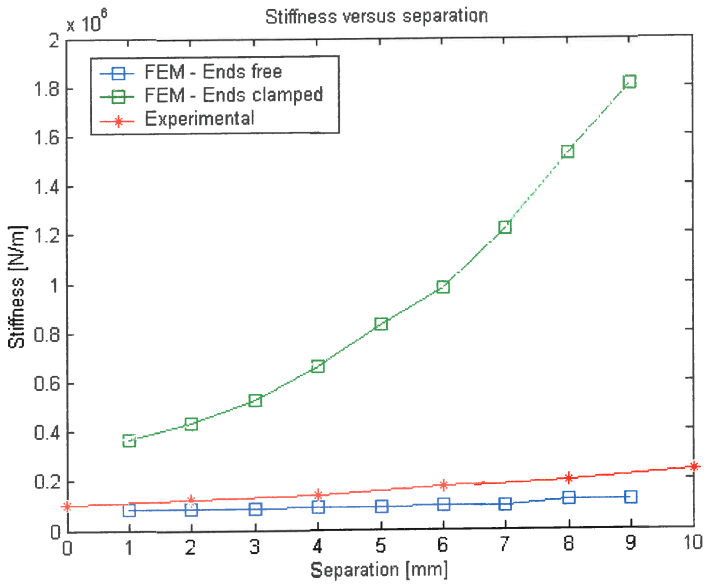

Figure 3. 11 Comparison between stiffness calculated by FEM and measured

The reason why the stiffness of the compound spring changes is because the separate springs are non-linear. Linear springs will not have an increase in stiffness as the displacement increases. Therefore the more non-linear the springs are, the more the stiffness change will be. The following two mechanisms are responsible for the non-linearity of the springs:

- Change in geometry
- Elongation of springs

The change in geometry is the most obvious. As the two leafs are separated, the change in geometry cause the spring to stiffen. It can be compared to an increase in the second moment of area of a beam. If the height of the beam is increased, the second moment of area and therefore the stiffness of the beam increases. The boundary condition will also not have a significant influence on this mechanism. The second mechanism can be explained with Figure 3. 12.

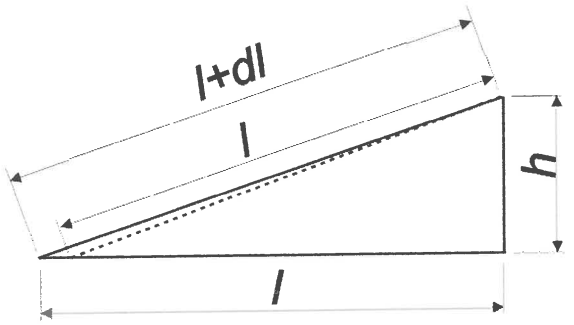

Figure 3. 12 Explanation of elongation of spring

If the centre of the spring is displaced upwards by *h*, one of the following two situations can occur:

- If the ends are free to move horizontally, the spring will deform as indicated by the dotted line. The centre of the spring will move upwards and the ends will move towards the centre. This cause the spring itself to keep a constant length and only bending of the spring is needed and no elongation.
- If the ends are clamped, the springs will have to stretch to be able to be displaced at the centre as illustrated by the solid line in the sketch. The tension generated in the springs is the same as tightening a guitar string. This causes the spring to be a lot stiffer and more non-linear. This mechanism is the main reason for the difference in stiffness of the two simulations and is an important aspect of these types of springs. To be able to get a significant stiffness change, the boundary conditions of the experimental spring must be as close to clamped as possible.

As said previously, the springs are non-linear with respect to the deflection of the spring. If two springs are combined in a spring assembly to form a variable stiffness spring, this spring can however be assumed to be linear around its neutral position if the spring is displaced by a small amount. That is the reason why a linear spring model can be used for such a spring although it consists of non-linear springs.

One last aspect of the FEM simulation that was investigated was the effect of the number of elements used in the model. In any FEM model, the question of "How many elements are enough?" will probably be asked at some stage. With modern

computers and software, it is really not more difficult or more time consuming to mesh a model with 10 or 10 million elements. The problem comes in at the solving of the model. The more elements the model has, the larger the matrices become and the longer the calculations take. It is not uncommon at all these days to have models that can take up to a few days to solve.

The problem is that only up to a certain point will more elements give you a more accurate answer. The accuracy of the results converges quite quickly to the actual answer with an increase in elements after which a further increase in elements will only increase the processing time dramatically and will not yield a significantly better answer.

Therefore the simulation of the leaf spring was run for different number of elements and the results combined in Figure 3. 13.

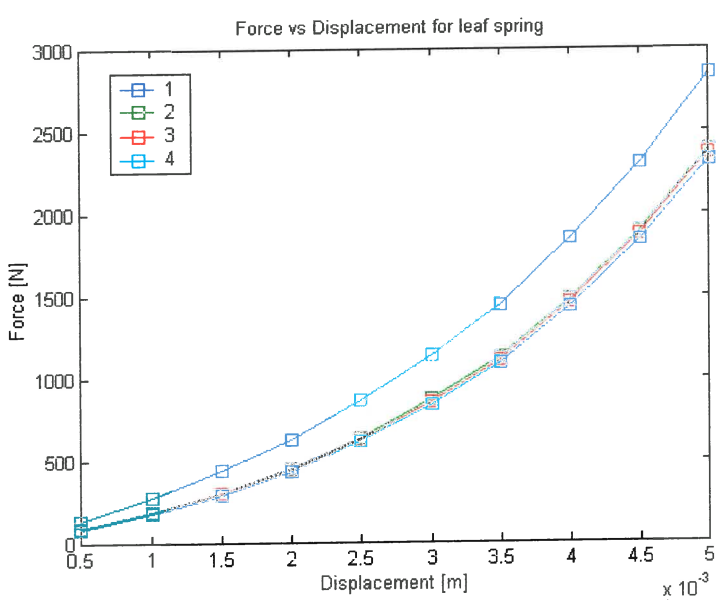

Figure 3. 13 Comparison between different number of elements in FEM model

The first test entailed the least number of elements and the fourth test the most. It can be seen that in the first test too few elements were used and that the results are not accurate (stiffness was over predicted). From the second test onwards, the results are

more accurate every time, but by such small a margin that it is not worth the extra processing time for that small amount of extra accuracy (test 2 took about 2 minutes of processing time and test 4 about 16 hours).

Out of this preliminary work the following conclusions could be made:

- The concept works and a significant stiffness change can be achieved with relatively low damping.
- Future designs need a way to practically clamp the ends of the springs for maximum stiffness change and to be able to compare it to the FEM model.
- The spring needs to be smaller and more compact to be used in an isolator.

This concept was chosen out of the three that were investigated and with these considerations the design process could progress into the final design of the spring.

3.3 Design of spring

3.3.1 Design concepts

The spring that needed to be designed must have the following properties as seen from the previous section:

- It must be smaller and more compact to be to implemented practically
- The ends of the spring must be as close to clamped as possible
- The design must produce repeatable test results.

The current design of two long straight leaf springs was not very well suited to be implemented in an isolator and has major problems as far as the clamping of the ends is concerned due to the fact that a very thick and stiff structure would be needed to achieve clamping. Therefore an entirely new design was needed.

LIVE isolators are usually circular in section and therefore a circular spring would probably be a suitable design to go with the isolator. For a circular spring, an inside

and outside ring will be needed that would move axially with respect to each other with elements between them that will deform and supply the stiffness. Figure 3. 14 show the simplest form of the design.

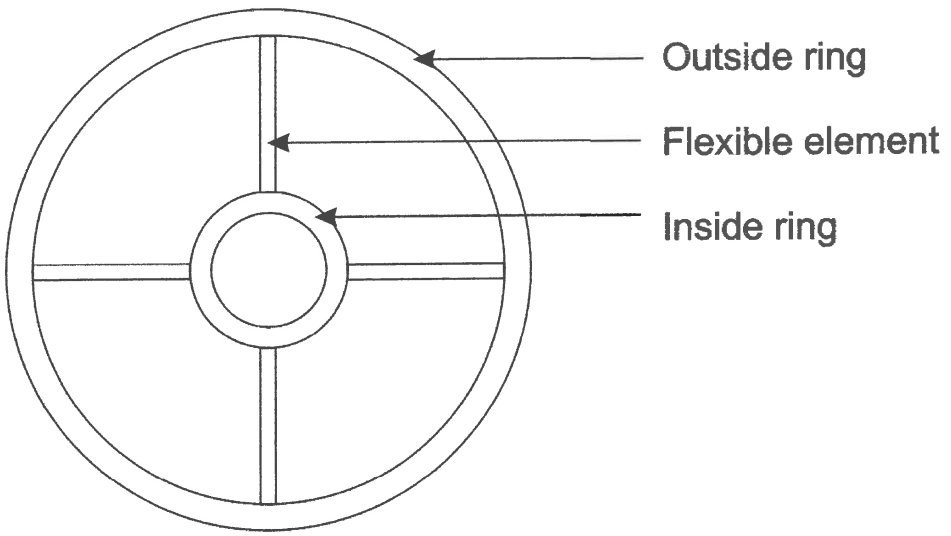

Figure 3. 14 Basic design of circular spring

Apart from the fact that the circular design will be nicely incorporated with the isolator, it has a few other advantages:

- It has a high lateral stability in all directions. This is important for an isolator.
- The outside ring already gives a clamped effect for the flexible elements due to the fact that a circle is a very strong shape. Furthermore, it will be possible to clamp the ring itself to produce a solid base that will result in a nearly perfectly clamped spring.

This design basically satisfies all the requirements. Within this design, the flexible elements can still be changed to suit the stiffness requirements needed. The simplest way to insert the flexible elements is to make the entire spring out of one piece from a thin spring steel sheet. This may sound impossible to manufacture, but with modern laser cutting techniques, it is actually much easier to manufacture in this way than by any other method.

To determine a suitable design, four designs were made and evaluated against each other with the FEM package. The four designs are depicted in Figure 3. 15.

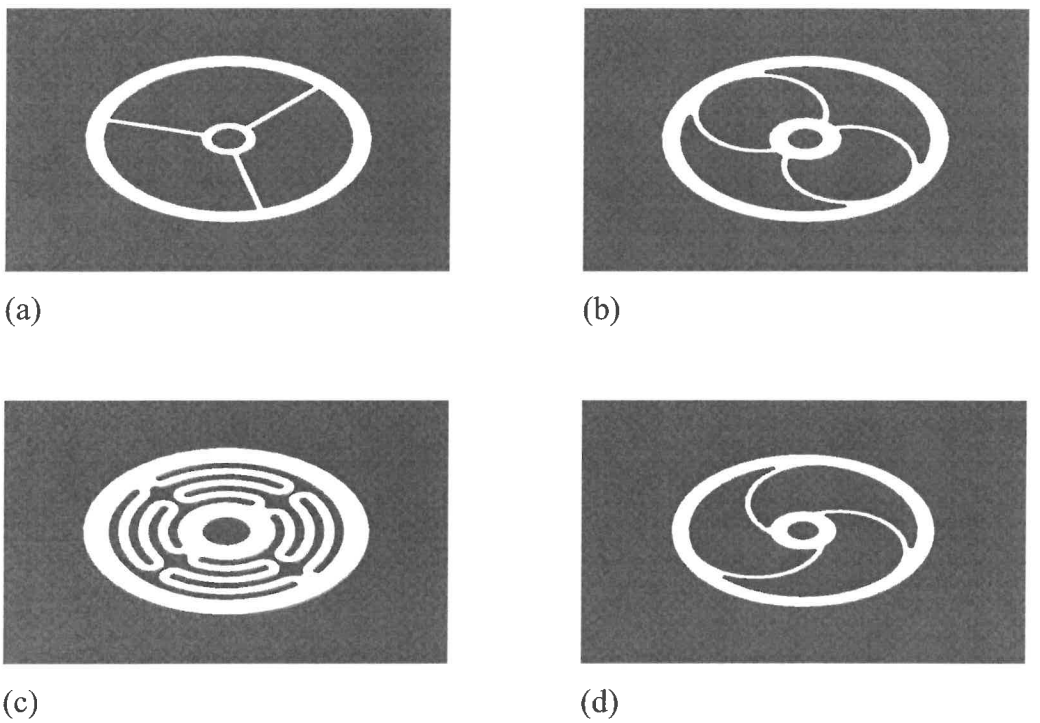

Figure 3. 15 Four designs of circular springs

The first design is the normal design with straight spokes. In the other three designs it was tried to obtain a less stiff spring but without increasing the size of the spring. All of these designs were simulated with MSC Patran and MSC Marc and the result compared to each other as shown in Figure 3. 16.

Out of the result it can be seen that the first design with the straight spokes yielded the best increase in stiffness. This is again due to the fact that the spokes have to stretch for the inside to move upwards, where the spokes in the other designs are able to bend or twist and do not have to stretch. It is noticeable that the third design did not yield the lowest stiffness. That however is due to the thicker spokes of the design compared to the last design that yielded the lowest stiffness. The first design was chosen due to the largest stiffness change. Although a less stiff spring is preferable in an isolator, the percentage stiffness change is the primary criteria for the application.

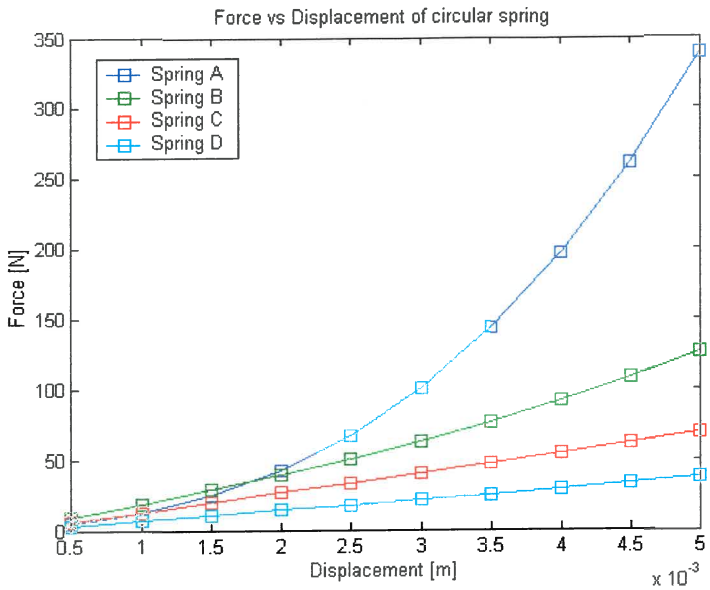

Figure 3. 16 **Stiffness of the four circular springs**

3.3.2 Final design

Three spokes were chosen in the first design, because it gave to lowest stiffness while still retaining stability and lateral stiffness in all directions that would not be the case with 2 spokes. To obtain the final design, many simulations were done with the FEM model to try and minimise the stresses in the spring while obtaining favourable stiffness values. The dimensions were kept as small as possible to keep the design compact. The design is depicted in Figure 3. 17.

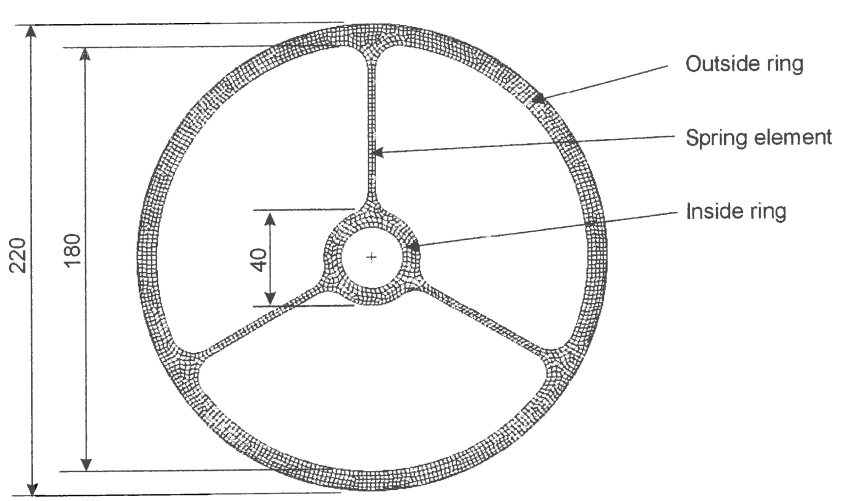

Figure 3. 17 **Mesh of circular spring**

In the FEM model the spring was meshed with about 4000 brick elements. The outside was clamped and the inside displaced 5mm upwards. 10 steps were used in the output so that data for every 0.5mm displacement were obtained. The displaced structure at 5mm displacement with corresponding stresses is given in Figure 3. 18.

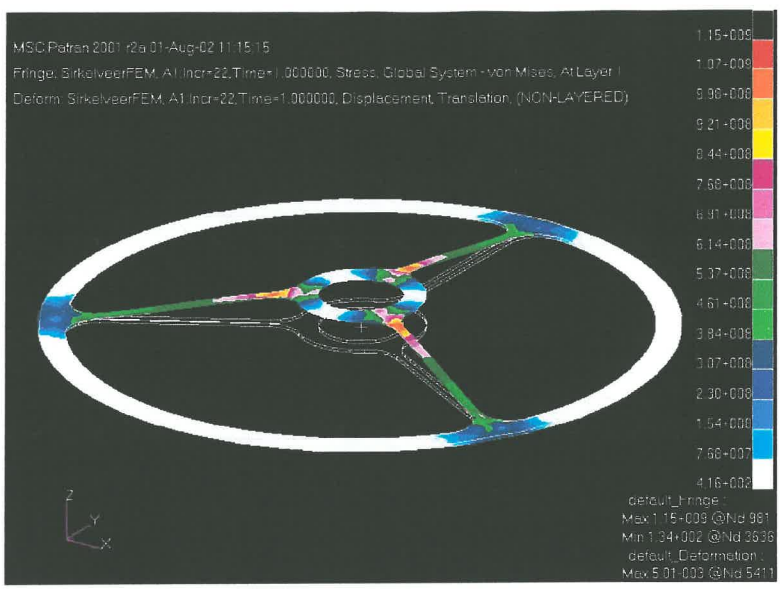

Figure 3. 18 Stresses in circular spring at 5mm displacement

The nodal forces and displacements were extracted from the results for all 10 steps. The vertical nodal reaction forces for the inside ring were added together to obtain a single force needed to displace the spring. From this the force vs. displacement graph in Figure 3. 19 was plotted.

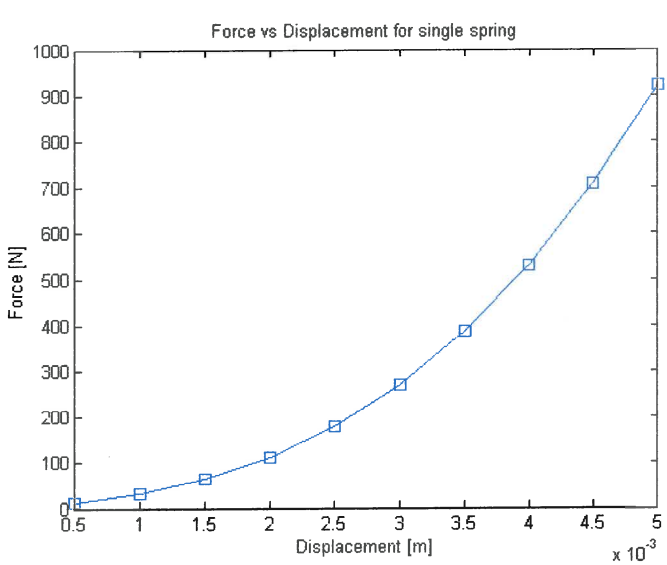

Figure 3. 19 FEM analysis results

3.3.3 Validation of FEM model

It is good practise to validate FEM results with an experimental test. For this purpose the designed spring was manufactured from hardened spring steel (EN42D). Laser cutting was used to manufacture the complex geometry of the spring. A frame was manufactured to clamp the spring on the outside and to mount the spring in order to do the test. A load cell was used to measure the applied force and a strain gauge displacement transducer was used to measure the displacement of the centre of the spring. The setup is depicted Figure 3. 20.

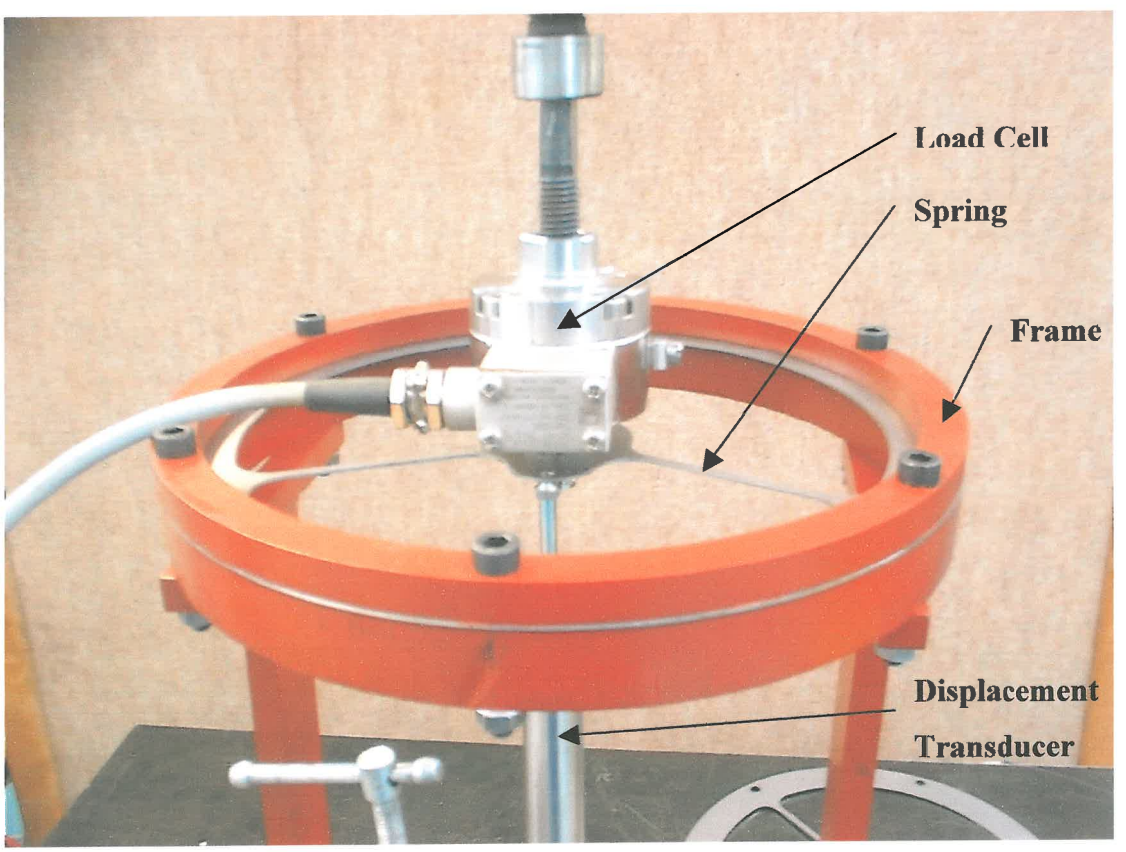

Figure 3. 20 Experimental setup

The spring was displaced 5mm and the displacement and force recorded every 0.5mm. After the first test it was seen that the spring slipped within the frame with

displacements larger than 4mm. That caused the change in gradient of the graph. The test was repeated with the spring tightened better, but the slipping occurred again.

The results from the FEM analysis and the practical test were compared to each other by plotting them on the same graph in Figure 3. 21.

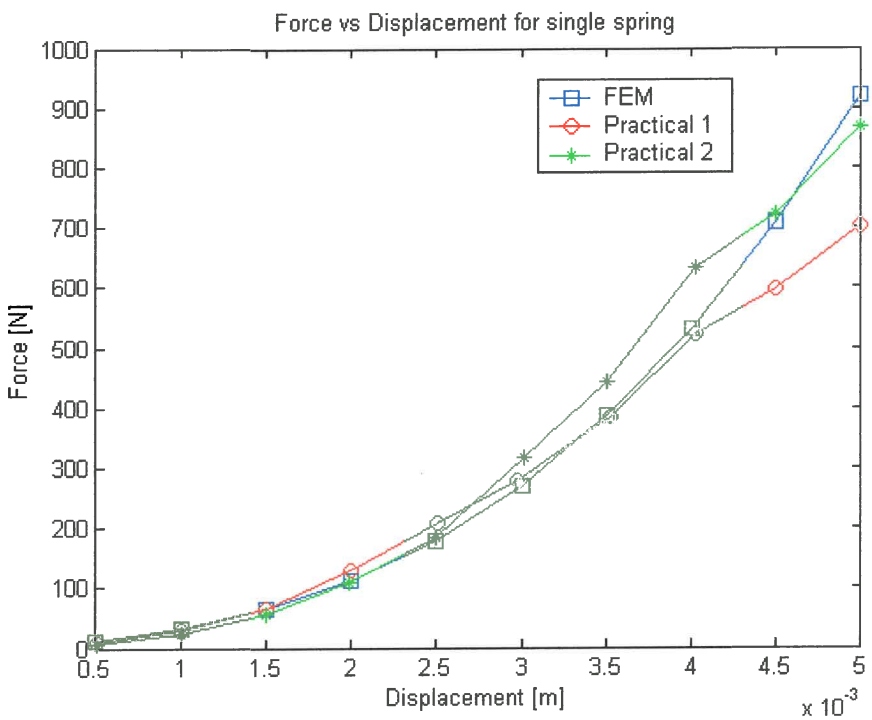

Figure 3. 21 Comparison between FEM and experimental results

It can be seen that there is a very good correlation between FEM and the experimental results with displacements up to 4mm. The slipping of the spring caused the difference above 4mm displacement and could be eliminated by better fixing the spring to the frame.

The spring has been designed, manufactured and compared to the FEM model. The last part of the spring assembly that has still not been addressed is the separation mechanism that will separate the two springs and control the stiffness of the spring. This will be addressed in the following section.

3.3.4 Separation mechanism

As stated in chapter one, it is preferable to use smart materials to accomplish the variation in stiffness of the variable stiffness spring. The current design consists of steel springs and do not comply with this aim. Therefore the separation mechanism will be the area where smart materials will be implemented. The separation mechanism must have the following properties:

- Must have a displacement of up to 10 mm.
- Must be able to deliver a force of up to 900 N at 10mm displacement (Figure 3. 21).
- Must be a simple mechanism with as few moving parts as possible. A solid-state type of actuator is preferable.
- The response time must be below 30 seconds and even less if possible.

These properties are guidelines for the optimal performance of the spring. It is therefore possible to use a mechanism that does not comply with all of the properties, but it will result in a spring with probably less stiffness change than possible.

3.3.4.1 Actuators

To minimise the moving parts in the separation mechanism, the actuator must preferably act directly upon the springs without an amplification device. The two major problems regarding smart actuators and the specifications are the displacement and force. The two most common smart actuators namely piezoelectric actuators and shape memory alloy actuators will not be able to produce displacements and forces of the required magnitude. Piezoelectric actuators have minute displacements (a few microns), but do have quite a large force. The problem is that the amount of displacement amplification needed will decrease the force to probably far below 1 N. Shape memory alloys on the other hand can in some cases give 10 mm displacement by means of bending, but result in very small forces. The amount of actuators needed to produce 900 N will just not be practical.

Other smart actuators that may possibly work are bi-metal strips and wax actuators. Bi-metal strips will probably have the same problem as shape memory alloys due the bending mechanism it uses. Wax actuators are a range of very compact actuators with quite a large force and displacement and were therefore well suited for the application.

3.3.4.2 Wax actuators

Wax actuators are not commonly sold commercially as actuators and the only company that could be found that do specialise in these types of actuators is Starsys. They manufacture these actuators (they call them paraffin actuators) for space applications and have a whole range offering different stroke length, force and accuracy.

Maximum values are 1.25 inches (32 mm) stroke, 500 lbf (2224 N) force and 0.3 micron accuracy. All of these figures can obviously not be obtained simultaneously, but gives an indication of the capabilities of these actuators. The 0.3 micron accuracy is obtained with a closed loop displacement control system. It is possible for them to design an actuator for a specific application regarding temperature range, force, stroke, internal spring and heating element. A quotation from them revealed that such a custom made actuator would be very expensive. One problem with the actuators is the response time, which is given in the region of 200 seconds. This will be a problem, but it will probably be possible to improve this with better heating and cooling.

A much more common and less expensive form of wax actuators is found in the thermostats of cars. The wax actuator in the thermostat is heated by the car's cooling water through forced convection. When the temperature of the water rises above a certain temperature, the wax actuator extends to open a valve that lets the water flow through the radiator. These thermostats can be obtained from any motor spares outlet for about R40. In the thermostat assembly there is usually a wax actuator, a spring to enable the actuator to retract and a housing to fit the thermostat to the vehicle.

Figure 3. 22 Thermostat and wax actuator

Taking the wax actuator out of the housing revealed a very small and compact actuator depicted in Figure 3. 22. The actuator consists of a copper cup filled with wax, a steel shaft and a rubber seal to prevent the wax inside the actuator from leaking (Figure 3. 23). The actuator works with a basic hydraulic principle in the sense that when the wax is heated, it changes from a solid to a liquid resulting in a volume increase or a pressure increase inside the copper cup. If the shaft is free to move, the shaft will extend. If the shaft is clamped, the pressure will rise inside the actuator and will increase the force on the shaft. Therefore it is important to note that the displacement of the actuator is dependant not only on the temperature, but also on the force produced on the shaft.

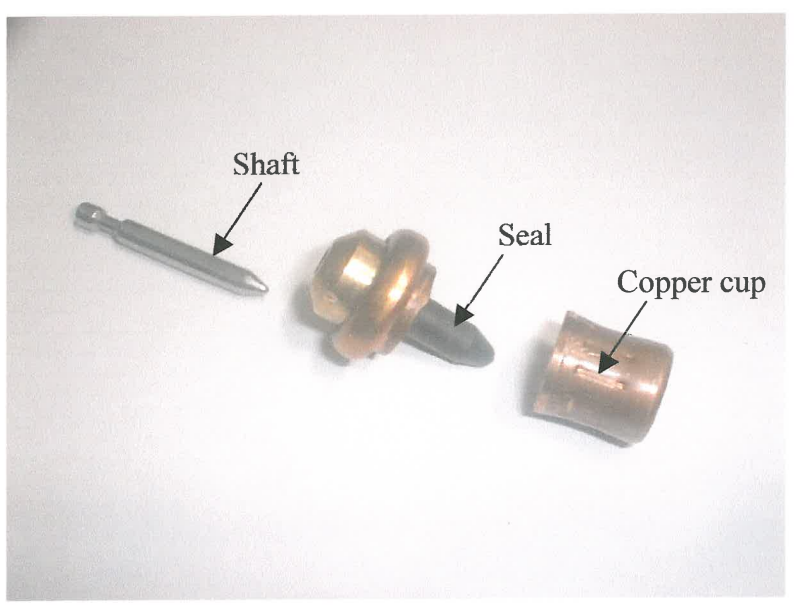

Figure 3. 23 Parts of a wax actuator

A study has been made on the heat transfer of such an actuator (Ogontz, 1998). It uses the normal heat flow equations to model such an actuator. The company, Ogontz, which sell valves actuated by wax actuators, indicates that these actuators have some level of hysteresis between heating and cooling. They indicated this with the graph in Figure 3. 24.

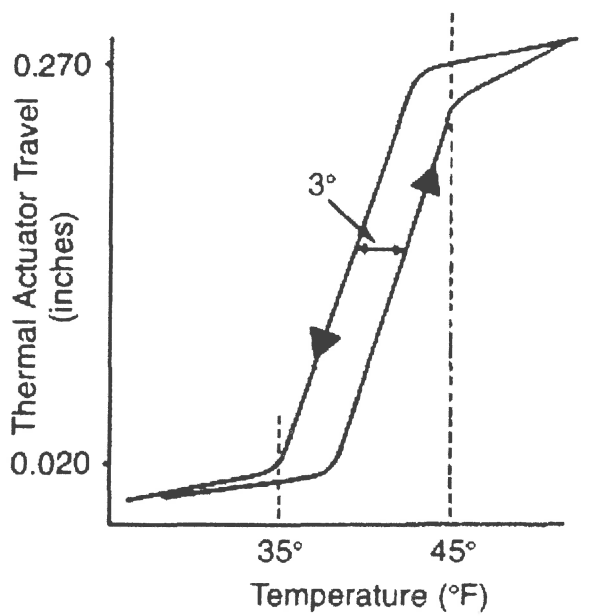

Figure 3. 24 Hysteresis loop of a wax actuator (Ogontz, 1998)

Note the low temperatures and small temperature range over which the actuator operates. This is another indication of the flexibility of these actuators.

The availability of the thermostats made it practically possible to use wax actuators and together with the excellent force and displacement characteristics, it was chosen as the actuators to be used. Because no information about the actuators themselves was available, it was necessary to characterise the actuator and determine its force and displacement characteristics.

The first test was to determine the maximum force and displacement of the actuator. For the maximum displacement, a dial gauge was used to measure the displacement while the actuator was heated. The experiment is depicted in Figure 3. 25.

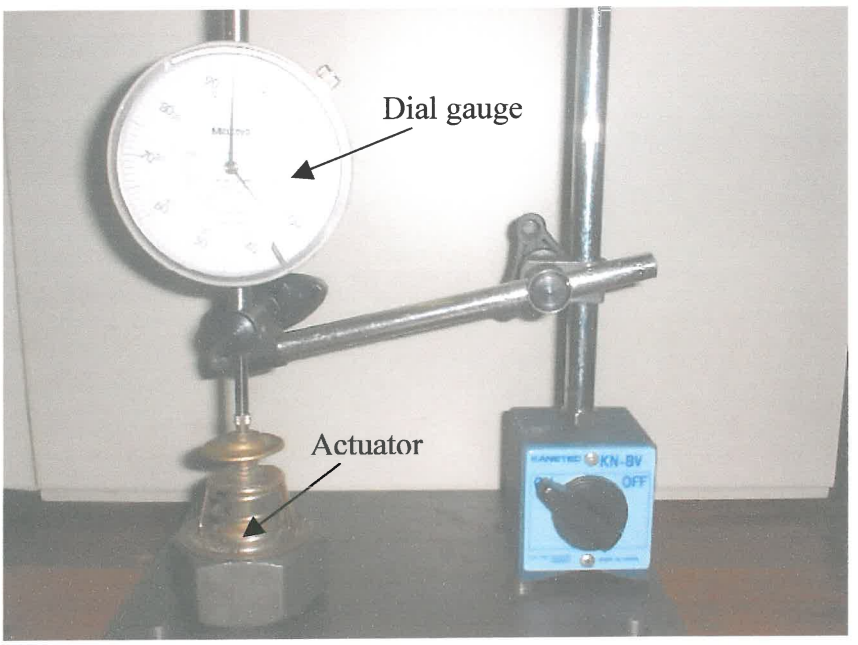

Figure 3. 25 Measurement of maximum displacement of wax actuator

The actuator was heated with hot air until it was extended to its maximum and the displacement documented. To measure the force of the actuator, the actuator was clamped with a load cell. Because of the hydraulic effect of the actuator, it was suspected that the maximum force would be dependant on the position of the actuator, so the maximum force was measured for different positions of the actuator. The force measurement experiment is depicted in Figure 3. 26.

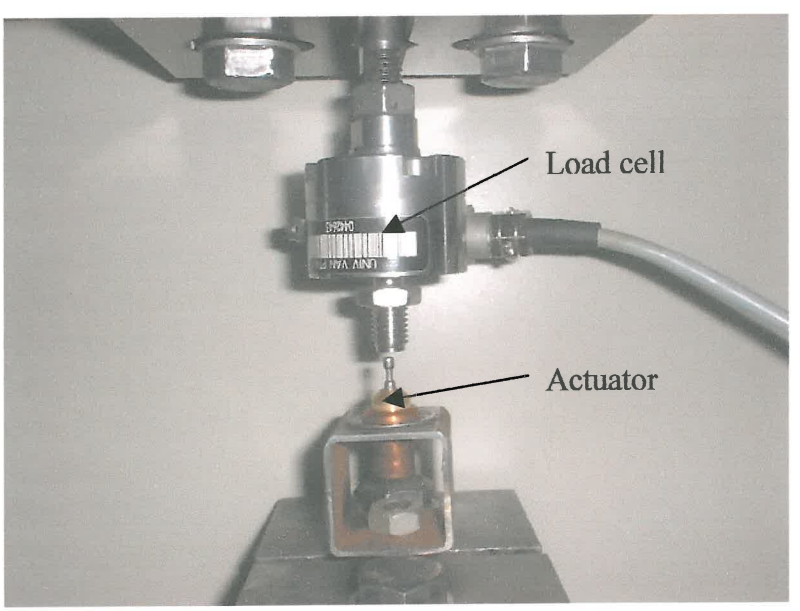

Figure 3. 26 Measurement of maximum force of wax actuator

The following results were obtained:

Table 3. 1 Maximum force of wax actuator

Displacement	Force [N]
0 mm	500 N
5 mm	430 N
10 mm	370 N

The last readings were at maximum displacement determined in previous tests. Further displacement caused the shaft end to be pushed out of the actuator. Considering that the shaft is a mere 3.8 mm in diameter, the pressure inside the copper cup must be 44 MPa and even higher in the walls of the cup for a force of 500 N on the shaft. The temperature of the actuator was also measured with a thermocouple to get an idea of the temperature range of these actuators. The actuator started to open at about 85 °C and the maximum force was obtained at about 170 °C. Therefore the temperature range of these actuators is quite large and it would probably be quite easy to control them.

The force values of the actuator are not enough to separate the springs 10 mm. As stated before, this will result in less stiffness change than ultimately possible, but because we do not want to use an amplification device, this actuator was accepted. It is actually possible to determine the amount that this actuator will separate the springs, by plotting the force vs displacement graphs of the actuator and the springs on the same graph as shown in Figure 3. 27. The displacement axis of the springs graph must only be scaled to display separation distance between the springs and not the displacement of the one spring.

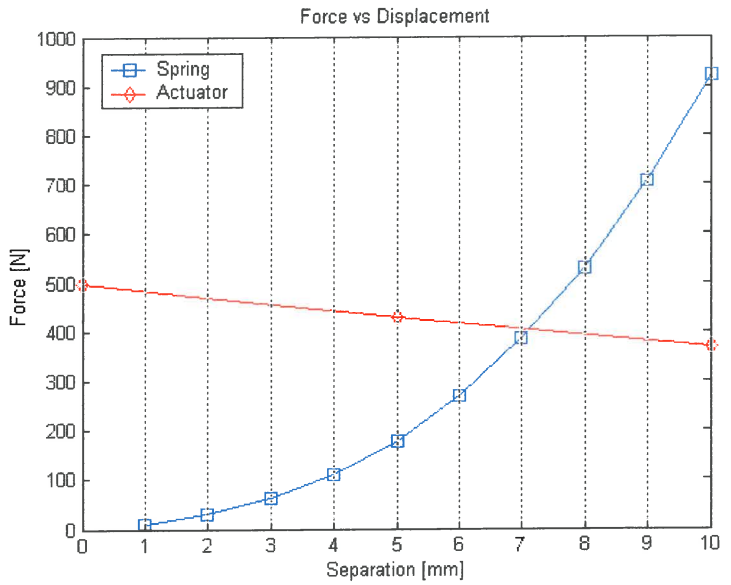

Figure 3. 27 Comparison between spring and actuator force

It can be seen that the actuator would be able to separate the springs about 7.2 mm. This will not result in the maximum possible stiffness change, but will be sufficient for the application in a LIVE isolator.

3.3.4.3 Heating mechanism

The wax actuator is controlled by controlling the temperature of the wax and through it the amount of phase transition in the wax from solid to liquid. Because the wax must be heated, it will be the best to insert a heating coil inside the wax, but that would require the manufacturing of an actuator, which was not part of this project. As far as external heaters are concerned, there are firstly normal heat conducting elements that consist of a heating element attached to the outside of the copper cup and the heat is conducted through the copper to the wax. Secondly, there are forced convection heaters that will make use of a hot fluid or gas that flows around the actuator to heat it.

The conduction is usually slower than forced convection, but the problem with forced convection is that a large volume of fluid or gas has to be heated that will result in a lot of losses. Reaction time is important, so forced convection will be used for

heating the actuator. To use water as medium to transmit the heat will slow the process down due to the large thermal capacitance of water. Air is a much better medium to use because it can be heated and cooled down more quickly than water.

The air must be heated well above 170 °C to be able to quickly heat the actuator to the maximum desired temperature. The easiest way to produce very hot air is with a hot air gun that can be bought commercially in a hardware store. A Bosch PHG 2 Hot air gun (Figure 3. 28) was used that was rated at 1.5 kW and that can produce air of up to 500 °C. The cover of the gun was removed and only the core-heating module used together with its integrated DC motor fan.

Figure 3. 28 Hot air gun

The wax actuator was mounted in the hole where the hot air exits, to form a closed controllable environment for the heating of the actuator. The fan was powered with 20V DC Power Supply, to supply the airflow necessary to heat or cool the actuator.

To be able to control the temperature of the actuator, the power dissipation of the heating coil in the hot air gun needs to be linearly controllable from zero to maximum power. This presented a challenge due to the large currents and voltages needed to drive the coil. The current of the coil can be calculated as follow:

$$I = \frac{P}{V} = \frac{1500W}{220V} = 6.818A \tag{3.1}$$

Therefore a controller is needed that can be controlled with a 0-10V DC signal from a computer and that can deliver about 7 A at 220 V or as close as possible to it. The controller can be AC or DC due to the fact that a coil is driven and that the type of current doesn't matter.

The first concept that was investigated was an AC drive that used pulse width modulation to control the power of the AC signal. The principle work as follows:

The basic idea is to control the part of the sine wave that is transmitted. A triac (switch) is used to switch the sine wave off after a certain time on every half cycle. Therefore only part of every half cycle will be transmitted and less power will be given. Figure 3. 29 show the concept in graphical form.

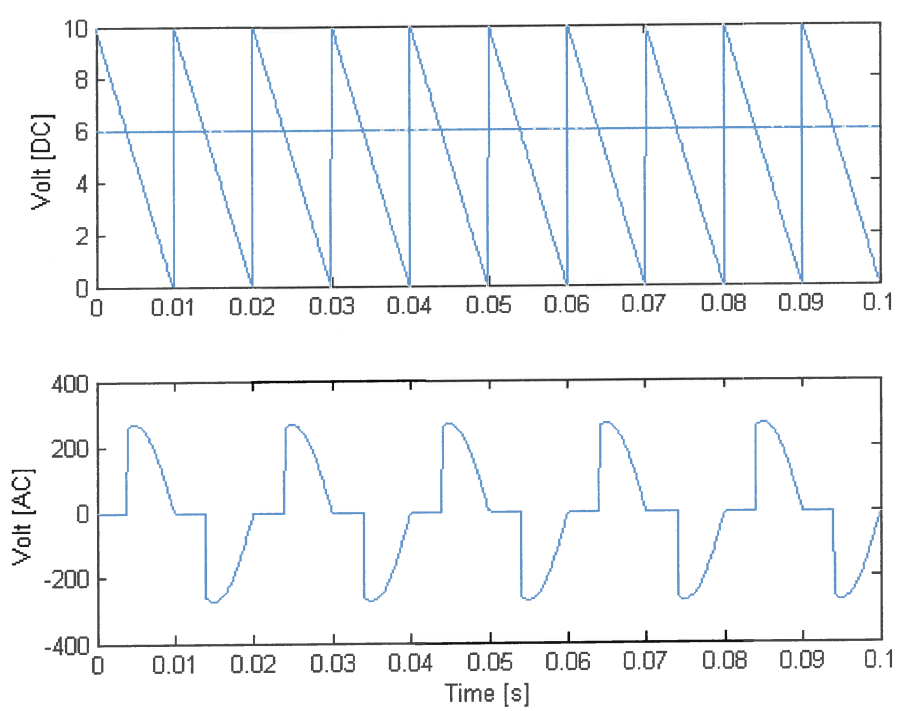

Figure 3. 29 Pulse width modulation principle

The top graph has a ramp signal in blue and a reference signal in green. The reference signal is the 0-10 V signal that is sent from the computer. The ramp signal is generated by the electronics by detecting the zero crossing of the sine wave. At every zero crossing (half cycle) a capacitor is charged to 10 V. The capacitor then discharges to 0 V in exactly the time of a half cycle of the sine wave after which is charged again to 10 V at the zero crossing. In this way the saw tooth signal is generated. The switching then works on comparing the reference and ramp signals to each other to see which one is larger. When the ramp signal is larger than the reference signal, the sine wave is switched off and when the reference signal is large than the ramp signal, it is switched on. In the bottom figure the chopped sine wave can be seen. Now it is possible to control the power delivered by changing the reference signal between 0 and 10 V.

This principle works well although it is not linear due to the fact that the power of a sine wave is not linear over time, but for the application it will work very well. The problem was that the electronic components to do all of this were not available. A complete unit will cost around R3000 to R4000, so another option was considered.

The other option was to look at DC signals. A normal DC motor controller was a perfect device to use for this application. It was capable of delivering the required current, but usually worked at about 180V instead of 220V. Such controllers were available in the laboratory and a simple test revealed that the coil could indeed be controlled with such a controller. After small modifications it was also possible to implement the control via a 0-10V DC signal. A Saftronics Quadro drive was used to control the heating coil.

Although convinced that the hardware was all in place, it was still not possible to drive the DC motor controller with the 0 – 10V DC signal from the computer. After investigation and research, it was discovered that the switching power supply of the computer caused the computer's ground to be different from the DC motor controller's ground. The difference was measured as a 110 V AC difference and that caused the problem. Therefore it was needed to isolate the grounds from each other.

For this an isolation amplifier was used. An isolation amplifier transfers the potential difference between the signal and ground, but isolates a difference of up to 1500 V between the grounds. A Burr-Brown ISO 124 isolation amplifier was used and its schematic can be seen in Figure 3. 30.

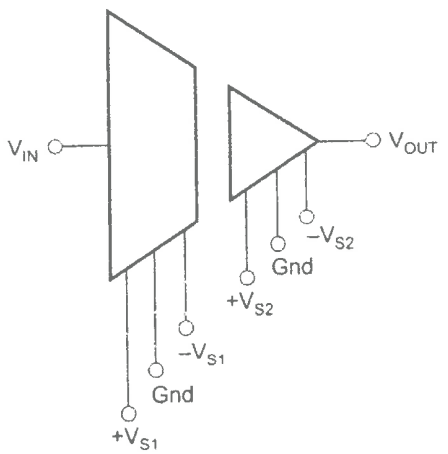

Figure 3. 30 Schematic of Burr-Brown ISO 124 isolation amplifier

This isolation amplifier was built into a box with connector terminals for the power supplies and signals and installed as depicted in Figure 3. 31.

Figure 3. 31 Isolation amplifier with power supplies

The four boxes at the bottom are four DC power supplies to supply the dual ρ12V power for the isolation amplifier. The box on top is the isolation amplifier with its connectors.

The whole heating mechanism worked well with the DC motor controller controlling the voltage over the coil of the hot air gun to control the temperature of the actuator. The DC motor controller is controlled with the computer through a digital to analog card. The whole system is schematically represented in Figure 3. 32.

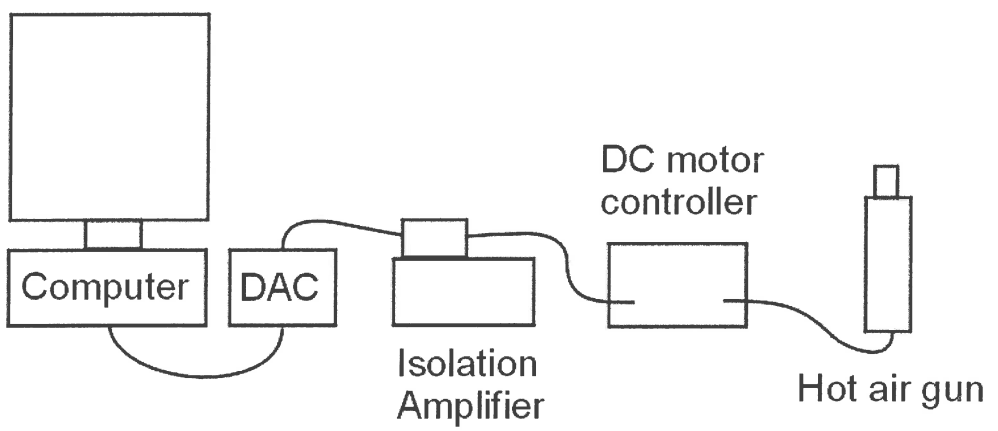

Figure 3. 32 Schematic of whole heating system

3.3.4.4 Displacement measurement

The last aspect to be addressed before control of the actuator can be obtained is the mechanism to measure the displacement of the actuator for the closed loop displacement control system. A very small and compact transducer is needed that has a stroke of at least 10 mm. A LVDT is an obvious choice, but it was found that a LVDT with 10mm linear stroke is quite large and would not fit in the allowable space. Another type of sensor was a laser displacement transducer that was a non-contact sensor, which is quite small and compact. The problem was that the sensor needed to be 80 mm from the surface that needed to be measured.

The last type of sensor considered was a linear potentiometer. Potentiometers are commonly used in volume controls and dimming devices and are usually found as rotational devices. Sliding potentiometers are also available and they are very small and compact with sufficient stroke and durability for the application. A 15mm linear sliding potentiometer (RS 855-377) was used and fitted to the springs to measure the displacement between the springs.

Calibration of the potentiometer against a laboratory quality strain gauge displacement transducer revealed that the potentiometer had a linear behaviour and a calibration factor was obtained. The potentiometer was supplied with 10V power and the output measured with an analog to digital converter on the computer.

The whole separation mechanism was designed and implemented complete with a displacement transducer and all the connections needed to control it with a computer. The control of the spring will be addressed in the next section.

3.3.5 Design of the controller

3.3.5.1 Characterisation of the system

It is important to characterise the open loop system before the loop is closed. The open loop system is the whole spring and actuator assembly and incorporates the isolation amplifier, DC motor controller and the potentiometer as shown in Figure 3. 33. Therefore the transfer function of the open loop system will be the transfer function between the voltage signal that is given to the DC motor controller and the output voltage signal from the potentiometer.

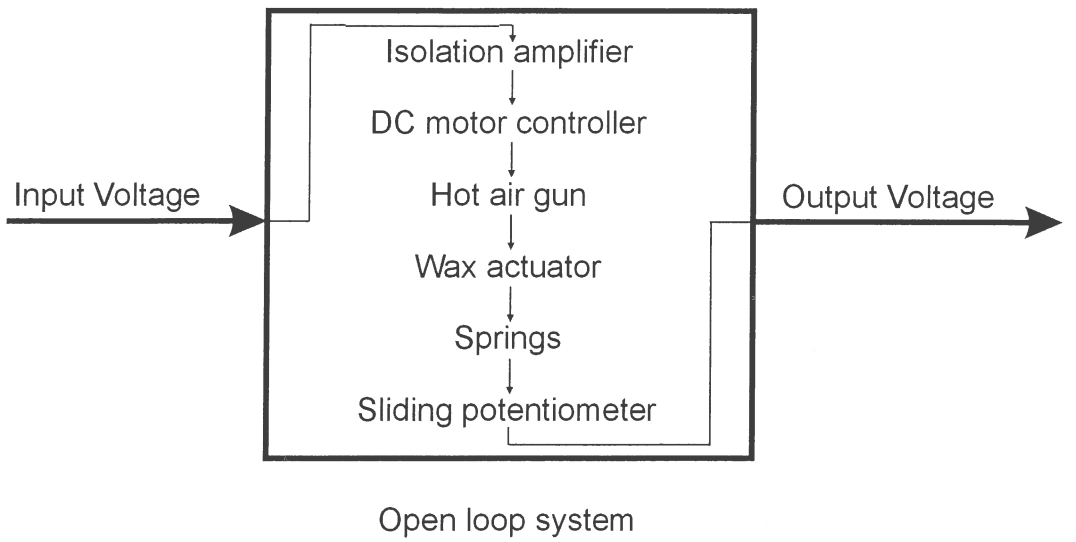

Figure 3. 33 Open loop system

The open loop system is obviously a very complex system, but to simplify the whole matter, the response of the open loop system will be measured and a theoretical model will be fitted to the response. This fitted model can be a first, second or higher order system, although it is preferable to keep it simple.

The first test that had to be done was to determine the range of the system. This is the steady state output of the system for certain input voltages. The system was therefore simply given a constant input voltage and the output was recorded after some time to make sure the system had stabilised. From these tests it was seen that the system starts to respond at 2 V and that maximum displacement of 7.2 mm is reached at an input of 3.4 V. This value would be the limit for the input to the open loop system.

It is difficult to determine whether a first or second order system will model the physical system the best, so both cases will be considered throughout the modelling and compared to each other at the end.

First we will consider a first order system. To characterise a first order system, it is necessary to measure the step response of the system. The step needed to be within the range of the system, so an input step between 2.2 V and 3.4 V was given to the system and the response measured. It was strongly suspected that the upward and

downward response of the system would differ, so both were measured. Figure 3. 34 give the results obtained.

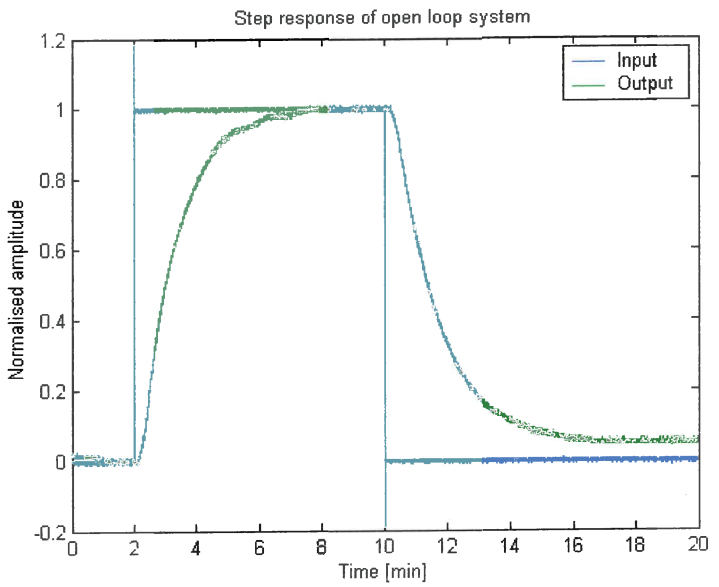

Figure 3. 34 Step response of open loop system

The input and output signals were scaled to fall between 0 and 1. To fit a first order system to such a response, the time constant has to be determined. Lets consider a first order system with the following transfer function (Theron, 2002):

$$G(s) = \frac{a}{s+a} = \frac{1}{\frac{1}{a}s+1} \tag{3.2}$$

The time constant of the system is defined as $\tau=1/a$.

To determine the response of the system with a step input the following can be done:

$$Y(s) = \frac{a}{s+a}\cdot\frac{1}{s} = \frac{a}{s(s+a)} = \frac{1}{s} - \frac{1}{s+a} \tag{3.3}$$

The 1/s is for the step input and the last term was obtained with partial fraction expansion. By performing an inverse Laplace transform, the response can be obtained as:

$$y(t) = 1 - e^{-at} = 1 - e^{\frac{-t}{\tau}} \tag{3.4}$$

After one time constant has elapsed, the response of the system would be the following:

$$y(\tau) = 1 - e^{-1} = 0.6321 \tag{3.5}$$

Therefore, any first order systems response would be 0.6321 after one time constant has elapsed from a step input to the system. If a step response was measured, the time at which the response reached 0.6321 will be the time constant of the system.

Figure 3. 35 give the results if this is implemented on the measured responses.

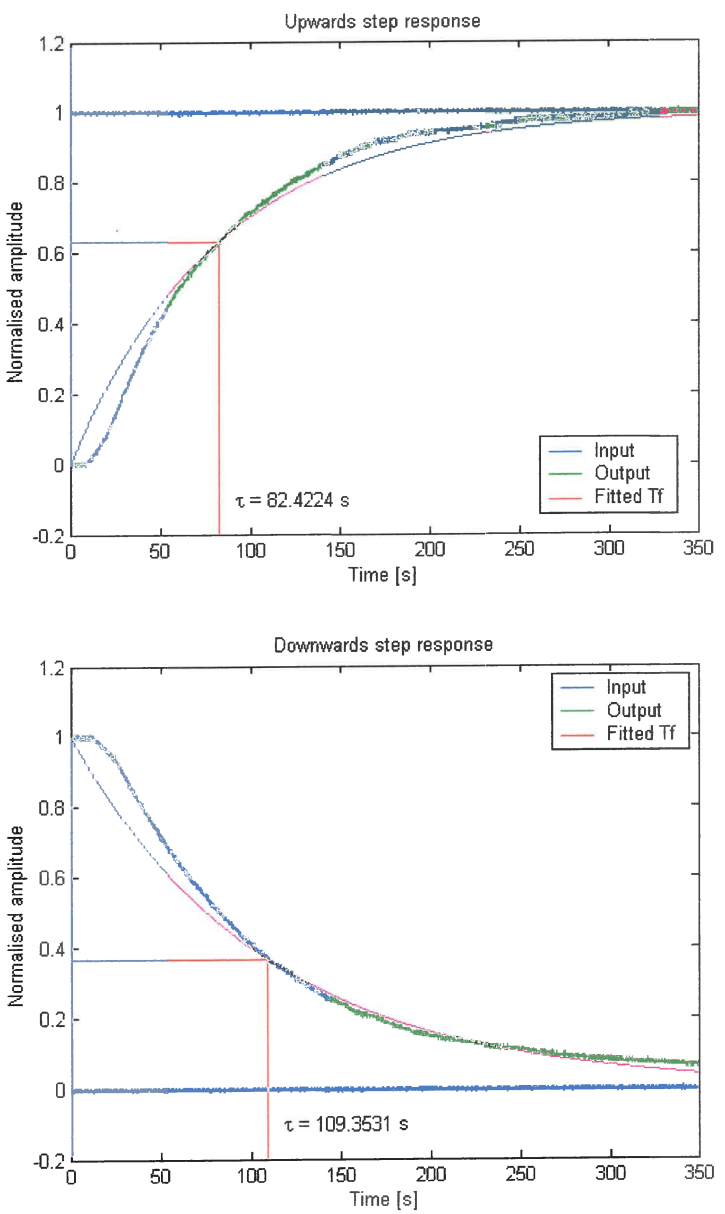

Figure 3. 35 Fitted first order system to upward and downward step response

It can be seen that the downward response is slower than the upward response due to the cooling that is less effective than the heating. The system is therefore non-linear, but to simplify the modelling, a linear system must be fitted to the response. Therefore the average time constant will be taken as 95.888s. The transfer function of the first order system would then be:

$$G(s) = \frac{1}{95.888s + 1} \tag{3.6}$$

The system has one pole at –0.0104.

If a second order system is considered, a step response is not sufficient to determine a theoretical model of the system. Therefore it was chosen to measure a transfer function of the system in the frequency domain. With a system with such a slow response, normal random or chirp excitation techniques are not possible. Therefore sine wave excitation must be used to determine the amplitude and phase of the transfer function at each frequency.

The same type of test was done as with the step response, except that a sine wave instead of a step input was used. The sine wave had an amplitude between 2.6 and 3 V and the period of the sine wave was varied between 100 and 5000 seconds to cover the whole frequency range. At each frequency measured, one sine wave input and output was measured. A theoretical sine wave was then fitted to the output to obtain amplitude and phase values for each frequency. A typical measurement is given in Figure 3. 36.

The red fitted line has been done using the following equation:

$$y(t) = A\sin(\omega t + \phi) \tag{3.7}$$

Where A is the amplitude, ω the circular frequency and ϕ the phase angle with which the output is leading the input. These values for all the frequencies were combined in a Bode diagram. For a second order system, the transfer function can be given as:

$$G(s)=\frac{\omega_n^2}{s^2+2\zeta\omega_n s+\omega_n^2} \tag{3.8}$$

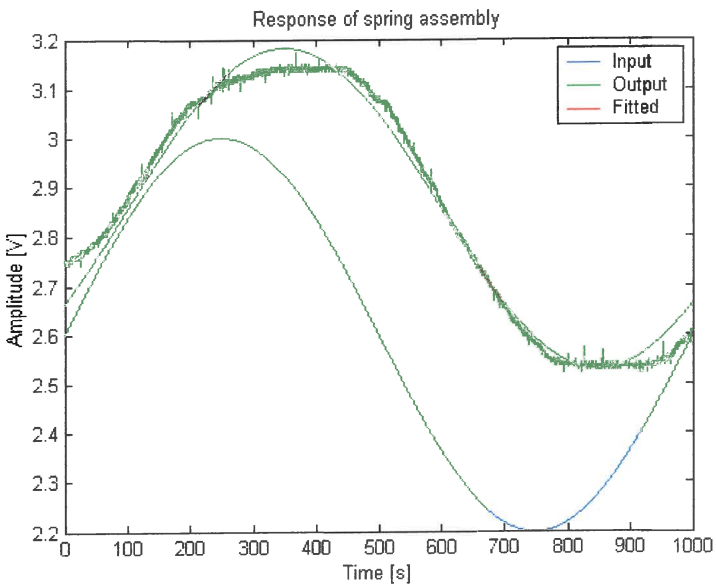

Figure 3. 36 Sine wave measurement

From this, the equations for the amplitude and phase graphs on the Bode diagram can be derived as:

$$\left|G(j\omega)\right|=\frac{1}{\sqrt{\left[1-\left(\frac{\omega}{\omega_n}\right)^2\right]^2+\left[2\zeta\frac{\omega}{\omega_n}\right]^2}} \tag{3.9}$$

$$\phi=-\tan^{-1}\left[\frac{2\zeta\frac{\omega}{\omega_n}}{1-\left(\frac{\omega}{\omega_n}\right)^2}\right] \tag{3.10}$$

Either one of these two equations can be used to fit a second order system to the measured bode diagrams. The result is given in Figure 3. 37.

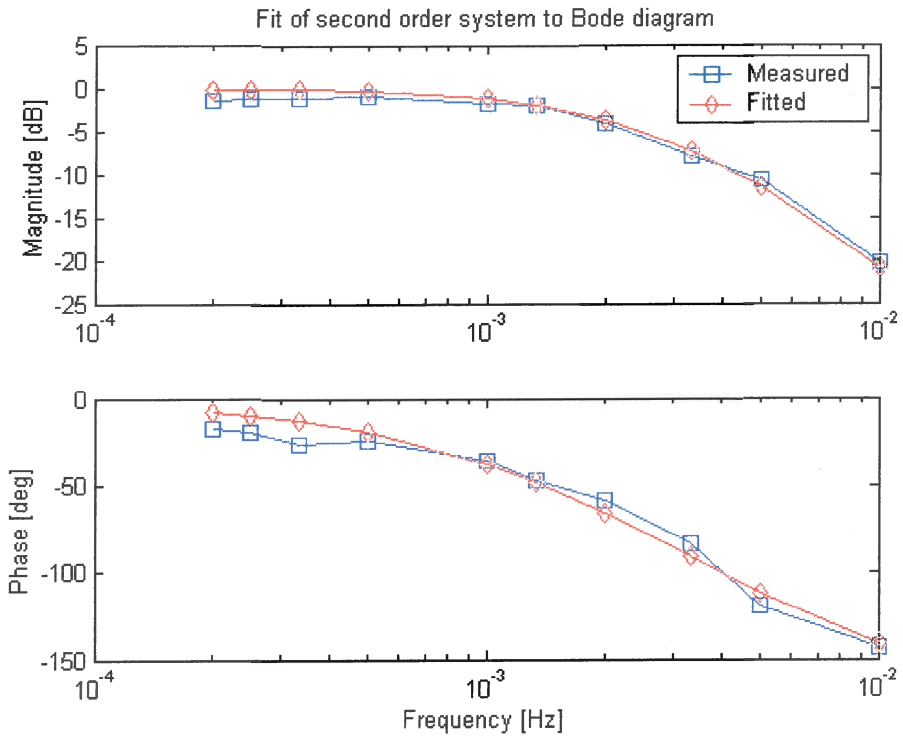

Figure 3. 37 Bode diagram

The fit on the phase graph yielded better results and were used. The fitted second order system had a natural circular frequency of ω_n=0.02055 rad/s and a damping ratio ζ=1.133. This means that it is an over damped second order system. The transfer function of the system is:

$$G(s) = \frac{P}{s^2 + 0.046566s + 0.0004223} \tag{3.11}$$

The poles of this system lie on -0.034228 and -0.012338.

The P in the numerator in equation (3.11) still has to be determined. This factor has to do with the amplitude scaling and time data is needed to determine the value accurately. A step response between 2.2 V and 3 V was measured and the step response of the system described in equation (3.11) was fitted to it by changing the value of P.

The result was a value of P=0.00046831. The response is given in Figure 3. 38.

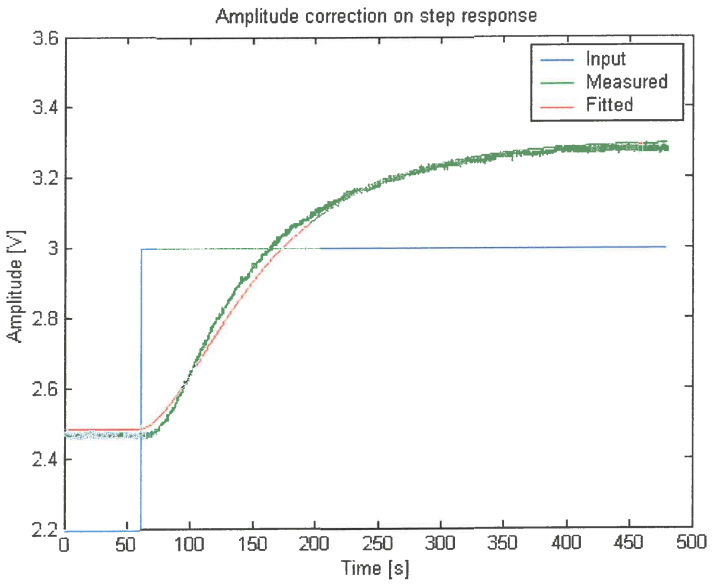

Figure 3. 38 Step response of second order system

Because the amplitudes needed to be fitted here, the graphs were not scaled to 0 – 1 like in the previous tests. Now a complete second order system was fitted to the response of the system and the transfer function of the system is:

$$G(s) = \frac{0.00046831}{s^2 + 0.046566s + 0.0004223} \tag{3.12}$$

3.3.5.2 Closing the loop

It was now possible to close the control loop by using displacement feedback to try and improve the system performance. The displacement signal was obtained from the sliding potentiometer that was installed for this purpose. The control was done in Matlab on the computer and a D/A and an A/D card were used to send and receive the voltage signals.

There are a few constraints on the system that must be pointed out.

- The input to the DC motor controller must be in the range of 0 to 10 V DC. 0 V will yield the maximum amount of cooling and 10 V the maximum amount

of heating. The control system may expect larger or smaller values, but it will be limited by this constraint.

- In a normal control system, an input of 0 V to the system will result in a static system at the current position. With this system it is definitely not the case because 0 V input will lead to maximum cooling and the system will not be stationary. To counter this effect, a constant of 2 V will be added to the output to the system. The reason for 2 V is because it is the value at which the system starts to respond.
- The system is non-linear. This must be remembered especially when the linear theoretical models are compared to the practical results.

The simplest way to close the loop is to use negative displacement feedback. This means that the current displacement is subtracted from the asked displacement, the difference multiplied with a gain input to the system. This is illustrated in Figure 3. 39 in block diagram form.

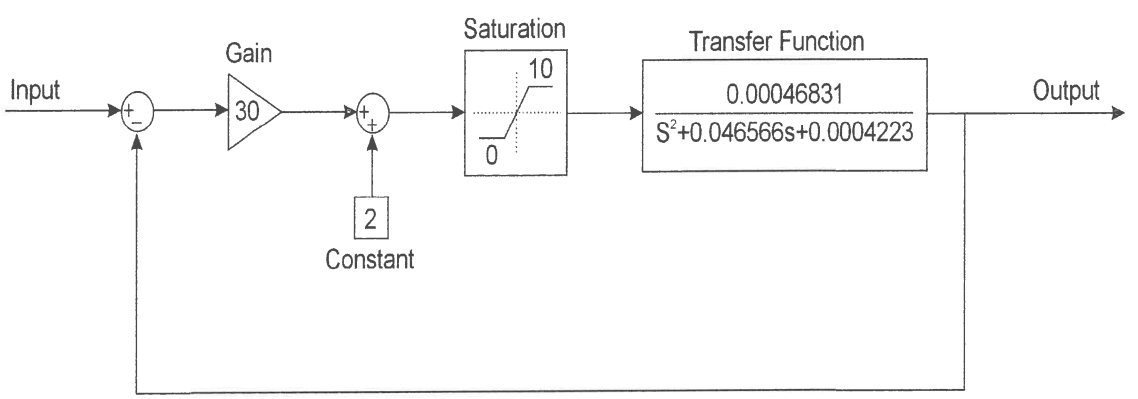

Figure 3. 39 Negative displacement feedback

Such a control program was written in Matlab and implemented on the actual spring. Different gain settings were used to obtain the best possible response. A step response was used to compare the different gain settings to each other. The responses were again normalised to range between 0 and 1 for easier comparison and are presented in Figure 3. 40.

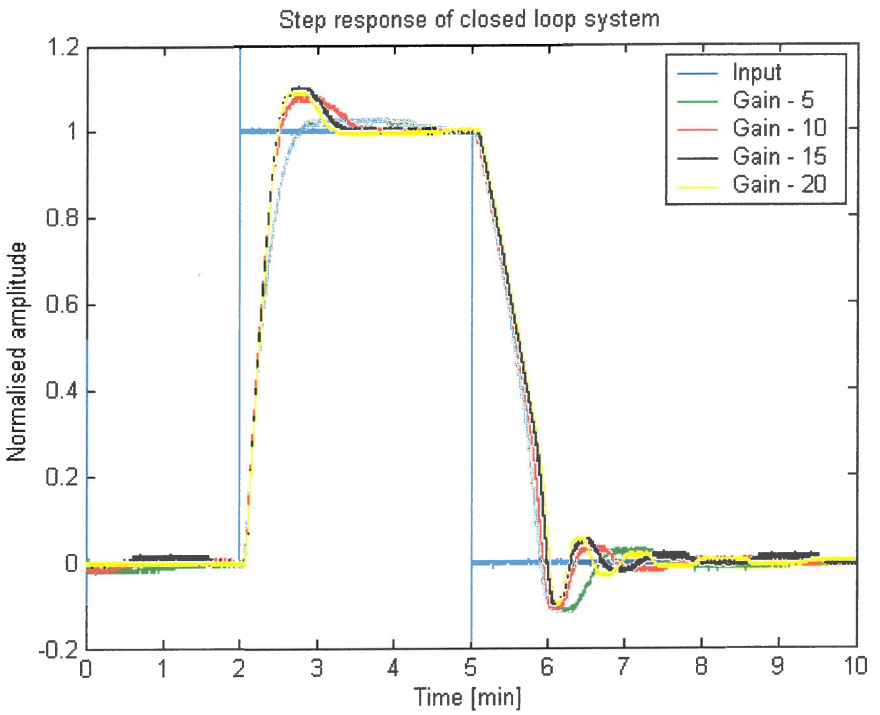

Figure 3. 40 Step response of closed loop system with negative displacement feedback

One of the important observations is the enormous decrease in response time compared to the open loop system. Furthermore, it can be seen that the response is improved by an increase in the gain, but that the overshoot and oscillation also increased. A large gain was needed to minimise the response time, but the overshoot and oscillation were unfavourable. The way to minimise overshoot and oscillation in a control system, is to implement a differentiator.

A differentiator determines the gradient of change of the system and adds that, multiplied by a differentiator gain, to the displacement of the system to account for the dynamics of the system. The effect will be that if the system is moving upwards, the differentiator will cause the measured displacement to appear larger than it actually is to account for the speed at which it is moving upwards. The control system will therefore start to brake the system before it reaches the desired position and therefore minimise the overshoot. The system is given in Figure 3. 41 in block diagram form.

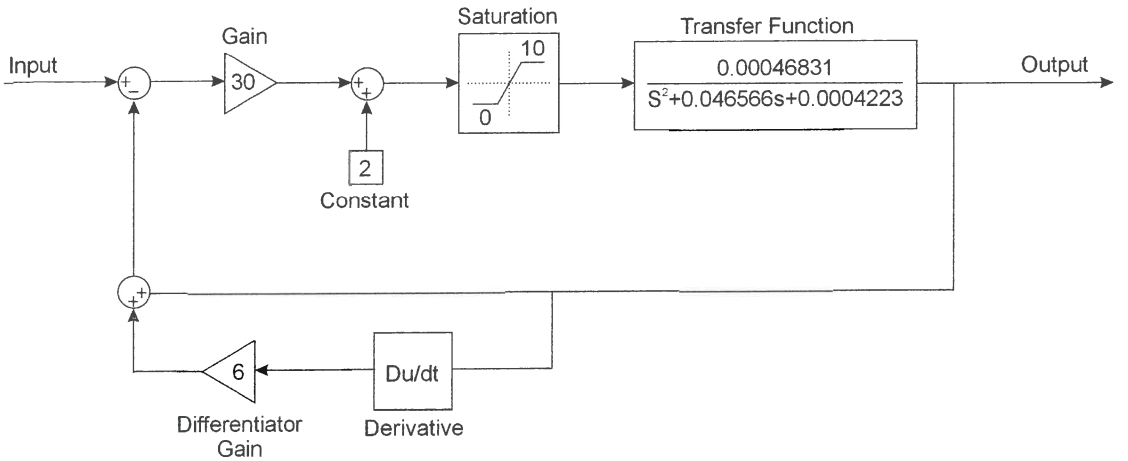

Figure 3. 41 Closed loop system with differentiator

This was also implemented in the Matlab program and the system was tested with this new control system. Different gains were again used to obtain the best results. Three gains were used (20, 30 and 40) and at each gain, the differentiator gain was varied between 2 and 10 and the response measured. Figure 3. 42 give the results.

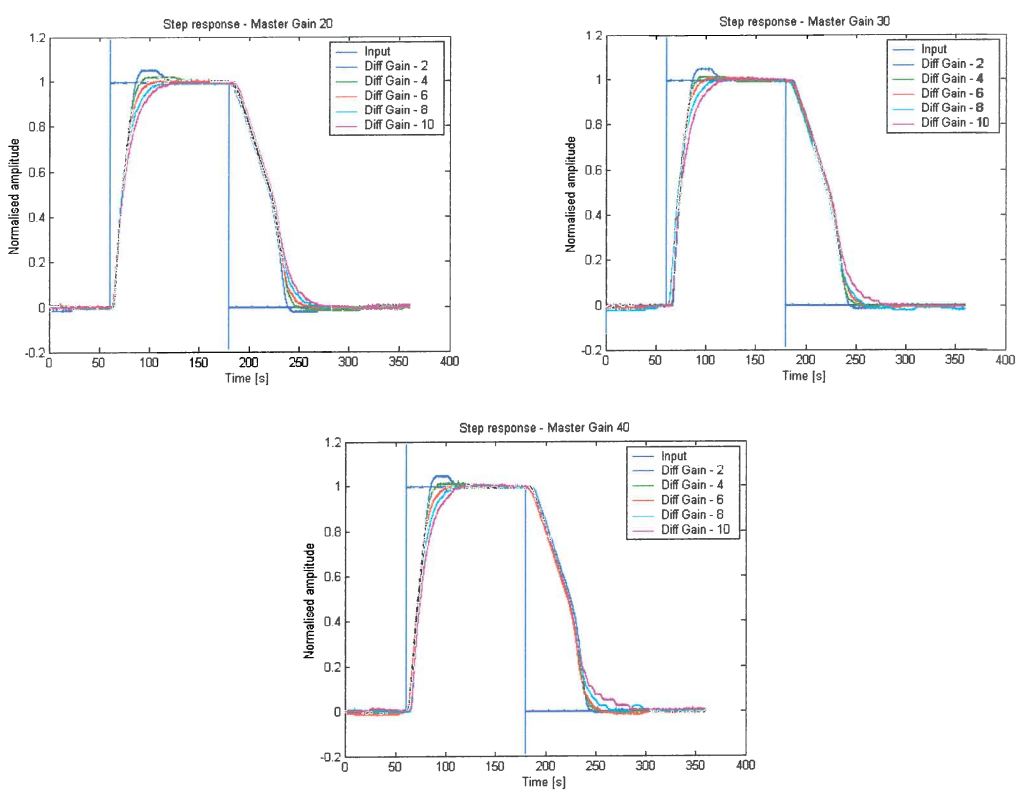

Figure 3. 42 Step response of closed loop system with differentiator

It can be seen that the overshoot and oscillation decreases as the differentiator gain is increased. The problem is now to determine which setting delivers the best response. To be able to determine this, an evaluation criterion must first be chosen. The different criteria available (Dorf & Bishop, 1995) are explained in Figure 3. 43.

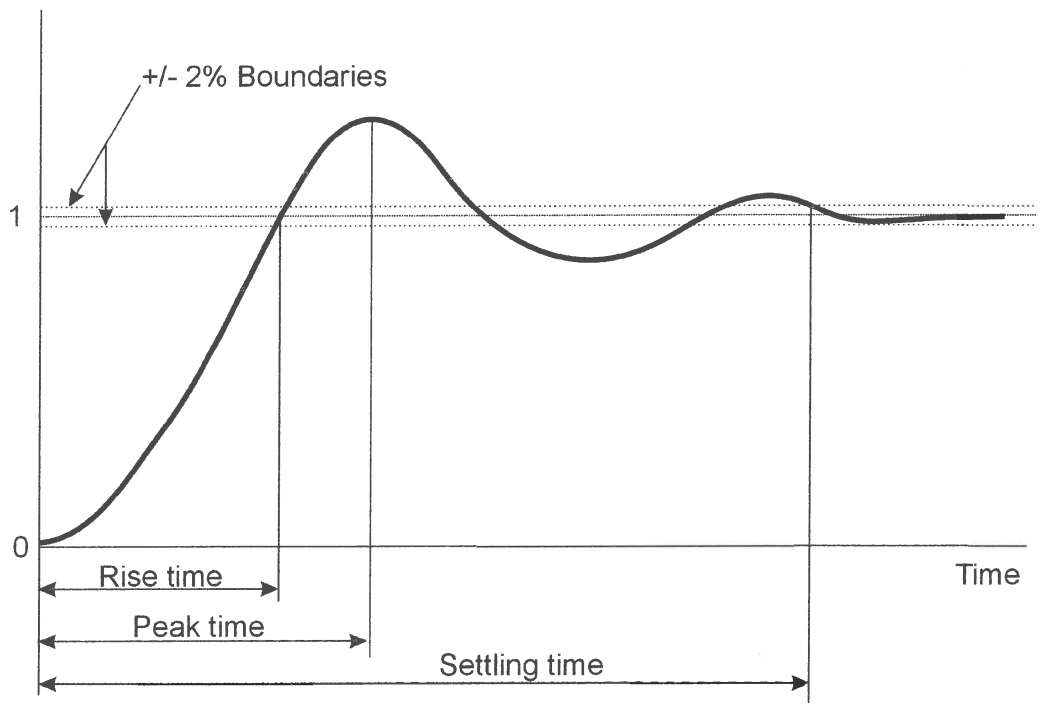

Figure 3. 43 Evaluation criteria

Rise time: The time the system takes to first reach the final value.

Peak time: The time the system takes to reach its maximum value.

Settling time: The time the system takes to settle within a ±2% region around the final value.

If the spring is considered, the stiffness has effectively changed to the new value once the system has reached the desired value and has settled on it. Therefore the settling time would be a valid criterion to evaluate the performance of the system.

The settling time for all the tests were determined for the upward and downward step as shown in Figure 3. 44.

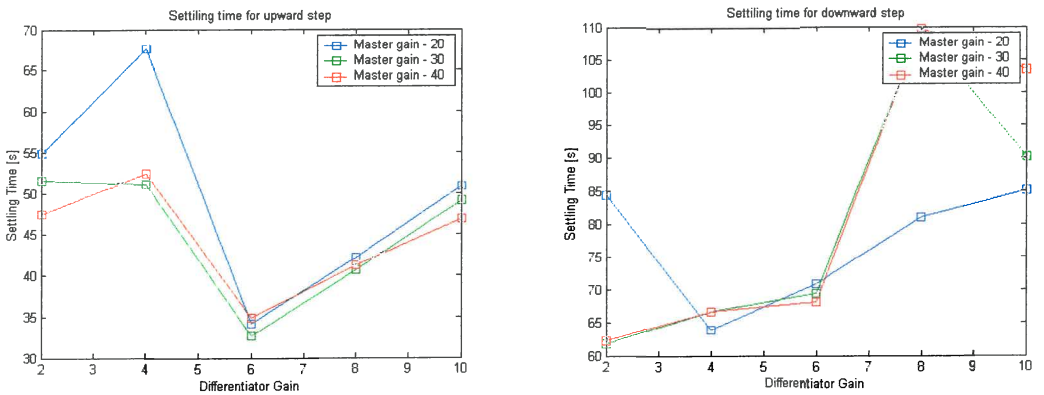

Figure 3. 44 Settling time for closed loop system with differentiator

From the graphs, it can be seen that a combination of a gain of 30 and a differentiator gain of 6 will yield the best performance for the upward step. For the downward step, there are a few discrepancies between the different gain settings. It seemed that a differentiator gain of 2 would yield the best performance. On closer investigation of the time signals, it was however noted that with a differentiator gain of 4 the graphs of the 30 and 40 gain settings just crossed the –2% boundary and increased settling time. It could very well have been that the graphs had not crossed the boundary, which would cause the differentiator gain of 4 to give the best performance as is the case with the gain of 20. Therefore a differentiator gain of 4 was chosen for the downward step. It is possible to implement different gain settings for upward and downward movement on the computer due to the fact that a Matlab program is used to control the settings. The block diagram of the final closed loop system is given in Figure 3. 45.

To validate the theoretical models that were developed, their predicted response must be compared to the measured response of the closed loop system. The previously mentioned constraints on the system complicated the analytical determination of the response of the theoretical systems. It is obviously necessary to include these constraints in the models otherwise the response would certainly not be comparable to the real system. Simulink, a simulation tool of Matlab, provided the tools to numerically implement all the constraints and determine the response of the theoretical models to certain inputs.

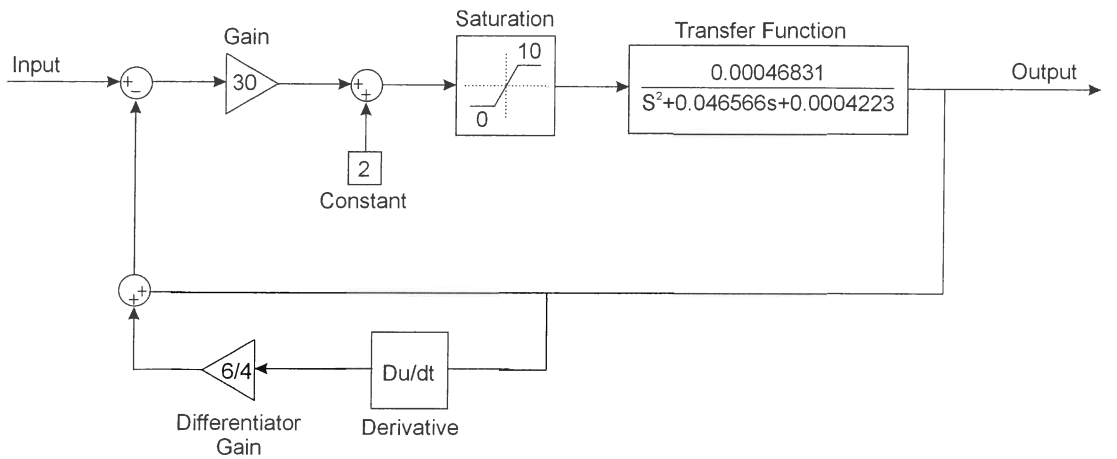

Figure 3. 45 Final closed loop system

A simulink model was developed to incorporate the first and second order system and the constraints to the system. The second order system model is given in Figure 3. 46.

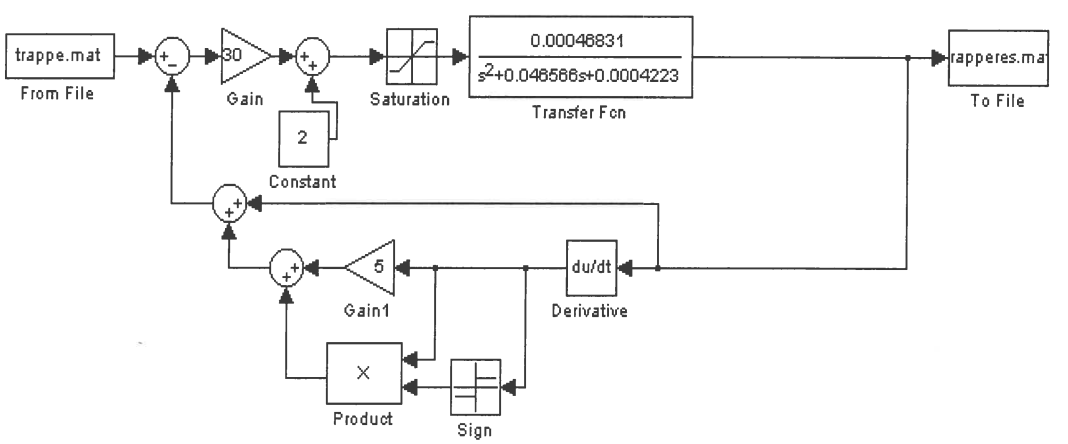

Figure 3. 46 Simulink model of second order closed loop system

To test the system, an input file was created that stepped from 2.2 V (in steps of 0.2 V) to 3.2 V and down again. The response of the actual system with the file as input was measured and the same file was used as input for the simulink model. The responses were plotted on the same graph to be compared in Figure 3. 47.

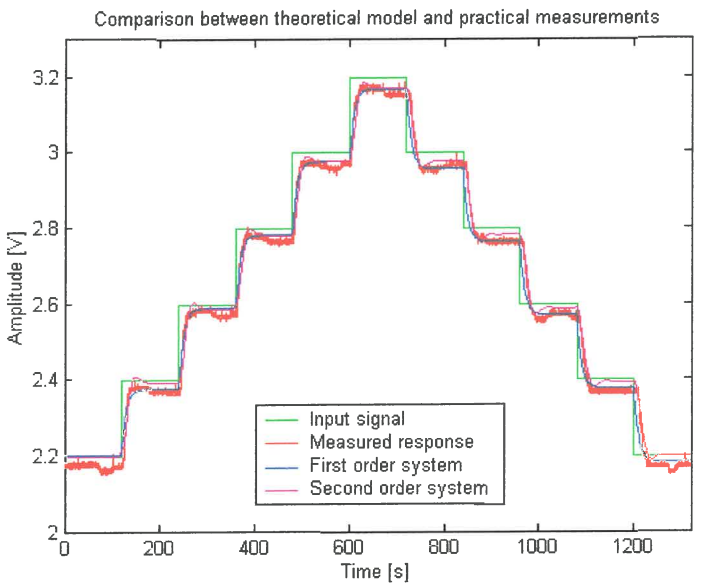

Figure 3. 47 Comparison between theoretical model and actual system response

It can be seen that both the first and second order models gave a quite good correlation to the actual response of the system. There is actually a very easy way to conclude that the second order system is the better fit: The overshoot. A first order system cannot have any overshoot and out of the tests it is clear that the system definitely has overshoot. Therefore the second order system yields the best theoretical model of the physical system.

From this last test it can also be seen that the smaller steps were completed in about 30 seconds. Therefore it was concluded that the time response of the system is adequate for the application. The last spring characteristic necessary to determine whether the spring complies with the specifications, are the stiffness and damping values. This will be reported in the next section.

3.4 Testing of the spring

The whole spring assembly with actuator, hot air gun, displacement transducer and frame was assembled to be able to test the spring on a servo hydraulic actuator. The Solid Edge model of the actuator and spring assembly is depicted in Figure 3. 48.

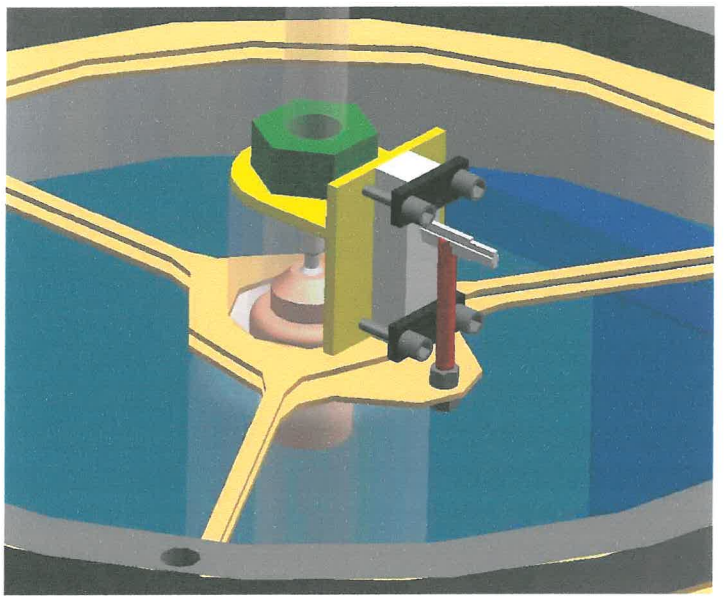

Figure 3. 48 Spring assembly

The actuator is between the two springs with the hot air gun beneath it. A cup-like part was made to fit on top of the actuator to act as a platform for the actuator to push against. The sliding potentiometer was fitted to measure the displacement between the two springs. In real life, the whole assembly is depicted in Figure 3. 49.

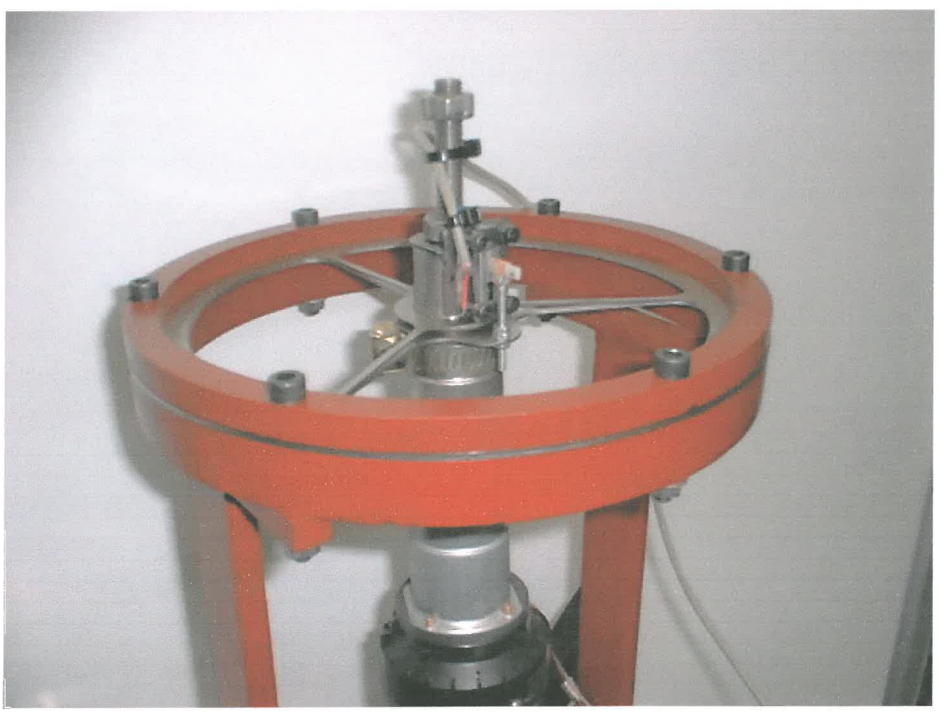

Figure 3. 49 Experimental spring assembly

This assembly was clamped at the top and the bottom was fixed to the servo hydraulic actuator. The force and displacement signals were measured and the stiffness and damping were determined. The results are given in Figure 3. 50.

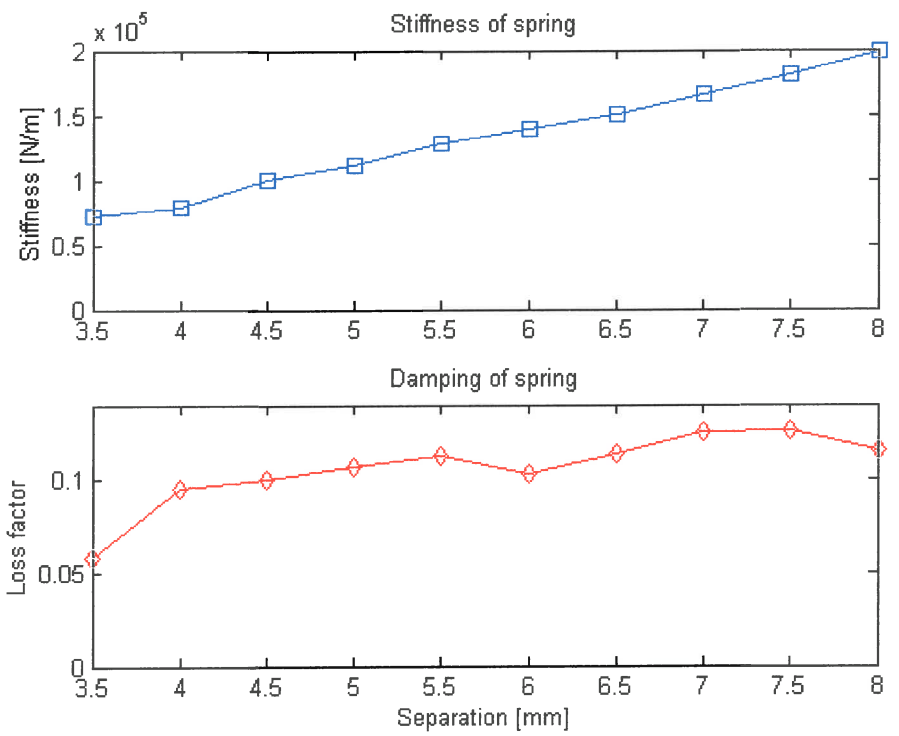

Figure 3. 50 Stiffness and damping of spring assembly

A stiffness change of 2.73 times was obtained and the loss factor ranged between 0.06 and 0.12. These values fulfil the requirements that were set for the spring and therefore the spring can be implemented on a LIVE isolator. The above stiffness and damping values can be used to design the LIVE isolator to obtain a desired frequency response.

3.5 Conclusion

In this chapter the whole development process of the variable stiffness spring was addressed starting at the concept phase with three concepts and then progressing to

the detailed design phase of the chosen concept. A control system was also implemented to control the stiffness of the spring by using a wax actuator. Closed loop displacement and velocity control was used to achieve the desired time response and accuracy of the actuator.

The final variable stiffness spring complied with the requirements set at the beginning and performs even better than needed, especially in light of the amount of stiffness change available. It is concluded that a successful variable stiffness spring was developed that can be implemented on a LIVE isolator or on various other practical applications.

CHAPTER 4

Design and testing of tunable isolator

4.1 Introduction

The previous chapter discussed the development of a practical variable stiffness spring for implementation on a LIVE isolator. It is also necessary to implement a variable damping mechanism in the isolator. The isolator will be designed to demonstrate that it is possible to build a tunable vibration isolator and will therefore not be designed for a specific application.

The isolator will be tested on a servo-hydraulic actuator in the laboratory and the capabilities of the actuator must be kept in mind in the design phase of the isolator.

4.2 Variable damping mechanism

As described previously, one of the aims is to be able to change the damping of the isolator. Structural damping as well as viscous damping is present in the isolator. In order to change the damping of the isolator, one or both of these damping constants must be increased. To change the structural damping of the spring or rolling membranes is quite difficult and therefore the viscous damping will be changed.

The main source of the viscous damping is the fluid going through the port at high velocity. This causes flow losses that in turn are reflected as viscous damping. The flow losses are created when a velocity difference exists between the fluid and surrounding bodies like at the port surface. These flow losses are further increased when turbulent flow or separation occurs at sharp edges, corners or holes. Therefore it will be possible to increase the flow losses by either increasing the surface contact area between the high-speed fluid in the port and the surrounding port or by inducing turbulent flow and flow separation in the port. To increase the surface contact area is not an easily executable option, so the second option was chosen.

The mechanism used must satisfy the following criteria:

- The mechanism must be easily operatable from outside the port.
- The connections to the outside must be watertight.
- It is preferable that the mechanism does not change the volume inside the isolator due to the problems it will create.
- In order to obtain maximum damping change, the minimum damping of the mechanism must be as low as possible.

There are basically two options to choose from, translational and rotational movement. With translational movement a plate or pen would be pushed further and further into the port to increase flow losses. The rotational concept would have a plate mounted in the port. When the plate is orientated vertically, there will be very little flow losses. As the angle of the plate increases, the flow losses will increase due to the turbulent flow over the edges of the plate. Maximum damping will occur when the plate is horizontal.

The translational movement will have a problem with either sealing or changing the volume. Compared to that, the rotational movement will have no influence on the volume and by connecting the ends of the plate to shafts will make the sealing very easy with normal oil seals. Therefore the rotational concept was chosen and the plate that would be inserted into the port is depicted in Figure 4. 1.

The thin plate like part fits into the port. The plate is thinner than the diameter of the port so that the flow will not be shut off completely, but only partly restricted. The cylindrical parts are for sealing and holding it in place. The ends are outside the port and the shaft can therefore be turned from the outside by some sort of actuator or motor.

Because rotation is used, an electrical motor would be the simple answer for turning the shaft. The only problem with a DC motor is position control. The angular position of the motor is very important and therefore some sort of position feedback will be needed if a DC motor is used. Another type of electrical motor that can be used is a stepper motor. Stepper motors are electrical motors that are controlled step by step and are therefore position control motors. They are used extensively in things

like printers and plotters where position control is needed. They are very cheap in comparison with a DC motor with shaft encoder. There is also no need for a closed loop control system to do position control on the motor.

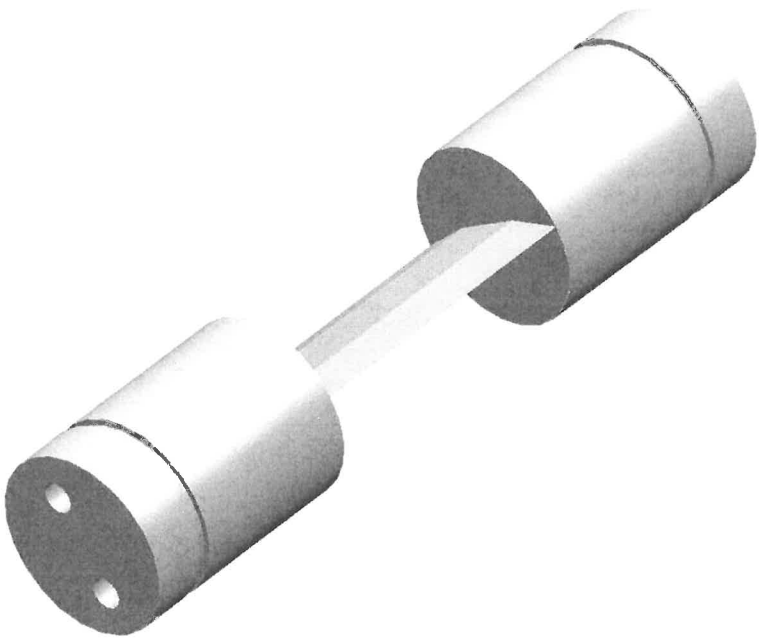

Figure 4. 1 Plate to be inserted in port

Although these types of motors are well known, the working principle of the motors and the control of them are not well known and therefore it is addressed in detail in Appendix C.

The circuitry developed to drive the stepper motor is depicted in Figure 4. 2.

4.3 Design of adaptable isolator

In this section the parameters of the isolator will be determined. The stiffness has already been determined to be variable between 80 000 N/m and 200 000 N/m. The loss factor of the structural damping has also been determined as being around 0.1. These values will now be used to determine the other parameters like port length, diameter and area ratio.

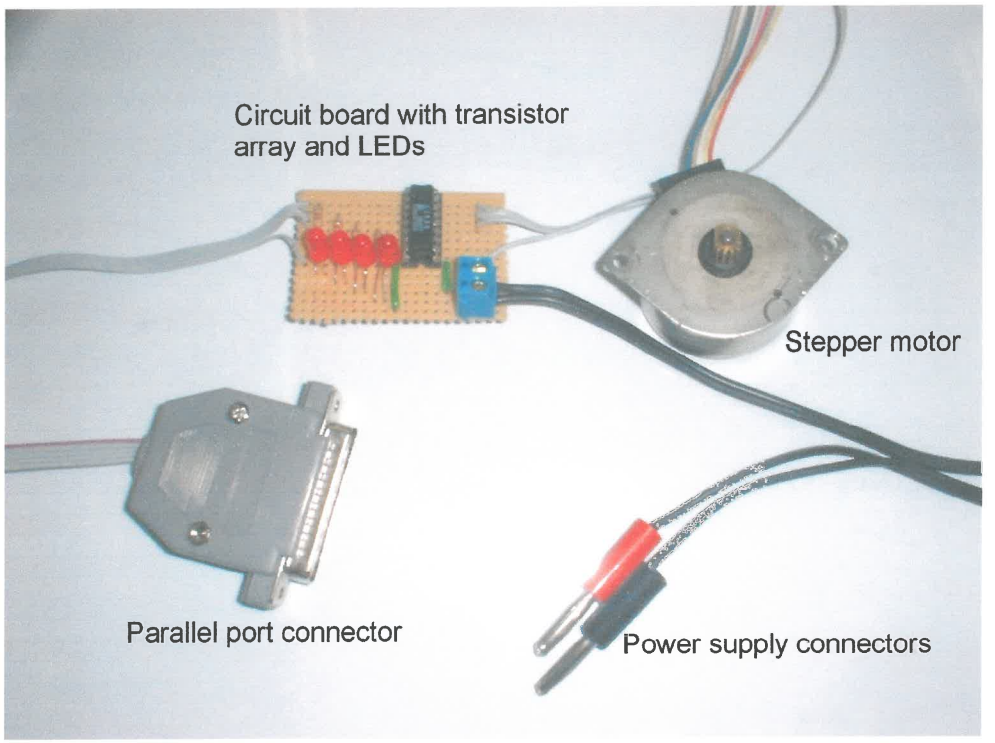

Figure 4. 2 Stepper motor circuitry

Before the design can be done, a few decisions have to be made regarding the properties of the isolator. The isolation frequency, mass and port length have to be chosen. The following values have been chosen:

Table 4. 1 Chosen parameters for isolator

Property	**Value**
Isolation frequency	30 Hz
Mass	4 kg
Port length	100 mm

The servo-hydraulic actuator can easily give excitation up to 50 Hz and therefore the 30 Hz isolation frequency was chosen. This will be the centre isolation frequency (for a stiffness of about 140 000 N/m). A mass of 4 kg was estimated to be a good representative value of what the mass of the isolator parts will be. It is not foreseen to add extra weights to the isolator to improve performance of the isolator. A port length

of 100 mm is sufficient to put the damping mechanism in without being limited by space.

There is another consideration regarding the stiffness. In the LIVE isolator, it is necessary to seal the fluid inside, while still allowing the port to move relative to the reservoir. This is usually done by moulding rubber in-between the two parts that act as a seal but also as the spring for the system as shown in Figure 4. 3.

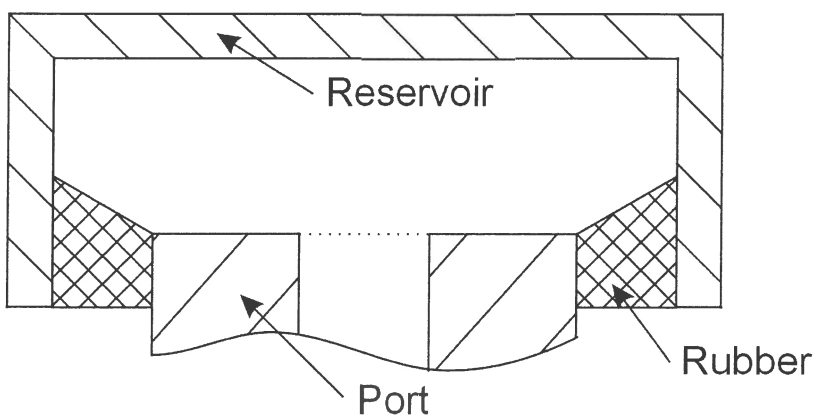

Figure 4. 3 Moulded rubber seal

In this case it is not preferable at all to add more stiffness to the system because it will decrease the overall stiffness change that can be achieved. Therefore another option must be considered.

Rolling diaphragms are sealing devices available on the market that seal two circular bodies while allowing movement with almost no stiffness. The diaphragms work as shown in Figure 4. 4.

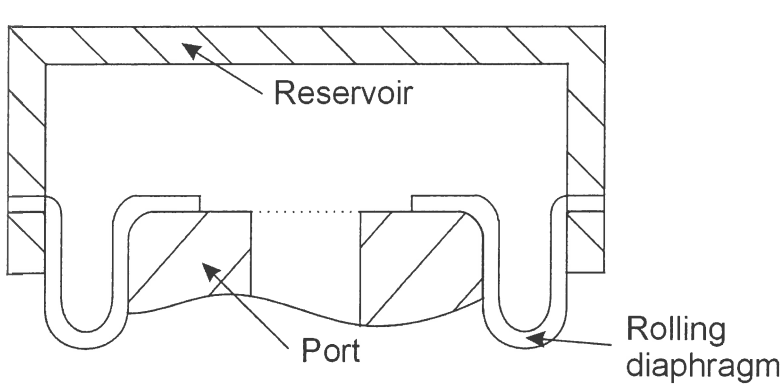

Figure 4. 4 Rolling diaphragm seal

These diaphragms are made of Nitrial rubber impregnated with a cotton woven sheet to prevent stretching. One other very important aspect of the diaphragms for the application is that they do not have a centre position and can work in any position. It will be remembered that the variable stiffness spring centre position changes as the leafs are separated. With a moulded rubber seal this would cause a major problem, but using rolling diaphragms solves it.

These diaphragms are therefore ideal for this application and will be used instead of moulded rubber. One problem with the diaphragms is availability. They can only be obtained in 3 sizes of which 2 are very small. Therefore the diaphragm determines the outside diameter of the reservoir. The diaphragm used is a Simrit Long-stroke-rolling diaphragm, type BFA 80x70x30. Figure 4. 5 gives the installation details for these diaphragms.

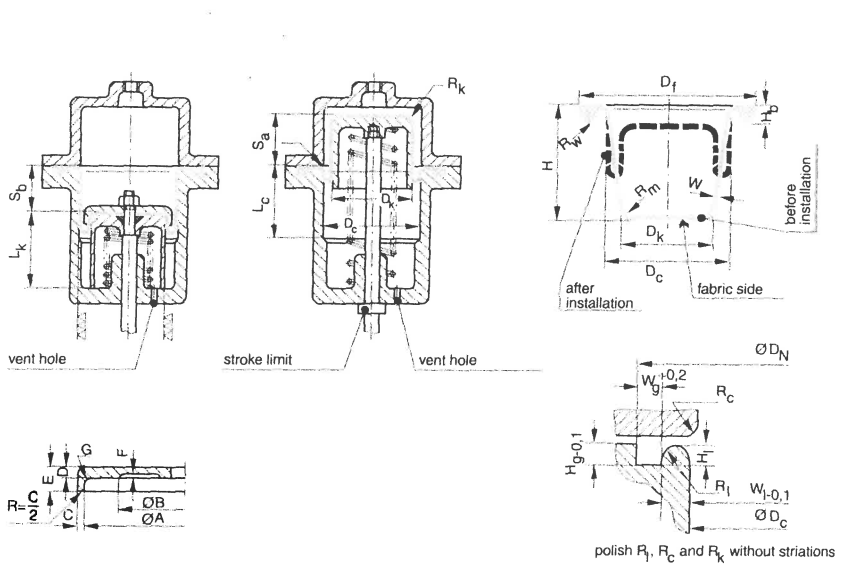

Figure 4. 5 Installation details for rolling diaphragms (Simrit)

Therefore the diameters of the reservoir will be as shown in Figure 4. 6.

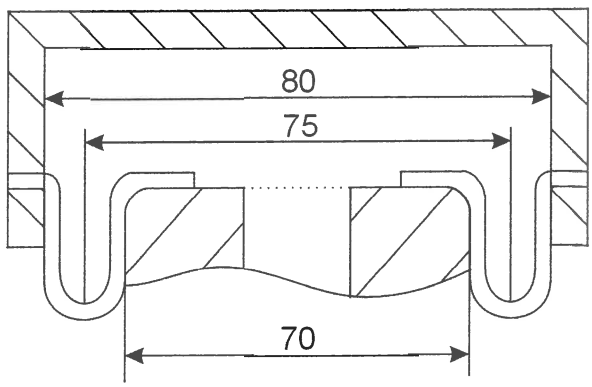

Figure 4. 6 Dimensions of reservoir

For calculation purposes, the outside diameter of the reservoir is the diameter of the piston that is moving upwards. Due to the fact that the diaphragm is also moving upwards, the outside diameter can be taken as 75 mm.

With all the values determined and chosen, the last parameter, the port diameter, can be calculated. The equation for the undamped isolation frequency will be used for this purpose due to simplicity. The equation is the following:

$$\omega_a = \sqrt{\frac{-k}{m_B\left(1-\frac{A_b}{A_a}\right)\frac{A_b}{A_a}}} \tag{4.1}$$

with

$$m_B = \rho \ell A_a \tag{4.2}$$

The area of the port and therefore the diameter of the port can be calculated as 25.5 mm. This will be rounded off to 25 mm. It is important to notice that the design is not done 100% accurately due to the fact that it is not necessary to have the isolation frequency at exactly 30 Hz. If it is 20% lower or higher, it will not matter because it is not designed for a specific application.

If such an isolator is designed for a specific application however, the design would be done in much more detail and greater care would be taken to accurately determine the masses, effective port length and the effect of damping. The damped isolation frequency would be used instead of the undamped isolation frequency and the flow

would be modelled to determine flow losses in the port. This would insure that the desired isolation frequency is obtained.

Figure 4. 7 show the transmissibility curves for the different stiffness values.

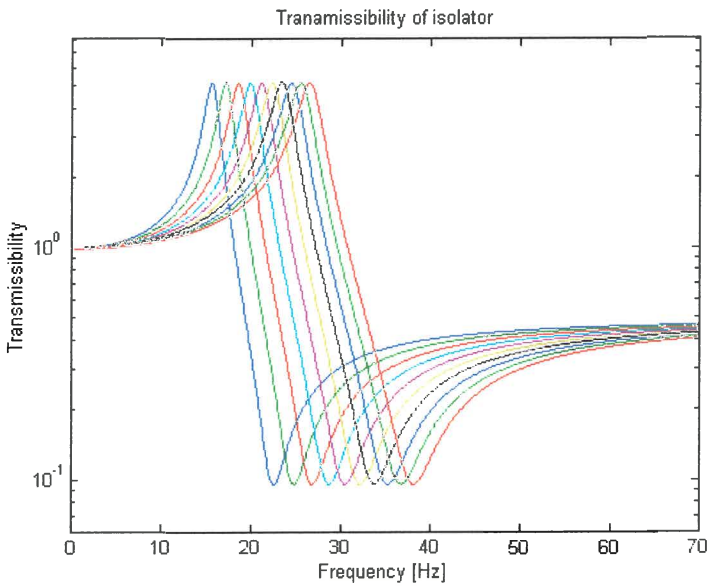

Figure 4. 7 Transmissibility form different stiffness values

This is what the designed isolator is supposed to be able to obtain, but this will probably change due to minor differences in the isolator itself. One factor that will certainly have an influence is the viscous damping value. It was taken as 0 for the above graphs, but will certainly not be 0 in the actual isolator.

Figure 4. 8 show a cross section through the designed isolator assembly.

It can be seen that edges around the port has been smoothed and rounded to minimise damping and that the rest of the design is quite simple and compact. It will be noted that there are no hole to fill the inside with water. The reason for this is that it was learnt from experience that it is almost impossible to get all the air out if the filling is done through a hole. Therefore the whole isolator was assembled while submerged in water to be sure that all the air is out of the reservoirs.

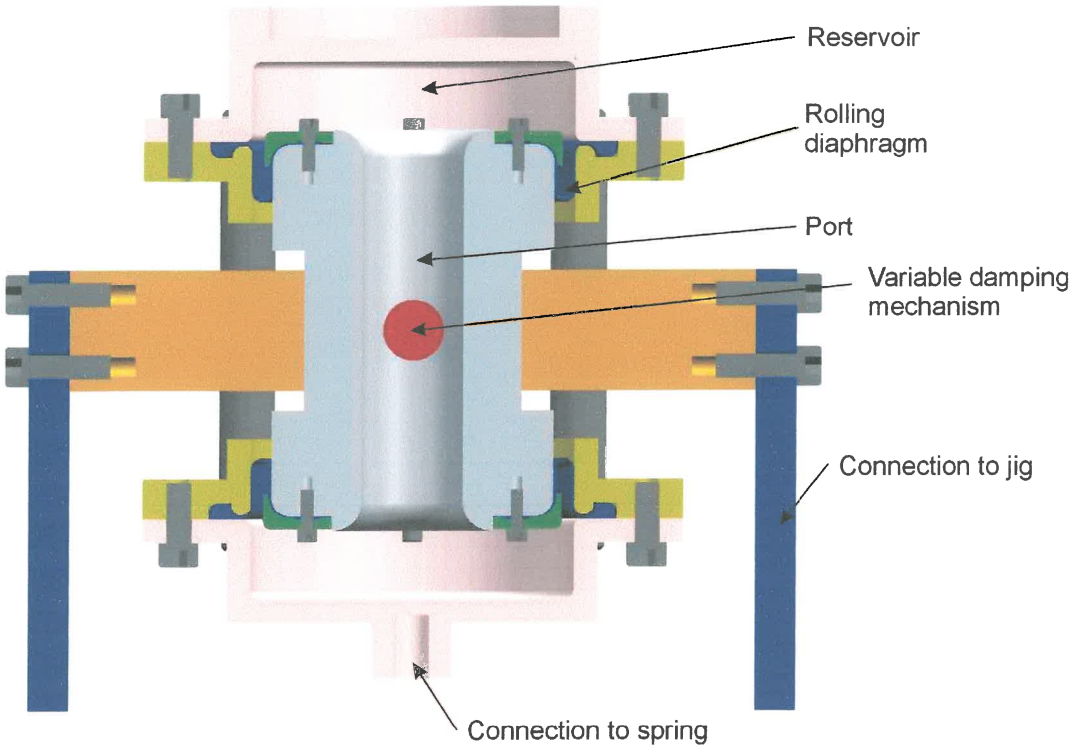

Figure 4. 8 Design of isolator

The isolator was manufactured, assembled and fitted to the variable stiffness spring to be tested. The whole assembly is depicted in Figure 4. 9.

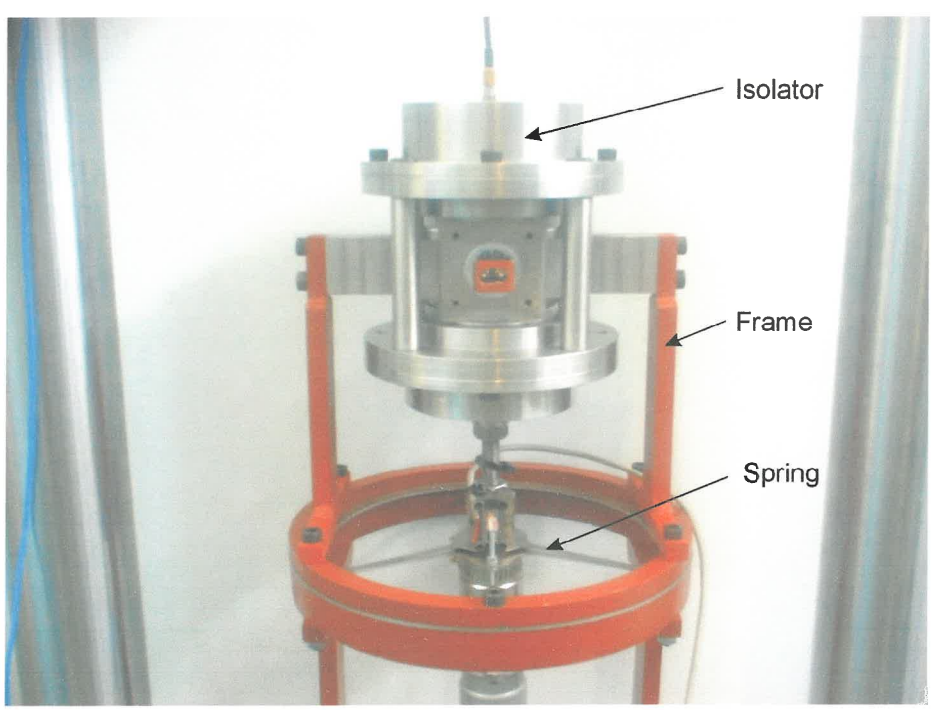

Figure 4. 9 Experimental setup

4.4 Testing of the isolator

As mentioned before, the isolator was tested on a servo-hydraulic actuator in the laboratory. To be able to measure transmissibility over the whole frequency range, the isolator has to be excited over the whole frequency range. This is usually done with one of the following two types of excitation:

- Random excitation
- Chirp excitation

Random excitation simply uses a white noise signal, usually band limited, to excite the structure. With chirp excitation, a sine wave is used of which the frequency is continuously swept from low to high frequencies to be able to excite all the frequencies. The two signals are represented graphically in Figure 4. 10.

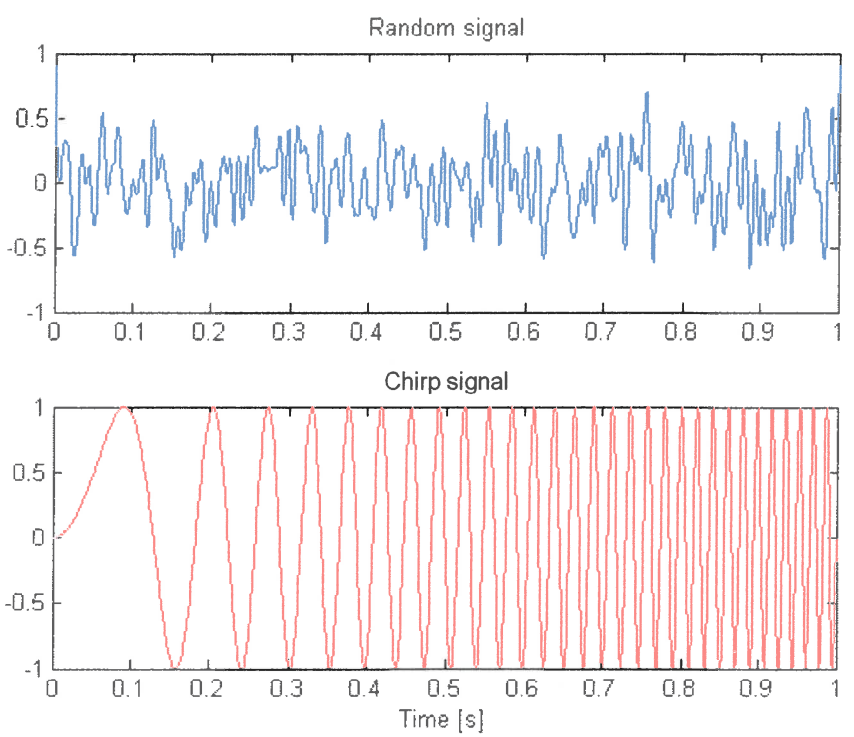

Figure 4. 10 Random and chirp excitation

The performance of the two excitation methods is application dependant and both were tested. It was found that random excitation worked better for the transmissibility measurement of the isolator. To measure the transmissibility, the acceleration of the input and output has to be measured and compared to each other. This was done by connecting an accelerometer to the actuator input and to the top of the isolator. Small 10 mV/g PCB ICP accelerometers were used together with signal conditioning amplifiers. The experimental setup is depicted in Figure 4. 11.

A Siglab measurement system was used to measure the signals and the transmissibility was calculated. The transmissibility is the H1 estimate between the two signals. Averaging is also used to smooth out the measured graphs and a Hanning window was used.

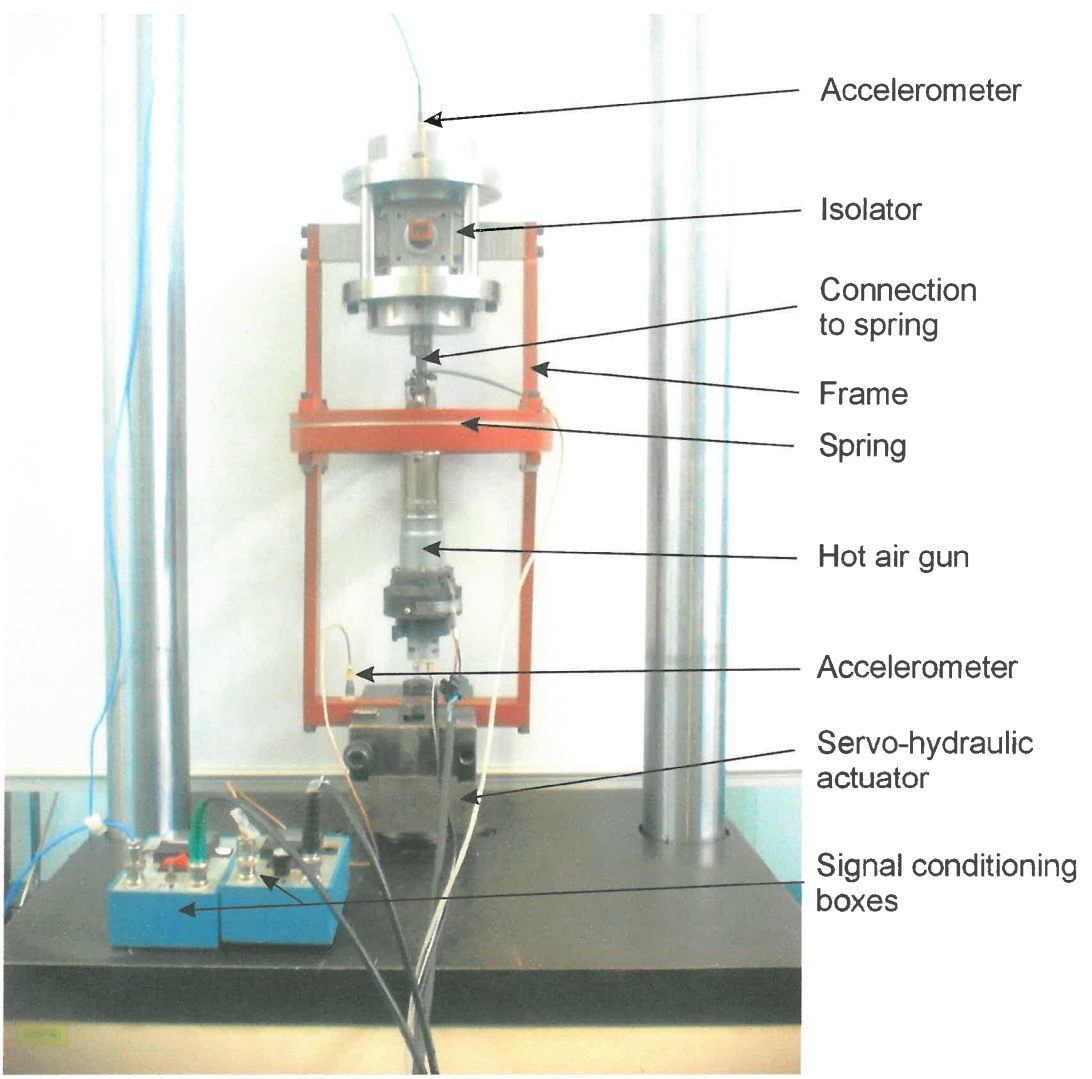

Figure 4. 11 Experimental setup

The first test was to measure the transmissibility of the isolator without any water inside. It is then essentially a mass-spring-damper system and the characteristics of the spring can be determined when connected to the isolator. The measured transmissibility is shown in Figure 4. 12.

It can very clearly be seen how the natural frequency of the system increases as the stiffness increases. The volt values in the legend refer to the setting on the spring controller (1 V = 2.3115 mm). It can also be seen that there is no isolation point present due to the absence of the water inside the isolator.

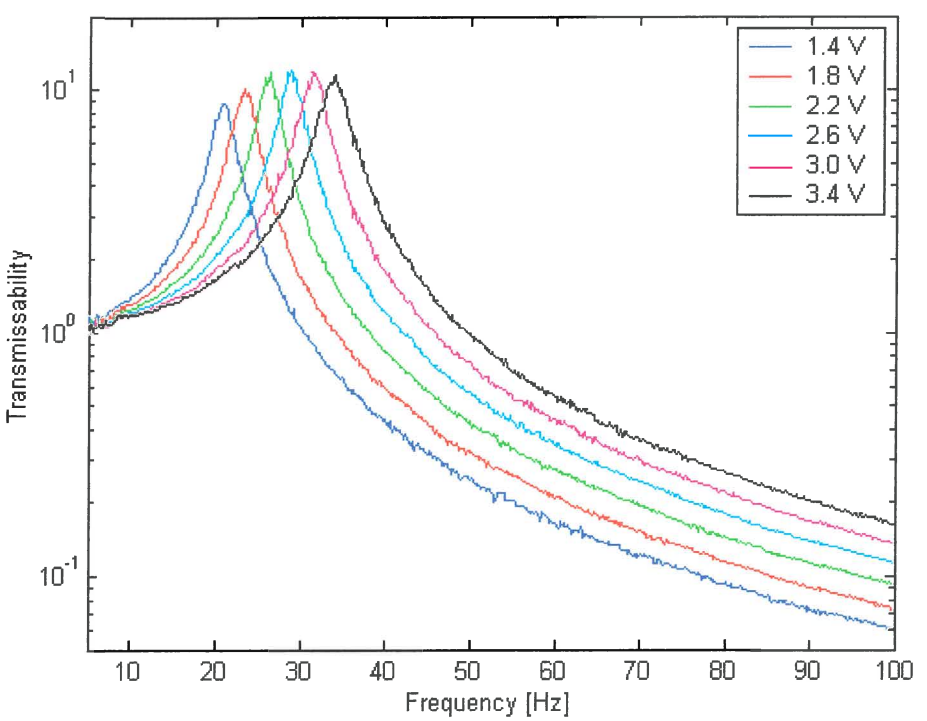

Figure 4. 12 Transmissibility of isolator without water

To determine the parameters of the spring from these graphs, a curve fit must be done on the graphs. The following equation gives the amplitude response of a mass-spring system with structural damping as given in equation (1.7):

$$|T| = \left| \frac{1 + i\eta}{1 - \left(\frac{\omega}{\omega_n}\right)^2 + i\eta} \right| \tag{4.3}$$

The Matlab function "nlinfit" was used to fit this equation to the measured graphs. It was of course possible to determine the mass of the system by measuring all the components. This was done and the total mass of the parts suspended by the spring weighed 4.287 kg. This was therefore used and the stiffness and loss factor were determined by fitting the graphs. Figure 4. 13 show the fit for the 1.4 V measurements.

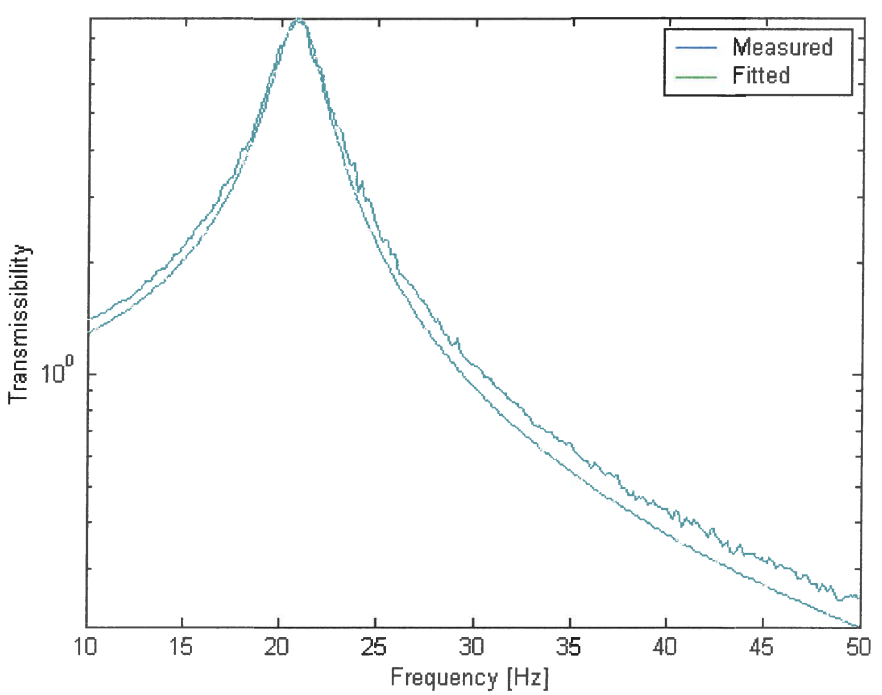

Figure 4. 13 Fitted transmissibility

It can be seen that the fit is quite accurate. By fitting all the graphs, the following results were obtained:

Table 4. 2 Fitted stiffness and damping values

Voltage	**1.4**	**1.8**	**2.2**	**2.6**	**3.0**	**3.4**
Stiffness [N/m]	73 328	92 098	115 690	140 530	167 040	193 930
Loss Factor	0.111	0.096	0.086	0.083	0.084	0.089

Figure 4. 14 give a comparison of the fitted stiffness values to the values obtained when testing the spring alone. It can be seen that the result are very similar and it looks as if the curve fit method used last produced better results at low separations. The structural damping loss factor is in the region of 0.09 for all the settings, so an average constant value of 0.0916 will be used in the following tests.

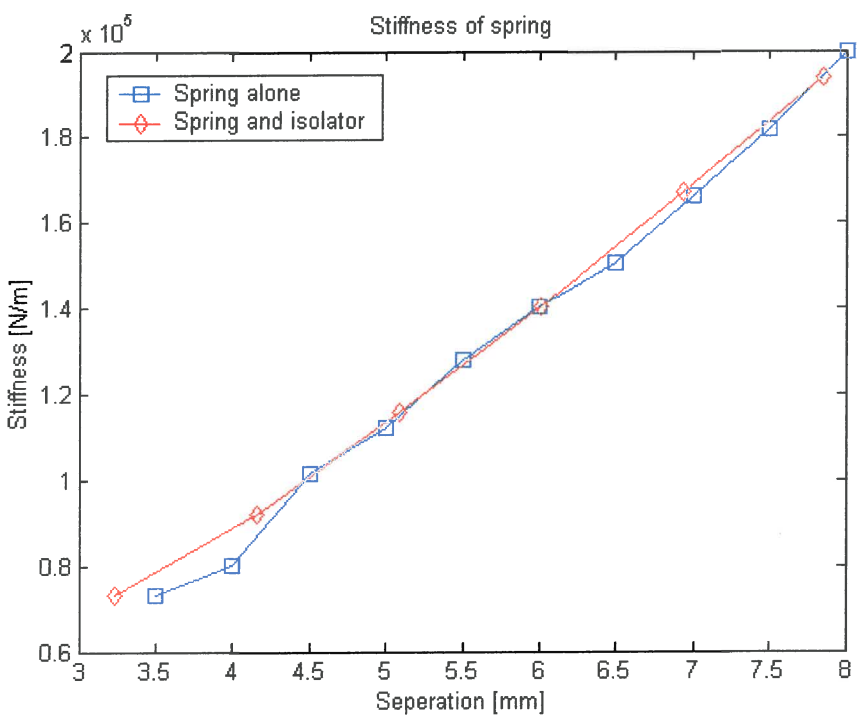

Figure 4. 14 Comparison of stiffness measurements

With the stiffness and damping of the spring determined, water was added to the isolator, the tests repeated and the transmissibility curves measured. The results are given in Figure 4. 15.

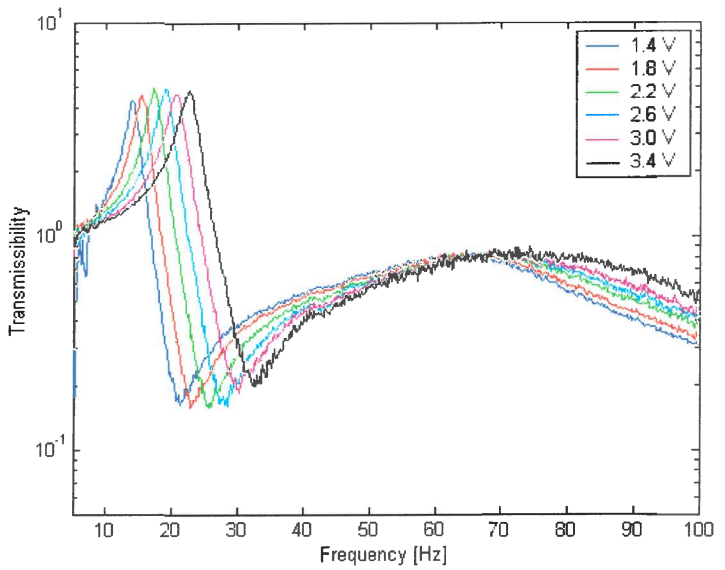

Figure 4. 15 Transmissibility with uncompressed water

The main observation from these graphs compared to the previous ones are the presence of the isolation point. The graphs still shift as the stiffness increases and it can be seen that the isolation frequency is shifted from 21 Hz to 33 Hz. This is quite a significant shift when the percentage difference is considered. Further it can be seen that an isolation of about 0.2 is obtained which is also quite significant. If the overall form of these graphs is compared to the form of the theoretical graphs in Figure 4. 7, it can be seen that they look similar up to about 40 Hz, but that the measured graph has a bump at about 65 Hz that is not present in the theoretical graphs. This can be explained by the fact that the water inside the isolator was not pressurised. Although the rolling diaphragms are lined with cotton to prevent it from stretching, it will still be able to expand a small amount. The effect of this is a second degree of freedom in the system created by the water being able to move without the port moving relative to the reservoir. The rolling diaphragms acts as the spring and the water as the mass and forms a spring-mass system with a natural frequency at about 65 Hz as can be seen in the graphs.

This second degree of freedom will cause serious problems when theoretical curves are fitted to the graphs. If the modal superposition principle is considered, it will be seen that the isolation point of the graph will be influenced the most by the second degree of freedom and that it will have a negative influence on the amount of isolation

achieved. The natural frequency will not be influenced very much. To try and eliminate this effect as far as possible, the water inside the isolator was pressurised. The effect of this will be that the diaphragms will stretch. That will increase the stiffness of the second degree of freedom significantly and shift its natural frequency hopefully high enough to have a negligible effect on the lower frequencies. It will therefore not be possible to take that second degree of freedom away completely, but it can be moved away far enough to eliminate its effect on the low frequencies.

This second degree of freedom is always a problem when building a LIVE isolator, because any deformation of the flexible element or any air trapped inside the isolator will cause such a second degree of freedom. It must therefore be ensured that this second natural frequency is high enough to have minimal effect on the lower frequencies.

The water inside the isolator was pressurised by changing the assembly process. It was not possible to measure the pressure inside the isolator, so the tests were redone to see if it had an effect. The results are shown in Figure 4. 16.

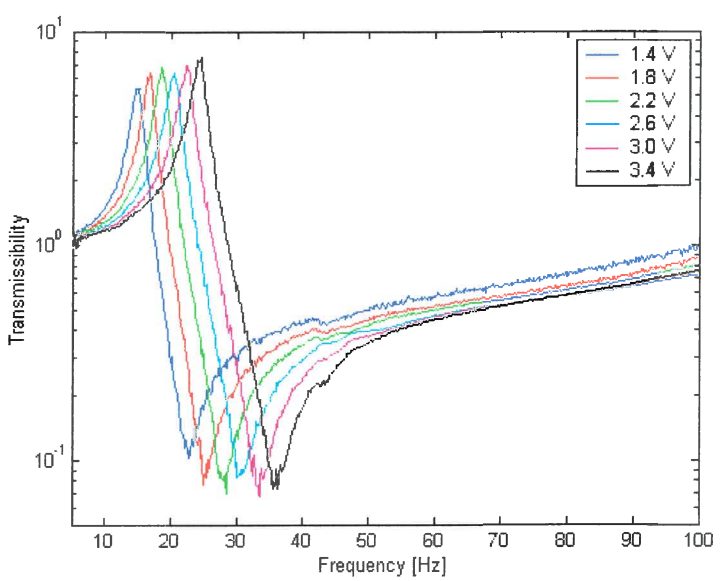

Figure 4. 16 Transmissibility with pressurised water

This time it can be seen that the bump is not present (or rather above 100 Hz). The amount of isolation has improved to about 0.1 and below. This can be seen as a good

amount of isolation. The fact the graphs still have a positive gradient at 100 Hz shows that the second natural frequency is still present but falls above 100 Hz. Therefore it can be assumed that the lower frequencies are not affected too much.

The numerical values of the measured natural and isolation frequencies are the following:

Table 4. 3 Measured natural and isolation frequencies

Voltage	**1.4**	**1.8**	**2.2**	**2.6**	**3.0**	**3.4**
Natural frequency [Hz]	14.625	16.75	18.5	20.375	22.25	24.5
Isolation frequency [Hz]	22.875	25	28.5	30.125	33.5	36.25

If the transmissibility curves for the different stiffness settings are combined to form one graph that shows the region of isolation that can be achieved, the graph in Figure 4. 17 is obtained.

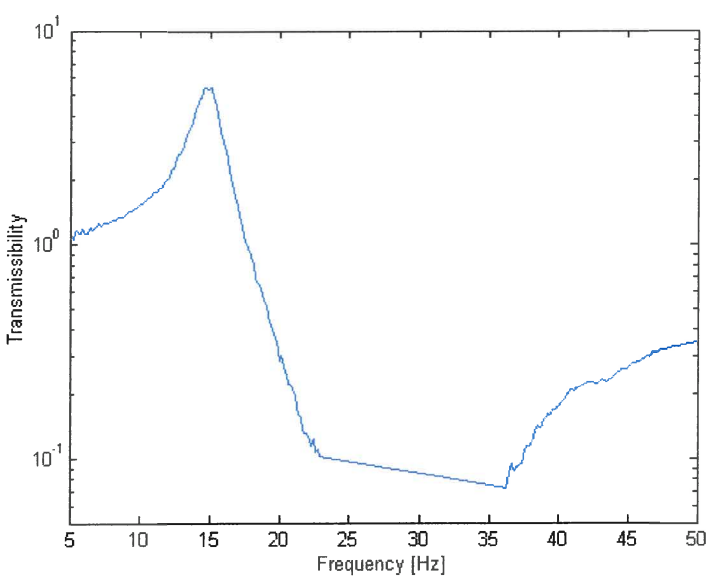

Figure 4. 17 Effective transmissibility of isolator

This gives an indication of what transmissibility the isolator can effectively obtain, although this cannot be obtained simultaneously. It must be mentioned that due to the

high pressure inside the isolator, the water did leak out slowly through the oil seals while in operation. This caused a problem and therefore some of the following tests like the optimisation test was done without the water being pressurised.

The next step is to fit theoretical graphs to these measured graphs to see whether they correlate. It may be suggested that all the parameters have already been obtained in the previous tests (without water) except possibly the viscous damping. This is true for the stiffness and structural damping, but with the addition of the water to the system, mass was added and would probably influence the mass of the isolator. Because it is not known exactly how the water flows inside the isolator, it is not possible to determine theoretically what the new mass of the isolator would be. It will off course be more than 4.287 kg, but could be more than the static mass of the system. Therefore the mass and viscous damping constant will be used as variables to fit theoretical graphs to the measured graphs. All other values will be kept constant as determined previously.

The equation that will be used for the theoretical graphs is the absolute non-dimensional transmissibility amplitude derived in equation (2.21). The equation is the following:

$$|T_r| = \left| \frac{k(1+i\eta) + i\omega c + \omega^2 m_b \left(1 - \frac{A_b}{A_a}\right)\frac{A_b}{A_a}}{k(1+i\eta) + i\omega c - \omega^2 \left[m + m_b \left(\frac{A_b}{A_a}\right)^2 \right]} \right| \tag{4.4}$$

with

$$\zeta = \frac{c}{2\left[m + m_b \left(\frac{A_b}{A_a}\right)^2 \right]\omega_n} \tag{4.5}$$

and

$$\omega_n = \sqrt{\frac{k}{m + m_b\left(\frac{A_b}{A_a}\right)^2}} \tag{4.6}$$

The fits were done with Matlab and results for the 1.8 V measurement are shown in Figure 4. 18. The complete set of results is presented in Appendix D.

It can be seen that the graphs fit very accurately below the isolation frequency, but that the second natural frequency has an influence above the isolation frequency due to the low amplitudes. The values fitted to the graphs are given in Table 4. 4.

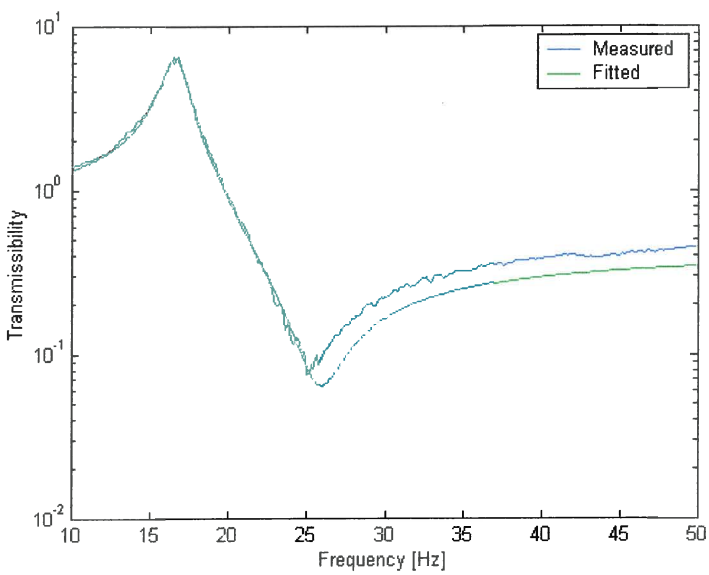

Figure 4. 18 Fitted transmissibility

Table 4. 4 Fitted values

Voltage	**1.4**	**1.8**	**2.2**	**2.6**	**3.0**	**3.4**
Mass [kg]	4.4239	4.4512	4.5271	4.6063	4.5194	4.3896
Viscous damping	0.006	0.00007	0	0.0007	0	0
Stiffness [N/m]	73 328	92 098	115 690	140 530	167 040	193 930
Loss factor	0.0916					

It can be seen that virtually no viscous damping was present and it can be taken as 0 for the lowest damping setting. This shows how effective the design of the isolator is with its round edges and large port. All these tests have been done with the damping mechanism set to its lowest damping setting. To measure the effect of the variable damping mechanism, the transmissibility was measured for each stiffness setting with the damping mechanism set to 0%, 50% and 100% of the angle. This correlates to the plate inside the port being set vertical, at 45 degrees and horizontally respectively.

Figure 4. 19 give the results that were obtained for the 1.4 V stiffness setting.

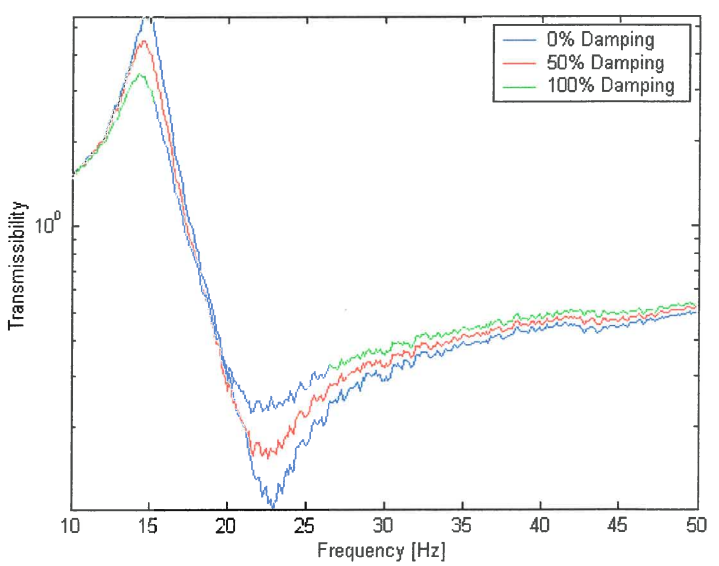

Figure 4. 19 Transmissibility for different damping settings

It can be seen that the variable damping mechanism works quite effectively and that the damping is increased significantly. Graphs were also fitted to the higher damping graphs, with the mass now kept constant at an average 4.486 kg. The only variable was therefore the viscous damping and the results are given in Figure 4. 20.

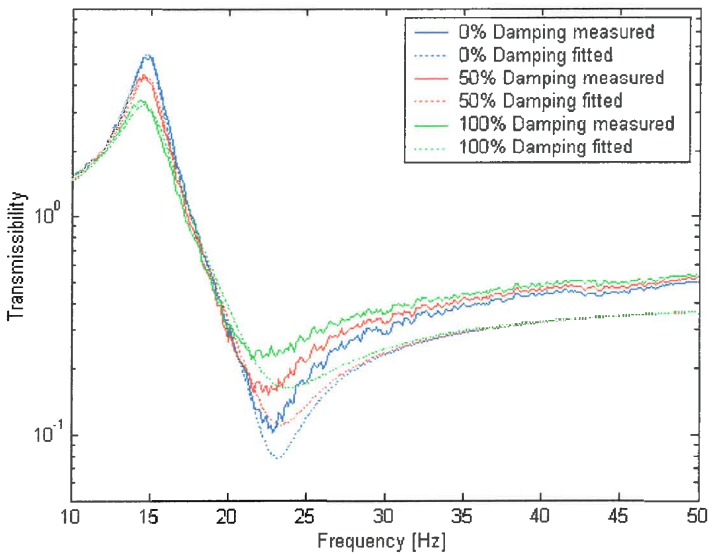

Figure 4. 20 Fitted transmissibility

The complete set of results is presented in Appendix D.

Again the fits are all very accurate below the isolation frequency, but not as good at and above the isolation frequency. The numerical values obtained for the viscous damping ratio are the following:

Table 4. 5 Fitted damping values

Volts	**1.4**	**1.8**	**2.2**	**2.6**	**3.0**	**3.4**
0% Damping	0.006	0.0001	0	0.0008	0	0
50% Damping	0.022	0.013	0.013	0.008	0.008	0.003
100% Damping	0.049	0.039	0.034	0.029	0.025	0.020

The slightly different 0% damping values is due to the constant mass of 4.486 kg that was used for these fits. It can be seen that the viscous damping constant values are quite low but that they increase as the damping is set higher. There is also a trend of a decreasing damping value as the stiffness is increased. This trend can be explained by means of the following equation:

$$\zeta = \frac{c}{2\sqrt{km}} \tag{4.7}$$

If the viscous damping coefficient, c, is taken as constant and the stiffness is increased, then the damping ratio, ζ, must decrease. The following average values for the viscous damping ratio can be determined:

Table 4. 6 Average damping values

0% Damping	0.001
50% Damping	0.011
100% Damping	0.033

The accuracy of these values can be debated due to their small values, but the values obtained show the tendency very clearly.

These tests showed that a successful tunable LIVE isolator has been designed and built. Its isolation frequency can be varied from 22.8 Hz to 36.2 Hz that is a 58.77 % shift in isolation frequency. The amount of isolation achieved at the isolation frequency was 0.078 on average. The damping of the isolator can also be changed with a viscous damping constant ranging from 0.001 to 0.033. The next section will deal with the design and implementation of a control system to automatically tune the isolator to perform optimally for specific excitation conditions.

4.5 Design and implementation of isolator control system

To be able to have a practical isolator, the isolator must be able to automatically tune itself and adapt to certain excitation conditions. The design and implementation of such a control system will be addressed in this section. The purpose is however not to design an optimal control system, but rather to prove that it is possible to implement such a control system and that it works in practice.

In principle the control system must be able to measure the performance of the isolator and must then vary the parameters (stiffness and damping) to obtain the best settings for the current excitation conditions. Thereafter the control system must keep the isolator at those settings and detect when the excitation conditions change and determine new settings. A block diagram of the global design of the control system is shown in Figure 4. 21.

It will be assumed that semi-stationary excitation conditions will be present meaning that the excitation conditions will be constant for a certain period of time to allow for the optimisation.

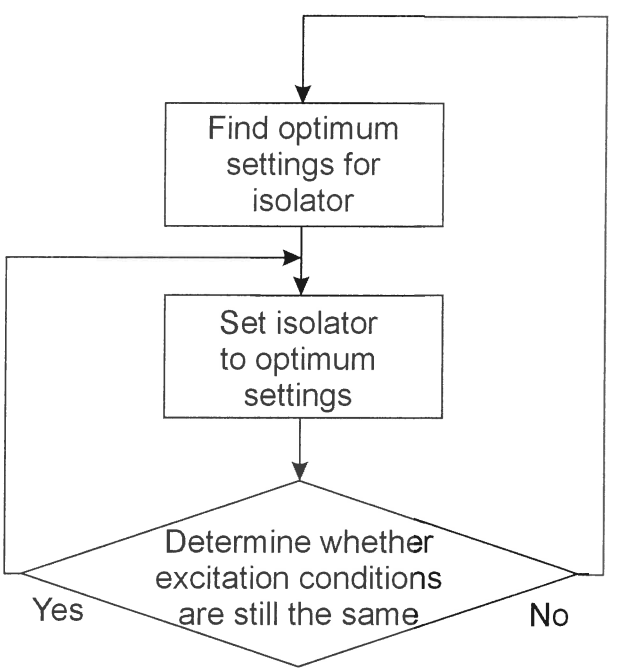

Figure 4. 21 Global design of control system

On implementation of the stepper motor on the variable damping mechanism, it was discovered that the torque needed to turn the shaft was more than what the motor could deliver due to the oil seals' friction. Therefore a gearbox would be needed to turn the shaft. Although possible, it was decided not to solve the problem due to the fact that the principle needed to be proven by the control system will be proven sufficiently by only changing the stiffness.

One parameter that has to be decided on is the criteria that will be used to evaluate the performance of the isolator. This must be a single value that can be used in the optimisation process to determine the performance of the system. Ideally this parameter must not be sensitive to changes in amplitude of excitation, but must be sensitive to frequency changes and changes in the ratio between noise levels and excitation levels. For the parameter to be insensitive to amplitude changes, the input and output signals must be measured and used to determine the parameter instead of only the output. The criterion that was chosen is the RMS ratio. This is calculated as follow:

$$RMS_{Ratio} = \frac{RMS_{Output}}{RMS_{Input}} \tag{4.8}$$

Therefore the time domain signals of the input and output will be measured and their RMS values determined. Then the RMS value of the output will be divided by the RMS value of the input to get the RMS ratio value.

The same experimental setup was used for this test as was used for the transmissibility measurements, except that the two accelerometers were not connected to the Siglab measurement system, but to the analog to digital converter that was used to control the wax actuator. The control system was implemented in Matlab and the optimisation algorithm "fminbnd" was used to determine the optimum stiffness setting for the current excitation. "Fminbnd" is a scalar bound non-linear function minimization. It uses the golden section method as well as parabolic interpolation to determine the minimum of a single variable continuous function.

An upper and lower bound can be supplied for the variable that would be the voltage setting in this case. The bounds were therefore set to 1.4 V and 3.4 V. In each loop of the function the stiffness was set to the desired value and then the time signals of the accelerometers were measured and the RMS ratio determined and sent back to the function. This is then repeated until the minimum RMS ratio has been reached according to certain tolerances. Figure 4. 22 give a graphical representation of the optimisation program.

Because an optimisation algorithm was used, the "guesses" of the stiffness values are actually calculated and not just random guesses. This part of the control system was programmed and tested on the servo-hydraulic actuator. The isolator was excited by different constant frequency sine waves and then the control system was activated and the response was recorded. The control system chose a random stiffness setting at the beginning to be able to get a value to start from and then started to search for the optimum position. Figure 4. 23 show how the RMS ratio improved as the number of iterations increased for the different excitation frequencies.

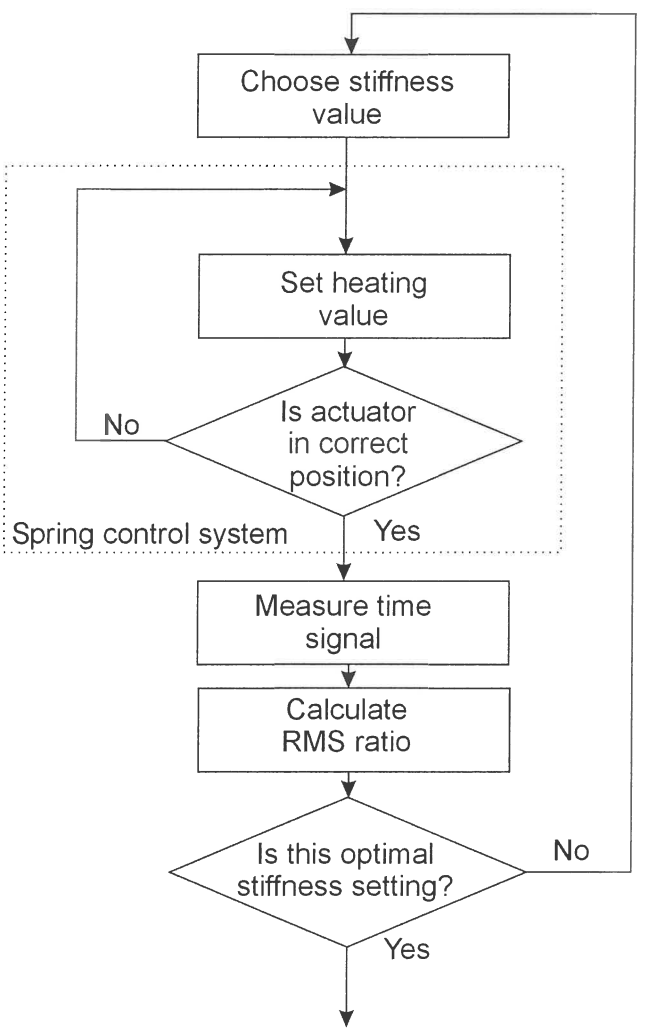

Figure 4. 22 Optimisation program

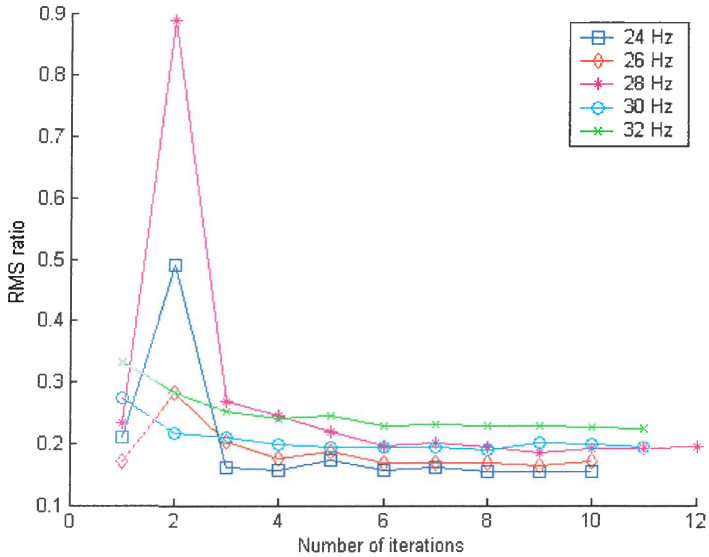

Figure 4. 23 Optimisation performance

Each time the optimal point was reached within 10 to 12 iterations. The RMS ratio values may seem a bit high, but it must be remembered that this is overall RMS values and not only at the isolation point. Although the servo-hydraulic actuator is supposed to excite the isolator only at a single constant frequency, other frequencies may also be excited. More significantly, these tests were done without pressurising the water inside the isolator, which decreased the amount of isolation achieved (see Figure 4. 15 and Figure 4. 16).

Numerical values obtained for spring settings and RMS ratio for the different excitation frequencies are the following:

Table 4. 7 Numerical values of optimum settings

Excitation frequency	Voltage setting for spring	RMS ratio
24 Hz	1.83 V	0.15
26 Hz	2.21 V	0.17
28 Hz	2.48 V	0.19
30 Hz	2.85 V	0.19
32 Hz	3.15 V	0.22

If the voltages that was obtained by the optimisation program are compared to the isolation frequency at different voltage settings as obtained from the transmissibility graphs (water not compressed), the graph in Figure 4. 24 is obtained. It can be seen that the results are similar and that it shows that the optimisation algorithm is working correctly and that the optimum setting was found every time.

A part of the control system that still needs to be addressed is the ability to keep the isolator at the determined settings until the excitation conditions change. This can be done by keeping the isolator at the determined settings and monitoring the RMS ratio of the isolator. If excitation conditions change, the RMS ratio will increase due to the fact that the isolator is not tuned to the excitation conditions any more. That is how the control system can sense when the excitation is changing and when the optimisation has to be started again. The whole control system is represented graphically in Figure 4. 25.

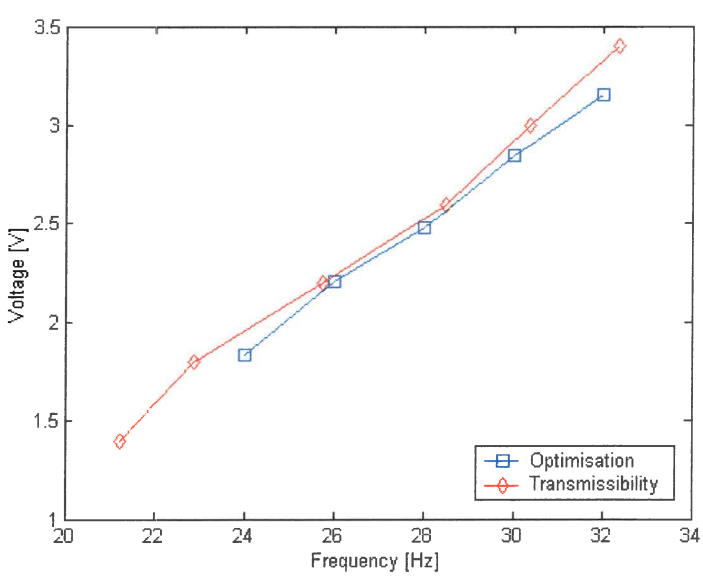

Figure 4. 24 Comparison of isolation frequencies

This control system will therefore keep the isolator at its best settings for the excitation conditions continuously. It is therefore proven that it is possible to implement a control system that can automatically change the settings of the isolator to be optimally tuned continuously. For the control system to change the damping as

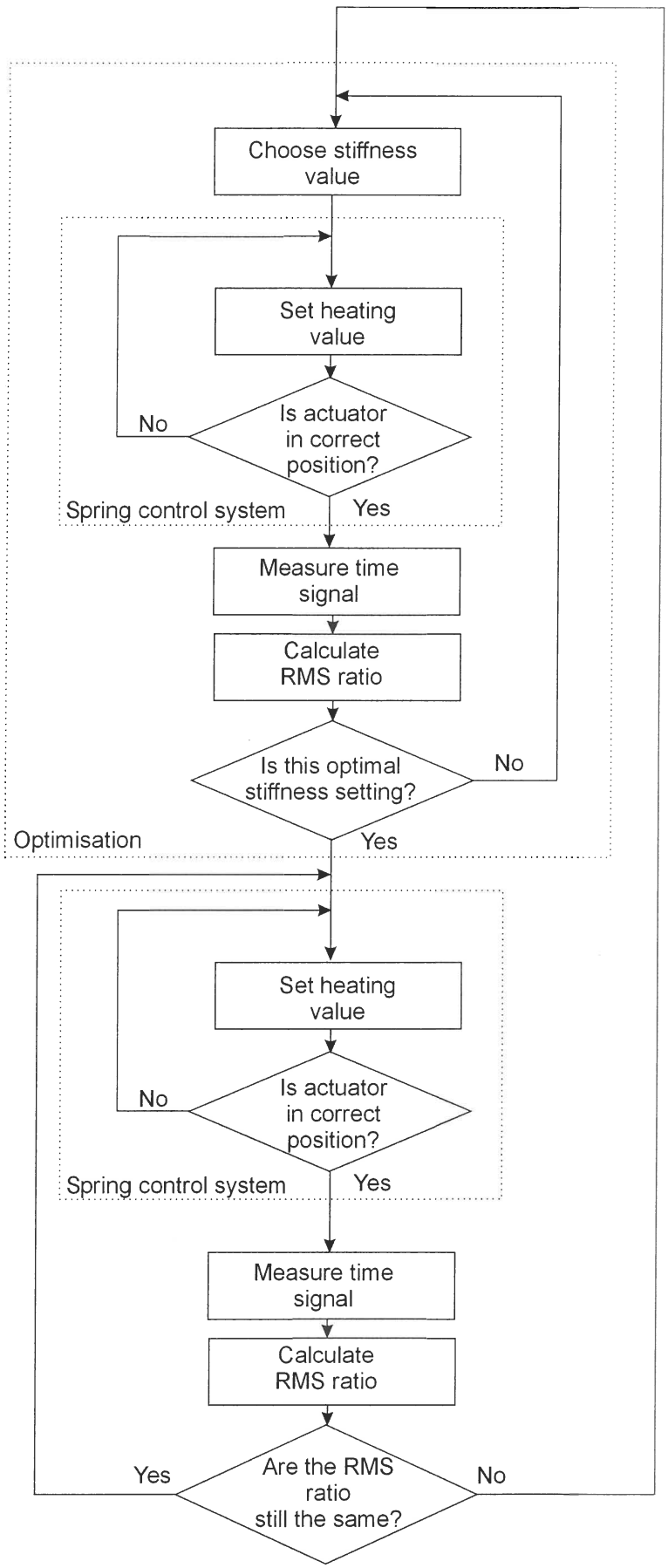

Figure 4. 25 Complete control system

well, it would make the optimisation a two variable optimisation. The whole structure of the control system would stay exactly the same.

4.6 Effect of variable damping

In section 4.4 the effect of the variable damping mechanism on the transmissibility graphs of the isolator was measured as given in Figure 4. 19. To illustrate how this change in damping can practically result in a lower RMS ratio, these graphs will be used to calculate the transmitted vibrations for various excitation conditions. The RMS ratio will be calculated and compared to each other to try and illustrate the gain that can be obtained by varying the damping.

The three graphs in Figure 4. 19 will be used for the calculations. To calculate the RMS ratio, the input and output time signals are needed. A theoretical signal will be created as input signal. This signal must represent tonal excitation together with wide band noise. The transmissibility of the isolator is in the frequency domain and therefore it is necessary to convert the input signal to the frequency domain by means of a FFT. Figure 4. 26 show the input signal that was used in the time and frequency domain. The excitation frequency was 23 Hz, the same frequency as the isolation frequency of the isolator.

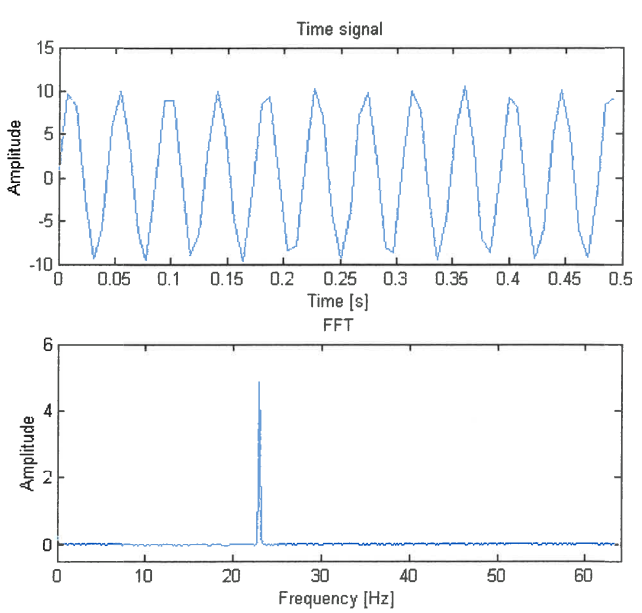

Figure 4. 26 Theoretical input signal with low noise levels

To determine the output FFT of the signal, the FFT in Figure 4. 26 must be multiplied by the transmissibility curves in Figure 4. 19. The result of this is given in Figure 4. 27.

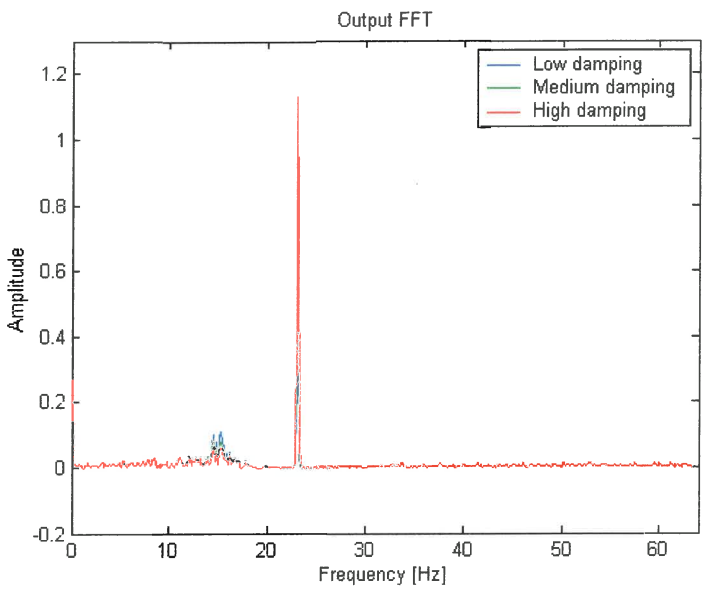

Figure 4. 27 Output FFT with low noise levels

To determine the RMS value of the output, the FFT of the output must be transformed back to the time domain by means of an IFFT. The RMS values of the input and output as well as the RMS ratio were calculated. This procedure was done three times for low, medium and high levels of noise and the results are as follows:

Table 4. 8 RMS ratio

Damping	**Low**	**Medium**	**High**
Low noise	0.076	0.103	0.146
Medium noise	0.201	0.195	0.204
High noise	0.364	0.317	0.278

From the results it is clear that higher damping results in a lower RMS ratio at higher noise levels. It is therefore shown that it is indeed necessary to change the damping to

be able to minimise the transmitted vibration in practical applications where noise is present. The graphs of the medium and high noise levels are presented in Appendix D.

4.7 Conclusion

In this chapter the design of the variable stiffness and damping isolator was addressed. The variable damping mechanism was first designed together with a stepper motor and driver to control the damping. The design of the whole isolator was done, drawings generated for manufacturing and all the parts manufactured. After assembling the isolator, the testing started. First the isolator was tested without water to be able to get accurate values for the stiffness and damping of the spring. After the addition of water the transmissibility of the isolator was measured and theoretical graphs fitted to it. A 58.77% variation in isolation frequency was achieved by shifting the isolation frequency from 22.8 Hz to 36.2 Hz. The viscous damping ratio was also changed from 0.0001 to 0.033. The second last section addressed the design and implementation of a control system to automatically tune the isolator to different excitation conditions. The final result was a tunable vibration isolator that can automatically adapt to changes in excitation conditions. The effect of the variable damping on the RMS ratio was investigated and it was found that the higher damping value did result in a lower RMS ratio value in noisy conditions as was expected.

CHAPTER 5

Conclusion

Vibrating machines are part of modern industry and in some cases the vibratory motion is an integral part of their working mechanism. These machines are therefore not suited to the implementation of a vibration absorber to minimise the vibration of the machine. In such cases it is necessary to make use of vibration isolator that minimise the vibration transmitted from the machine to surrounding bodies without effecting the vibratory motion of the machine. This study was done to develop a tunable vibration isolator that is able to automatically adapt itself to excitation conditions so that it can perform optimally all of the time. The isolator was based on the LIVE concept and it was decided to change the stiffness of the isolator to shift the isolation frequency. A variable damping mechanism was also designed and implemented to be able to control noise.

A variable stiffness spring was developed for implementation on the LIVE isolator. After investigation of different concepts, a compound leaf spring was chosen as a suitable concept for the spring. Circular springs were designed and manufactured to form the leafs of the spring. A wax actuator was used to separate the springs in the middle to obtain the stiffness change. The wax actuator was controlled by a closed loop displacement and velocity feedback system to form a smart actuator that could be controlled by a computer. The variable stiffness spring that was developed was capable of a change in stiffness of 2.7 times which is sufficient for implementation in a LIVE isolator. The spring was practical and the circular design made it suitable for the LIVE isolator.

The LIVE isolator was designed by using the derived equation for the transmissibility and isolation frequency. Equations for the damped natural and isolation frequency were also derived. A variable damping mechanism was implemented that consisted of a plate that was mounted in the tuning port of the isolator. Changing the angle of the plate caused a change in the damping of the isolator. The isolator was characterised in the laboratory on a servo-hydraulic actuator to determine the effect of the stiffness and damping change. The transmissibility functions were measured for all the different stiffness and damping settings. The variable stiffness resulted in a 58% shift in the isolation frequency from 22.8 Hz to 36.2 Hz. An isolation of 10% and lower was achieved over the whole stiffness range. The variable damping mechanism changed the viscous damping ratio from 0.001 to 0.033. The

effectiveness of the higher damping on the RMS ratio in noisy conditions was also illustrated.

A control system was developed to change the parameters of the isolator automatically and to tune the isolator optimally to various excitation conditions. The control system changed only the stiffness, but illustrated that it is possible to optimise the RMS ratio of the isolator by changing the parameters while in operation. The control system found the optimum settings and kept the isolator at that settings until the excitation conditions changed.

It is therefore concluded that a successful tunable vibration isolator was built which is able to automatically change its stiffness to adapt to excitation conditions. The isolator was able to isolate quite a wide range of frequencies, although not simultaneously. The objectives of this project were met, with exception that the damping was not automatically changed.

Future work that may be conducted would include a in depth study of the wax actuator to try and incorporate the heating and cooling elements inside the actuator, making it a very compact actuator. Response time of the actuator can be improved by using more effective ways of heating and especially cooling. Other work would be to find other more effective ways of separating the compound leaf spring to achieve better results. The control system can be developed further to include the damping control. Other applications for the variable stiffness spring could also be investigated. The design of the LIVE isolator with rolling diaphragms showed that it worked well and that opens the field to use any type of spring externally on such an isolator that could improve its performance.

References

Baz, A., Iman, K. & McCoy, J. 1990. The dynamics of helical shape memory actuators, *Journal of Intelligent Material Systems and Structures,* Vol. 1, January, p. 105-133.

Braun, D. 1980. Development of anti-resonance force isolators for helicopter vibration reduction, *Sixth European Rotocraft and Powered Lift Aircraft Forum,* Bristol, England, September 16-19, Paper no. 18, p. 1-17.

Bo, Z. & Lagoudas, D.C. 1995. A unified thermodynamic constitutive model and finite element analysis of active metal matrix composites, *Active Materials and Smart Structures,* SPIE Vol. 2427, p. 276-288.

Brennan, M.J., Elliot S.J., Long, T. 1996. Automatic control of multiple vibration neutralisers, *Proceedings of Inter-noise,* Vol 96. p.1597-1602.

Brennan, M.J. 2000. Actuators for active vibration control – Tunable resonant devices, *Applied Mechanics and Engineering,* Vol. 5, No. 1, p.63-74.

Carlson, J.D. & Weiss, K.D. 1995. Magnetorheological materials based on alloy particles, *U.S. Patent 5,382,373.*

Chen, Q. 1999. Development of mesoscale actuator devices with microinterlocking mechanism, *Mechanical and Aerospace Engineering Department, University of California.*

Davis, L.C. 1999. Model of magnetorheological elastomers, *Journal of Applied Physics,* Vol. 85, Nr. 6, p. 3348 – 3351.

Desjardins, R.A. & Hooper, W.E. 1976. Rotor isolation of the hingeless rotor B0-105 and YUH-61A helicopters, *2nd European Rotorcraft and Powered Lift Aircraft Forum,* Buckeburg, F.R.G., September, Paper no. 13, p. 1-13.

Desjardins, R.A. & Hooper, W.E. 1980. Antiresonant rotor isolation for vibration reduction, *Journal of the American Helicopter Society,* Vol. 25, no. 3, July, p.46-55.

Dorf, R.C. & Bishop, R.H. 1995. *Modern Control Systems,* Addison-Wesley Publishing Company, Inc.

Du Plooy, N.F., 1999. The development of a vibration absorber for vibrating screens, *M. Eng, University of Pretoria.*

Duerig, T.W., Melton, K.N., Stockel, D. & Wayman, C.M. 1990. *Engineering Aspects of Shape Memory Alloys,* Butterworth-Heinemann Ltd.

Dyke, S.J., Spencer Jr., B.F., Sain, M.K.& Carlson, J.D. 1996. Modeling and control of magnetorheological dampers for seismic response reduction, *Smart Materials and Structures*, Vol. 5, August, p. 565-575.

Feng, Z.C. and Li, D.Z. 1996. Dynamics of a mechanical system with a shape memory alloy bar, *Journal of Intelligent Material Systems and Structures,* Vol 7 July, p.399-410.

Flanneley, W.G. 1966. The dynamic anti-resonant vibration isolator, *22nd Annual AHS National Forum,* Washington, p.153-158.

Flatau, A.B., Dapino, M.J., Calkins, F.T. 1998. High bandwidth tunability in a smart vibration absorber, *SPIE Smart Structures and Materials Conf,* Paper #3329-19/3327-42.

Flower, W.C. 1985. Understanding hydraulic engine mounts for improved vehicle noise, vibration and ride qualities, Technical report 850975, *Society of Automotive Engineers.*

Ford, D.S., Hebda, D.A. & White, S.R. 1995. Constitutive and transformation behaviour of TWSM nitinol, *Active Materials and Smart Structures,* SPIE Vol. 2427, p.218-233.

Fosdick, R. & Ketema, Y. 1998. A thermoviscoelastic dynamic vibration absorber, *Journal of Applied mechanics,* Vol. 65, March, p.17-24.

Franchek, M.A., Ryan, M.W., Bernhard, R.J. 1995. Adaptive passive vibration control, *Journal of Sound and Vibration,* Vol. 189, No. 5, p.565-585.

Ginder, J.M., Nichols, M.E., Elie, L.D., Clark, S.M. 2000. Controllable-stiffness components based on magnetorheological elastomers, *Proceedings of SPIE Smart Structures and Integrated Systems,* Vol. 3985, March, p.418-425.

Ginder, J.M., Nichols, M.E., Elie, L.D., Tardiff, J.L. 1999. Magnetorheological elastomers: Properties and applications, *SPIE Conference on Smart Materials Technologies,* Vol. 3675 p. 131 – 138.

Halwes, D.R. & Simmons, W.A. 1980. Vibration suppression system, *U.S. patent no. 4,236,607.*

Halwes, D.R. 1981. Total main rotor isolation system analysis, Bell helicopter textron, *NASA Contractor Report No. 165667.* Langley Research Center, Hampton, Virginia, June.

Herakovic, N. 1998. Smart actuators in robotics, *University of Ljubljana*

Hodgson, D.A. & Duclos, T.G. 1991. Vibration isolator with electrorheological fluid controlled dynamic stiffness, *U.S. Patent 5,029,823*

Hodgson, D.E., Wu, M.H. & Biermann, R.J. 1999. Shape memory alloys, *http://www.sma-inc.com/SMAPaper.html*

Hooker, M.W. 1997. Properties and performance of RAINBOW piezoelectric actuator stacks, *Smart Materials and Structures : Industrial and Commercial Applications of Smart Structures Technologies*, Proc. SPIE vol. 3044, p. 413-420.

Janker, P. 1998. Development of high-performance piezoelectric actuators for transport systems, *Daimler-Benz AG Research and Technology*

Jolly, M.R., Carlson, J.D., Munoz, B.C., Bullions, T.A. 1996a. The magnetoviscoelastic response of elastomer composites consisting of ferrous particles embedded in a polymer matrix, *Journal of Intelligent Material Systems and Structures,* Vol. 7 p. 613 – 622.

Jolly, M.R., Carlson, J.D., Munoz, B.C. 1996b. A model of the behaviour of magnetorheological materials, *Smart Material Structures,* Vol. 5 p. 607-614.

Ketema, Y. 1998. A viscoelastic dynamic vibration absorber with adaptable supression band: A feasibility study. *Journal of Sound and Vibration,* Vol. 216, No. 1, p.133-145.

Liang, C. & Rogers, C.A. 1993. Design of shape memory alloy springs with applications in vibration control, *Journal of Vibration and Acoustics,* Vol. 115, January, p. 129-135.

Lin, R. 1996. Shape memory alloys and their applications, *http://www.stanford.edu/~richlin1/sma/sma.html*

Lin, H.C., Wu, S.K. & Yeh, M.T. 1993. Damping characteristics of TiNi shape memory alloys. *Metallurgical Transactions,* Vol. 24A, October, p. 1993-2189.

Longbottom, C.J. & Rider, M.J.D.E. 1987. A self-tuning vibration absorber, *UK Patent,* GB 2189573 B, London.

Mashinostroeniya, V. 1987. Variable-stiffness springs with packs of cylindrical panels, *Soviet Engineering Research,* Vol. 67, Issue 4, p. 44-47.

Maw, A.N. 1991. The design of resilient mounting systems to control machinery noise in buildings. *Plastics, Rubber and Composites Processing and Applications*, Vol. 18, No. 1, p.9-16.

McKeown, W.L., Smith, M.R. & Stamps, F.B. 1995. Hydraulic inertial vibration isolator, *U.S. Patent 5,439,082*

Meghdari, A., Jafarian, M., Mojarrad, M. & Shahinpoor, M. 1993. Exploring artificial muscels as actuators for artificial hands, *Intelligent Structures, Materials and Vibrations,* ASME, Vol. 58, p. 21-26.

Monkman, G.J. 2000. Advances in shape memory polymer actuation, *Mechatronics,* Vol. 10, p. 489-498.

Nagem, R.J., Madanshetty, S.I., Medhi, G. 1997. An electromechanical vibration absorber, *Journal of Sound and Vibration,* Vol. 200, no. 4, p.551-556.

Ogontz Corporation. 1998. The wax actuator, *http://www.ogontz.com/html/wax_tech.html*

Onoda, J., Sano, T., Kamiyama, K. 1992. Active, passive, and semiactive vibration supression by stiffness variation, *AIAA Journal,* Vol. 30, No. 12, December, p. 2922-2929.

Rao, S.S. 1995. *Mechanical Vibrations,* 3rd Edition, New York: Addison Wesley.

Raw, S. 1999. Ergonomic hand-grip for attenuating vibrations in hand-held power tools, *Health an Safety,* May.

Ribakov, Y. & Gluck, J. 1998. Optimal design of base isolated active controlled MDOF structures, *ISMA 23.*

Rita, A.D., McGarvey, J.H., Jones, R. 1976. Helicopter rotor isolation utilizing the dynamic antiresonant vibration isolator. *32nd Annual AHS National Forum,* Washington, May, p. 22-29.

Segalman, D.J., Parker, G.G. & Inman, D.J. 1993. Vibration suppression by modulation of elastic modulus using shape memory alloy, *Intelligent Structures, Materials and Vibrations,* ASME, Vol. 58, p. 1-5.

Seto, K. & Yamanouch, M. 1978. On the effect of a variable stiffness-type dynamic absorber with eddy-current damping, *Bulletin of the JSME*, Vol. 21, No. 160, October, p.1482-1489.

Siler, D. & Demoret, K.B. 1996. Variable stiffness mechanisms with SMA actuators, *SPIE,* Vol. 2721, p. 427-435.

Simrit. Standard Catalogue Standard Range Part A, *Freudenberg*

Smith, K.E. 1991. Smart tuned mass dampers, *Proceedings of ADPA/AIAA/ASME/SPIE Conference on Active Materials and Adaptive Structures.*

Smith, M.R. & Stamps, F.B. 1995. Vibration isolation system, *U.S. Patent 5,435,531*

Smith, M.R. & Stamps, F.B. 1998. Vibration isolation system, *U.S. Patent 5,788,029*

Stalmans, R. & Van Humbeeck, J. 1995. Shape memory alloys: Functional and smart, *Smart Materials and Technologies – Sensors, Control Systems and Regulators,* October, Prague, Czech Republic, http://www.mtm.kuleuven.ac.be/Research/ADAPT/publicat/ShapeMemory/smatext.htm.

Sun, J.Q., Jolly, M.R. & Norris, M.A. 1995. Passive, adaptive and active tuned vibration absorbers – A Survey. *Transactions of the ASME*, Vol. 117, June, p.234-242.

Tentor, L.B. & Wicks, A.L. 2000. Electromagnetic tuned dynamic vibration absorber – Theoretical foundations, *IMAC 18,* San Antonio, February, p.440-447.

Theron, N.J. 2002. Some notes on first order systems, *University of Pretoria,* February.

Von Flotow, A.H., Beard, A., Bailey, D. 1994. Adaptive tuned vibration absorbers: Tuning laws, tracking agility, sizing, and physical implementations, *Noise-Con 94,* May, p. 437-454.

Walsh, P.L., Lamancusa, J.S. 1992. A variable stiffness vibration absorber for the minimisation of transient vibrations, *Journal of Sound and Vibration,* Vol. 158, No. 2, p.195-211.

Williams, K.A., Chiu, G.T.-C., Bernhard, R.J. 1999. Passive-adaptive vibration absorbers using shape memory alloys, *Proceedings of SPIE Smart Structures and Integrated Systems,* Vol. 3668, March, p.630-641.

Williams, K.A., Chiu, G.T.-C., Bernhard, R.J. 2000. Controlled continuous tuning of an adaptively tunable vibration absorber incorporating shape mamory alloys, *Proceedings of SPIE Smart Structures and Integrated Systems,* Vol. 3984, March, p.564-575.

Witting, P.R. & Cozzarelli, F.A., 1995. Experimental determination of shape memory alloy constitutive model parameters, *Active Materials and Smart Structures,* SPIE Vol. 2427, p. 260-275.

Yu, Y., Naganathan, N.G. & Dukkipati, R.V. 2000. A literature review of automotive vehicle engine mounting systems, *Mechanisms and Machinery Theory,* Vol. 36, p. 123-142.

APPENDIX A

Measurement of spring stiffness and damping

A.1 Theory

Most springs have an amount of structural damping. The only springs without it would probably be magnetic springs or other non-contact type springs. All the springs considered in this study had structural damping and it was necessary to measure this damping very accurately.

Structural damping is a phenomenon where if the spring is excited with sinusoidal excitation, the displacement of the spring and the force transmitted are not in phase as is expected. Furthermore, the force is leading the displacement, which is even more unexpected. Structural damping is usually given as the loss factor η. The loss factor can be related to other constants with the following equations:

$$\eta = \frac{h}{k} \tag{A.1}$$

$$h = c\omega \tag{A.2}$$

Another way in which structural damping is sometimes expressed is tan δ. This can be related to η with the following equation:

$$\eta = \tan\delta = \tan\left(\phi_{Force} - \phi_{Displacement}\right) \tag{A.3}$$

Where ϕ_{Force} and $\phi_{Displacement}$ are the phase angles of the force and displacement signals.

Therefore, it is possible to relate any of the constants to the loss factor, and therefore any constant can be determined out of experimental results. The most obvious way to determine the loss factor is to determine the phase shifts of the force and displacement signals and to determine tan δ. With sinusoidal excitation the force and displacement signals are sine waves and a fit can easily be obtained.

A sine wave is described with the following equation:

$$y(t) = A\sin\left(\omega t + \phi\right) \tag{A.4}$$

A least squares fit can be done to the measured force and displacement signals by substituting the known frequency into ω and to assign A and ϕ as the two variables. Therefore an amplitude A and a phase shift ϕ will be determined for the force signal and the displacement signal. From that the loss factor of the spring can be determined with equation (A.3) and the stiffness of the spring can be determined with:

$$k = \frac{f_{x=X}}{A_x} \tag{A.5}$$

Where $f_{x=X}$ is the force at maximum displacement and A_x is the amplitude of the displacement.

Figure A. 1 explains the whole concept.

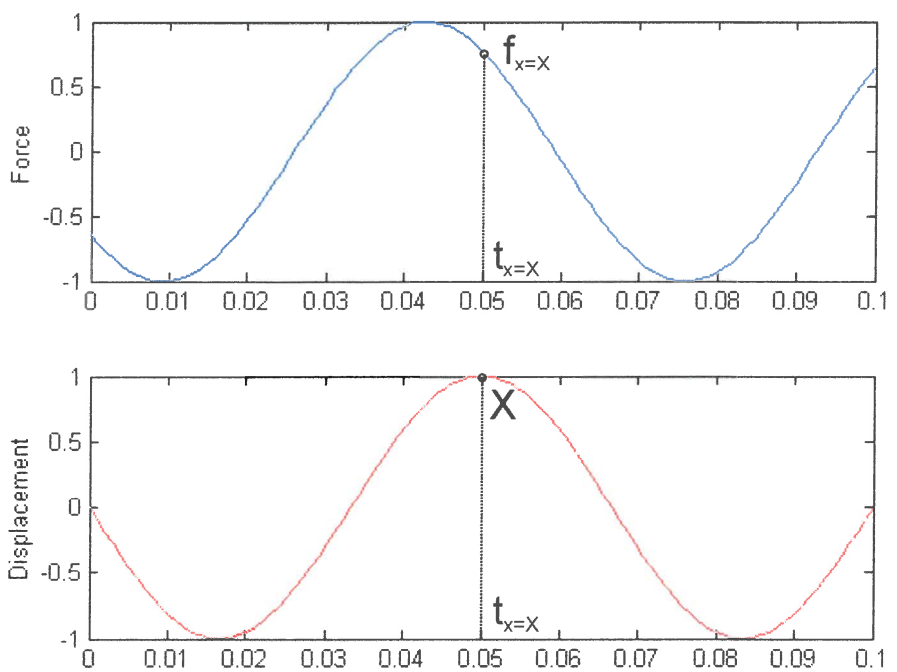

Figure A. 1 Force and displacement time signals

Another method of determining the stiffness and damping, is by using the hysteresis loop method and determining the viscous damping constant *c* and then translating it back to the loss factor.

A hysteresis loop is obtained when the force and displacement are plotted against each other on the same graph. Due to the phase shift, an ellipse is formed. Figure A. 2 explains the concept.

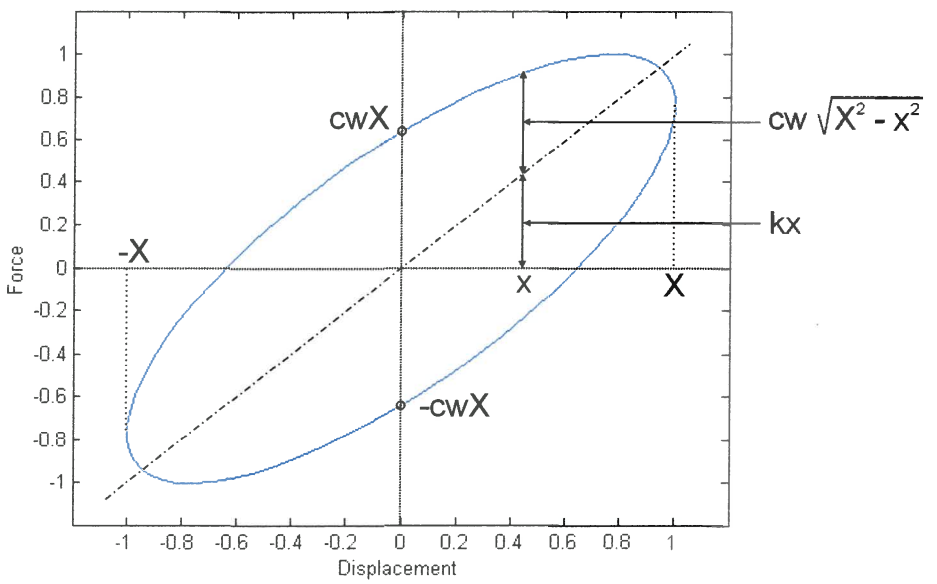

Figure A. 2 Hysteresis loop

The equation of the ellipse can be derived as follow (Rao, 1995):

Consider a spring and viscous damper. The force needed for a certain displacement is:

$$F = kx + c\dot{x} \tag{A.6}$$

For harmonic motion of frequency ω and amplitude X:

$$x(t) = X \sin \omega t \tag{A.7}$$

Combining the equations give:

$$\begin{aligned} F(t) &= kX \sin \omega t + cX\omega \cos \omega t \\ &= kx \pm c\omega\sqrt{X^2 + (X \sin \omega t)^2} \\ &= kx \pm cw\sqrt{X^2 - x^2} \end{aligned} \tag{A.8}$$

From experimental results, the hysteresis loop can be produced. A least squares fit can be done on the hysteresis loop with equation (A.8) and the stiffness k and the

viscous damping constant c can be determined. The loss factor can then be determined with equations (A.2) and (A.1).

A.2 Practical considerations

If the theory is considered, one important practical aspect that comes forward is accurate measurement, especially as far as the phase is concerned.

Let us evaluate the normal laboratory experiment with the measurement transducers that are usually used for these measurements as depicted in Figure A. 3.

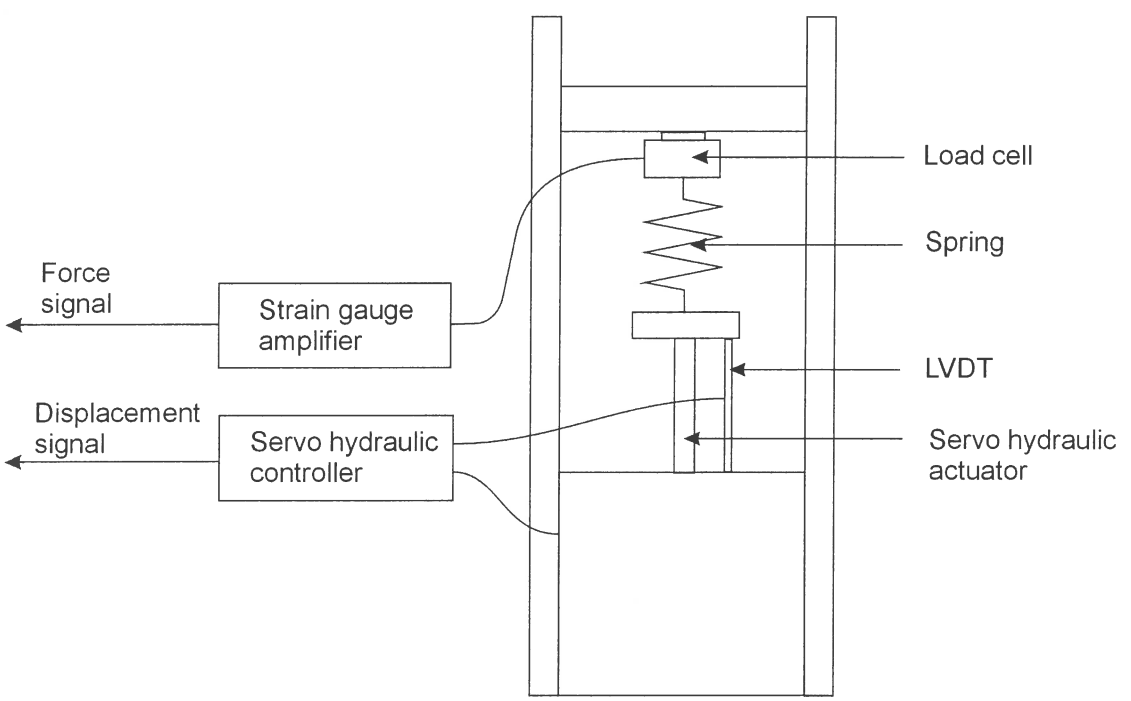

Figure A. 3 Experimental measurement system

As far as the amplitude of the signals are considered, there are no problem with this experimental measurement technique because the transducers are usually calibrated and should be accurate. If the phase of the signals is considered, there seems to be some amount of confusion. The reason for this is that the strain gauge amplifier and servo hydraulic controller with its LVDT amplifier are seen as black boxes and it is unknown what exactly is happening inside them. To try and find out what exactly is

done to the signals is also a fruitless exercise. If the basic principal of strain gauge (or LVDT) amplifiers is considered, it comes to light that all of them have some sort of filter in them. These filters' characteristics are unknown and can sometimes be altered by the user by setting cut-off frequencies etc. Let us consider the characteristics of a 4th order Butterworth filter shown in Figure A. 4.

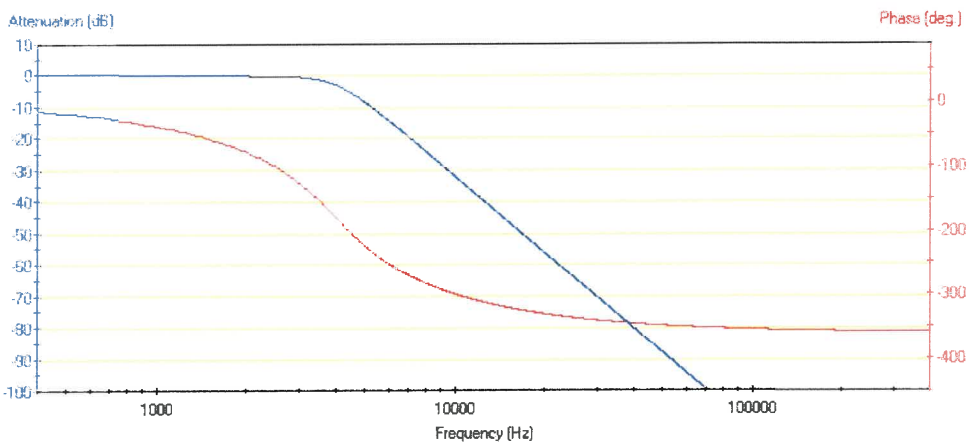

Figure A. 4 Characteristics of a 4th order Butterworth filter

It can be seen that the amplitude is not altered below the cut off frequency, but that is certainly not the case with the phase. There is a phase shift from 0 Hz onwards and it is also not constant over frequency, not even in a certain region. This causes a problem for damping measurements because it is exactly this phase shift that is measured to determine the amount of damping. A filter would therefore alter the measured damping considerably.

It is therefore noted that the most widely accepted way of measuring force and displacement yielded the wrong values and that a very specific measuring technique must be used to accurately measure the damping of a spring. The only way in which this way of measuring could be accurate, is if the phase shift of the strain gauge amplifier and the LVDT amplifier is the same. It is possible, especially when the strain gauge amplifier in the controller is used for the load cell instead of an external amplifier as shown in the sketch, but it must first be confirmed. There could still be a phase shift due to the internal working mechanism of an LVDT, which would not be present in the strain gauges in the load cell.

To accurately measure the damping of a spring, there are two possibilities. Either transducers with zero phase shift must be used, or the phase shift of the two transducers must be exactly the same. The first option is not practically possible, so the phase shift of the transducers must be kept exactly the same. As mentioned above, an LVDT could have some phase shift internally so it will not be an option. The only way to be sure that the two transducers will respond identically is if both worked on the same principle. Therefore a strain gauge displacement transducer was used for the measurements. The load cell and strain gauge displacement transducer were amplified with the same HBM MGC strain gauge amplifier with both channels set to a 400 Hz Bessel filter. This would ensure exactly the same phase shift on both transducers and would therefore yield an accurate damping value.

APPENDIX B

Determining separation force

B.1 Separation force

The separation force is defined as the force needed to keep the two leaf springs apart in the centre. In FEM tests, the stiffness of the individual springs is known and it is necessary to determine the separation force from that.

Consider a single spring with the following characteristic:

Table B. 1 Spring characteristics

Displacement	Force
1 mm	100 N
2 mm	220N
3 mm	360 N
4 mm	520 N
5 mm	700 N

Now it is desirable to determine the stiffness of a compound spring separated by different amounts and also the separation force needed to separate the two springs. This can be done as follows:

Let us assume the compound spring is displaced 1mm upwards in the centre from its neutral position for different separation distances. The following table can then be compiled:

Table B. 2 Spring forces

Separation	Force on top spring	Force on bottom spring
2 mm	220 N	0 N
4 mm	360 N	100 N
6 mm	520 N	220 N
8 mm	700 N	360 N

Let us consider the situation graphically in Figure B. 1.

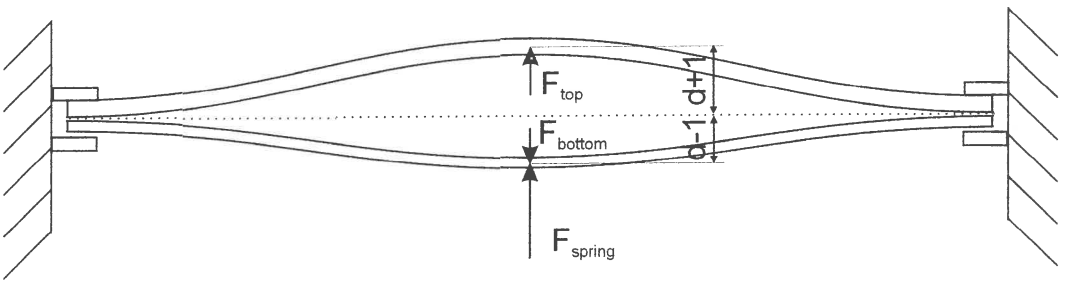

Figure B. 1 **Separation forces**

The actuator is located between the two springs and therefore the separation force will be the same on the two springs. In the case shown in Figure B. 1 it will be equal to the force on the top spring. The stiffness of the compound spring will be the spring force divided by the displacement of the spring (1 mm). The resultant force on the bottom spring must be F_{bottom}. Therefore the spring force will be:

$$F_{spring} = F_{separation} - F_{bottom} = F_{top} - F_{bottom} \tag{B.1}$$

If the above tables are extended the following values will be obtained:

Table B. 3 **Stiffness of spring**

Separation	Stiffness	Separation Force
2 mm	220 000 N/m	220 N
4 mm	260 000 N/m	360 N
6 mm	300 000 N/m	520 N
8 mm	340 000 N/m	700 N

In this way it is not necessary to measure separation force because it can be calculated from the stiffness of a single spring.

APPENDIX C

Stepper motor

A stepper motor consists of a magnetic rotor and a lot of windings on the outer stator. The windings on the outside are usually arranged in groups of four so that the groups alternate as you go round. It is illustrated graphically in Figure C. 1.

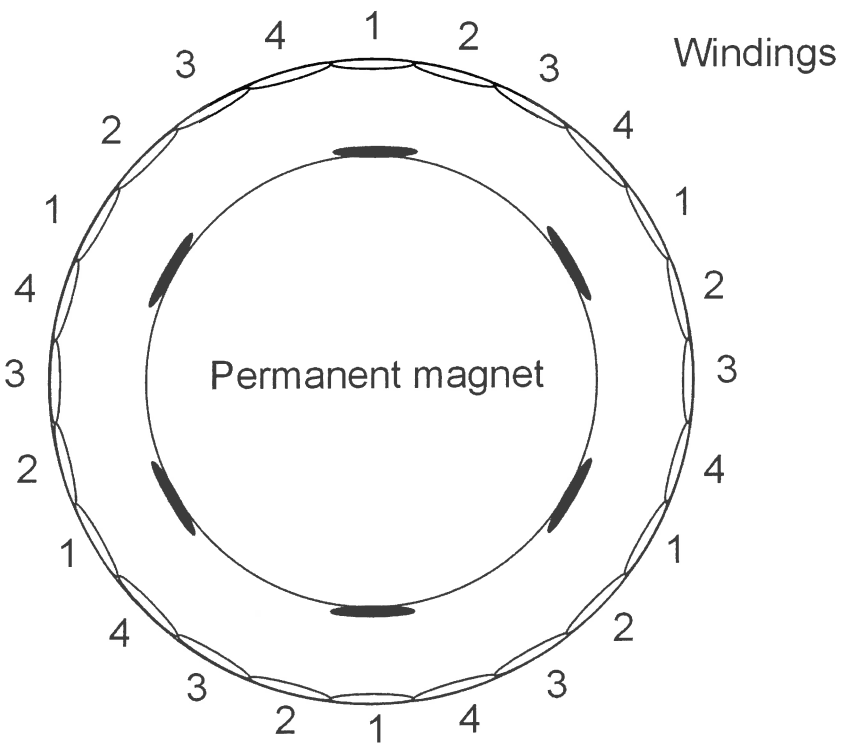

Figure C. 1 Working of a stepper motor

When the first group of windings are activated, all the windings with the number 1 are energised and the permanent magnet is pulled into the orientation as shown above. To let the motor turn 1 step clockwise, the second group of windings are energised so that the permanent magnet will be pulled one step clockwise so that all its poles will be pointing to a number 2 winding. All stepper motors work like this with the only difference being the total number of steps per revolution. This will off course always be a multiple of 4 and common values are 48 or 72 steps per revolution.

With this concept understood, it can be seen that it is very easy to control the motor accurately. To let the motor rotate clockwise, the coils must be energised as follows:

Table C. 1 Clockwise rotation

Step	Coil 1	Coil 2	Coil 3	Coil 4
1	1	0	0	0
2	0	1	0	0
3	0	0	1	0
4	0	0	0	1
5	1	0	0	0
6	0	1	0	0

For anticlockwise movement, the order will be as follows:

Table C. 2 Anticlockwise rotation

Step	Coil 1	Coil 2	Coil 3	Coil 4
1	1	0	0	0
2	0	0	0	1
3	0	0	1	0
4	0	1	0	0
5	1	0	0	0
6	0	0	0	1

It is also possible to use sub-steps to let the motor turn very slowly, but accurately. This can be done as follows:

Table C. 3 Sub-step rotation

Step	Coil 1	Coil 2	Coil 3	Coil 4
1	1	0	0	0
2	1	1	0	0
3	0	1	0	0
4	0	1	1	0
5	0	0	1	0
6	0	0	1	1

When two adjacent coils are energised, the permanent magnet will stop in-between the coils and that is called a sub-step. Sub-steps are only used while the motor is turning and must not be used to keep the motor stationary.

The last utility that can be used is high torque rotation. It can be achieved as follows:

Table C. 4 High torque rotation

Step	Coil 1	Coil 2	Coil 3	Coil 4
1	1	1	0	0
2	0	1	1	0
3	0	0	1	1
4	1	0	0	1
5	1	1	0	0
6	0	1	1	0

Because two coils are energised each time, the force on the permanent magnet is increased and results in a higher torque during rotation.

A very important thing to remember about stepper motors is that they can and will slip if the torque required is too large. This results in a loss of position and usually causes problems. Therefore it is important to ensure that the required torque does not exceed the capabilities of the motor.

To control a stepper motor, some sort of controller or driver is obviously necessary. There are two possibilities, a stepper motor driver or using a computer directly. A stepper motor driver is usually used when more than two stepper motors are used. The reason for this is that it is much cheaper and easier to use a computers parallel port to directly control the coils of the stepper motor. The problem is that there are only 8 channels on a parallel port and therefore only two motors can be controlled. A stepper motor driver uses a serial link to a computer that sends the direction and number of steps for each motor to the controller and the controller does the rest by activating the coils in the correct order. These controllers are quite expensive and are

not easily obtainable, so because only one motor needed to be controlled, the parallel port of a computer was used to do the control.

To control one motor, only 4 channels on the parallel port were used, one for each group of windings. The parallel cannot supply the necessary current to drive the motor, so some kind of driver must be used to supply the current. This driver must have at least 4 channels and must be able to supply the required current. A ULN 2003 transistor array IC was used. It is a 7-channel driver and can supply 0.5 A current in total. It can be triggered directly from the parallel port and no other components are required. LED's were added on the 4 channels to indicate which channels are active. The IC has to be supplied with external power to drive the motor. The circuit is depicted in Figure C. 2.

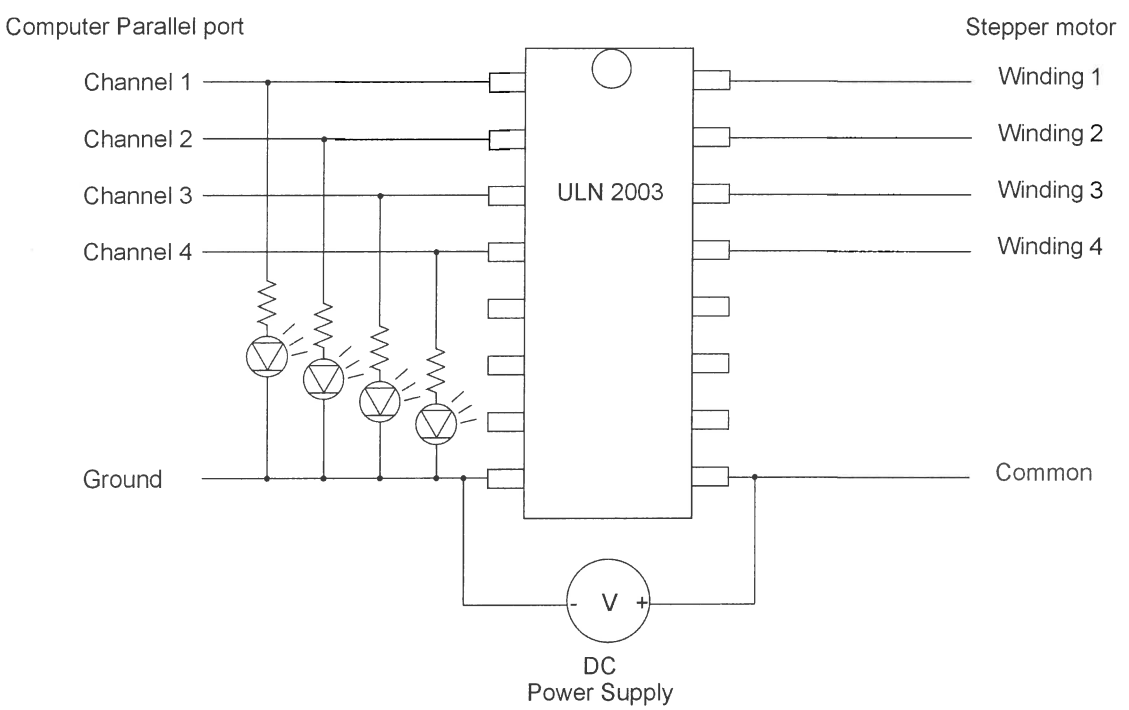

Figure C. 2 Stepper motor driver

If the stepper motor itself is considered, there are usually 6 wires of different colours. The reason for the 6 wires is that 2 sets of windings are connected to the same ground or common. Therefore a multimeter can be used to determine the layout of the wires. The two common wires can be connected to the common on the circuit above and the

other wires to the winding connections. If the wires are connected in the wrong order, the motor will not turn continuously, but jump around.

Once the motor is connected, a Matlab program downloaded from the Internet (http://www.isibrno.cz/~ivovi/matlab.htm) allows you to give output to the parallel port of the computer and the stepper motor can be controlled. To do angular position control, the number of steps per revolution of the motor must be counted and then the angle per step calculated. Once the current position of the motor is known, it can be positioned in any way by letting it move the correct number of steps.

APPENDIX D

Isolator test results

D.1 Transmissibility without water

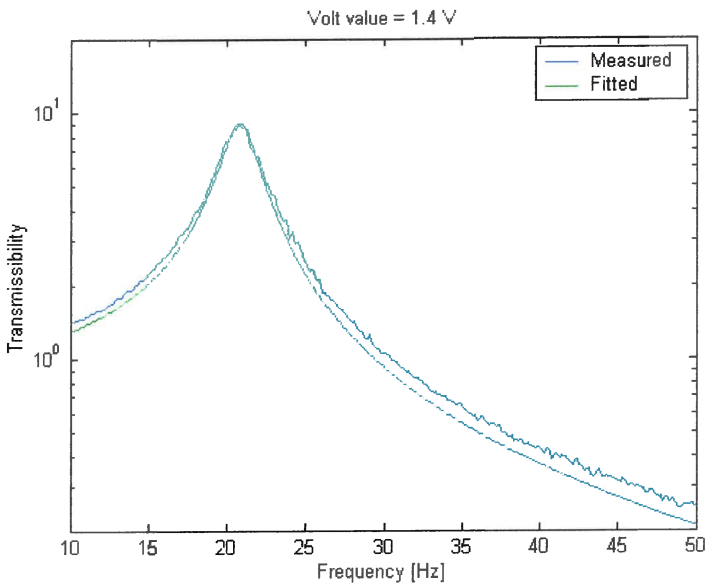

Figure D. 1 **Transmissibility – 1.4 V**

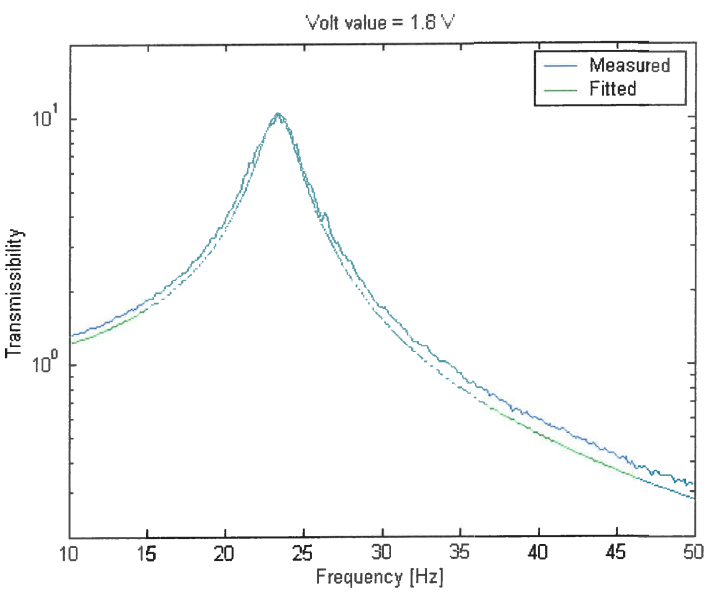

Figure D. 2 **Transmissibility – 1.8 V**

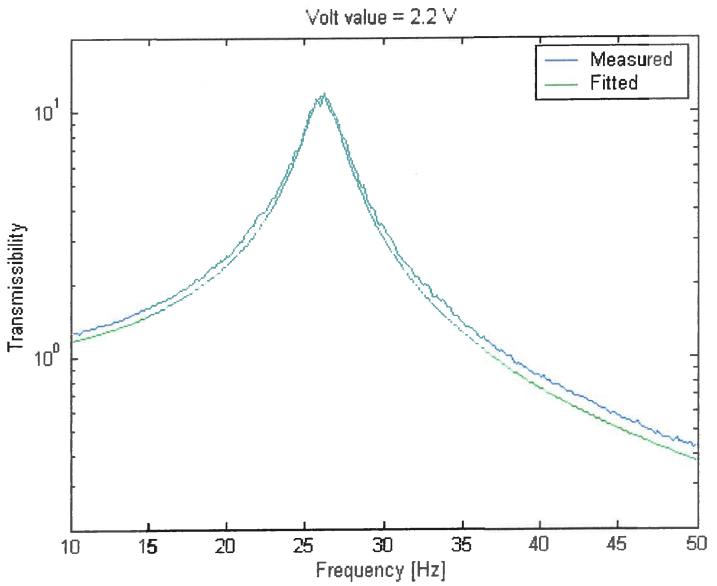

Figure D. 3 Transmissibility – 2.2 V

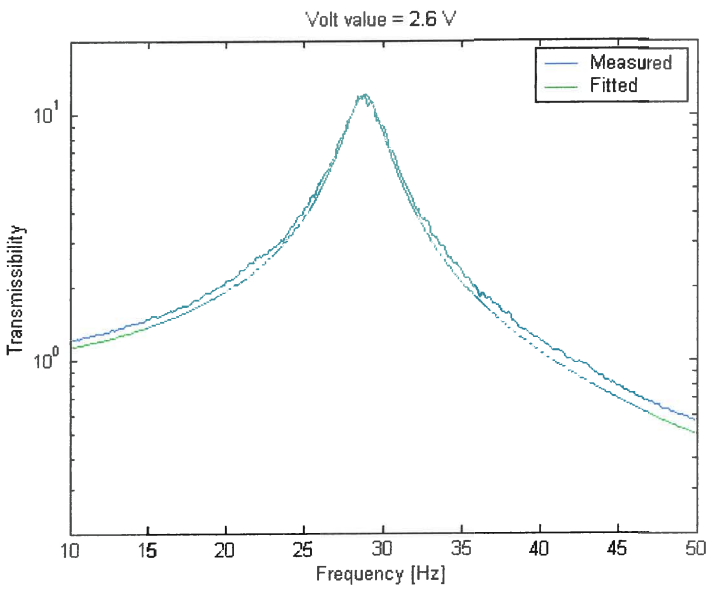

Figure D. 4 Transmissibility – 2.6 V

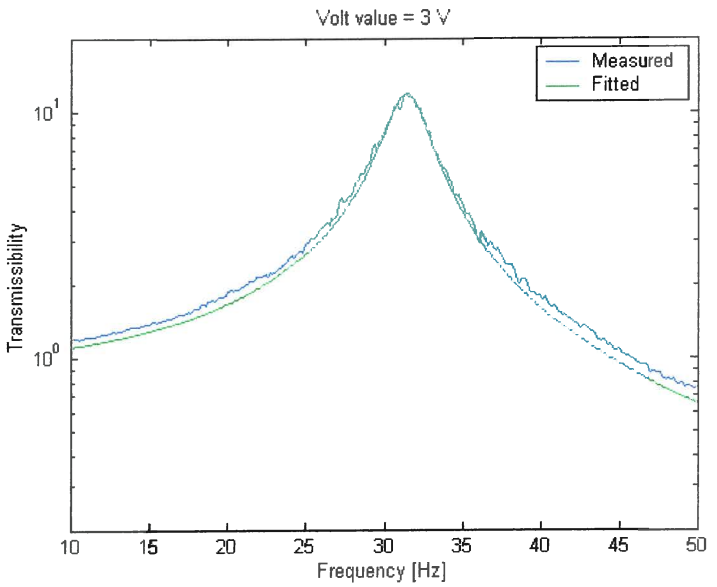

Figure D. 5 Transmissibility – 3.0 V

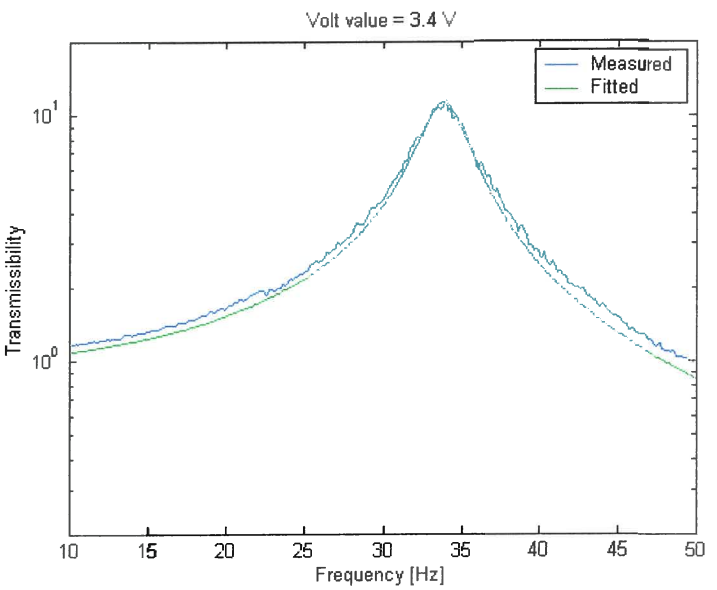

Figure D. 6 Transmissibility – 3.4 V

D.2 Transmissibility with water

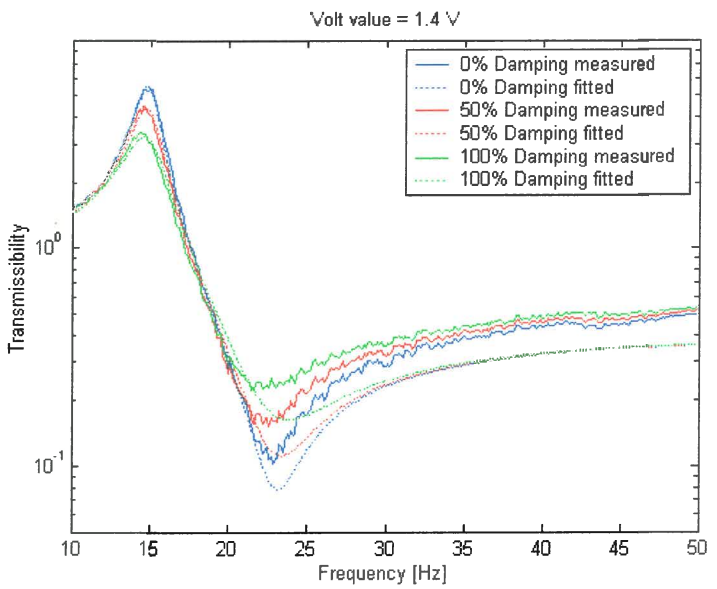

Figure D. 7 Transmissibility – 1.4 V

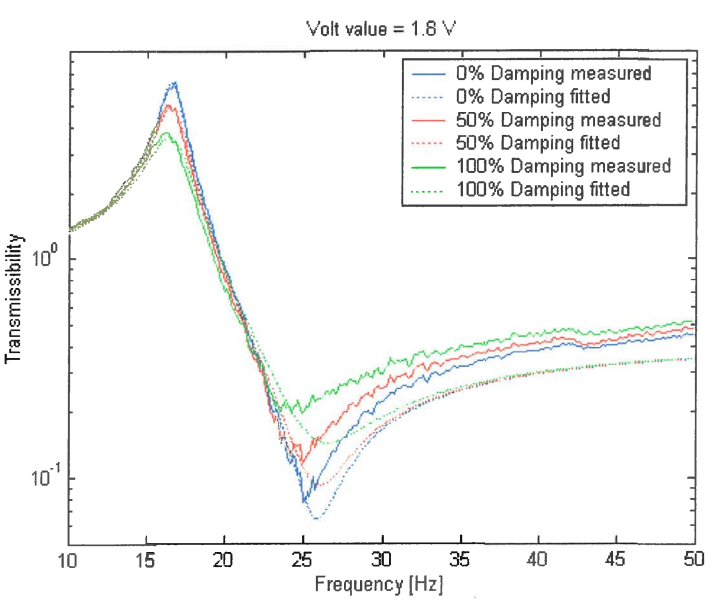

Figure D. 8 Transmissibility – 1.8 V

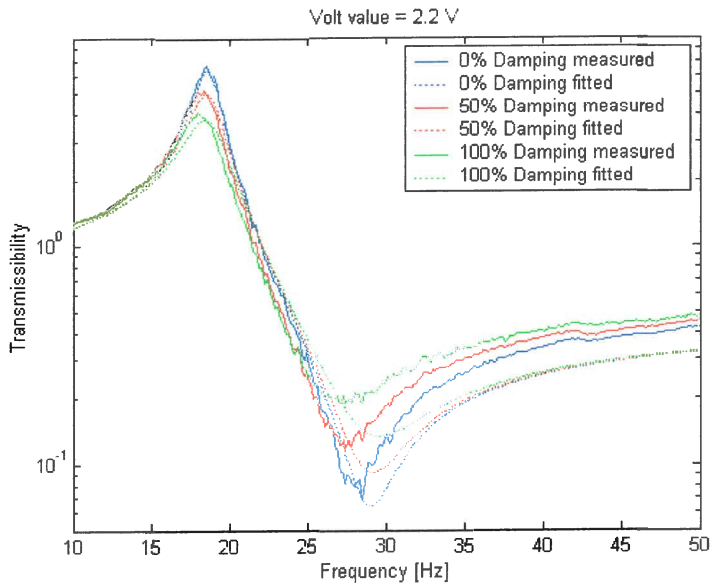

Figure D. 9 **Transmissibility – 2.2 V**

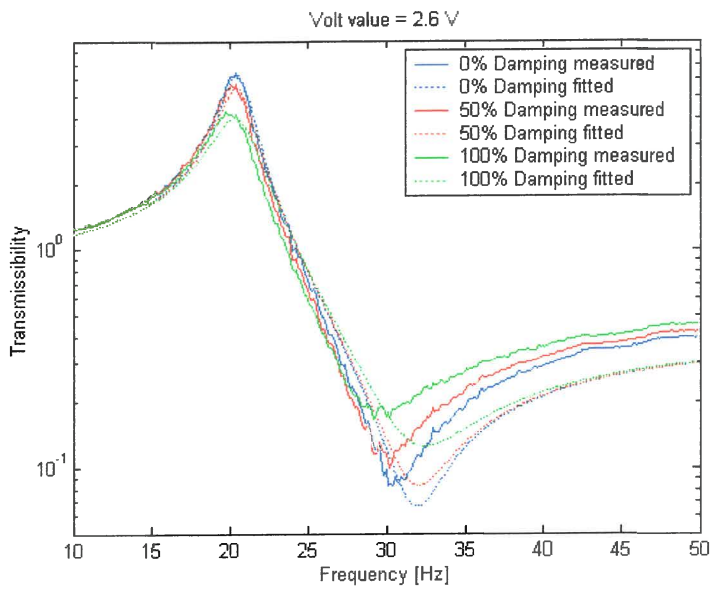

Figure D. 10 **Transmissibility – 2.6 V**

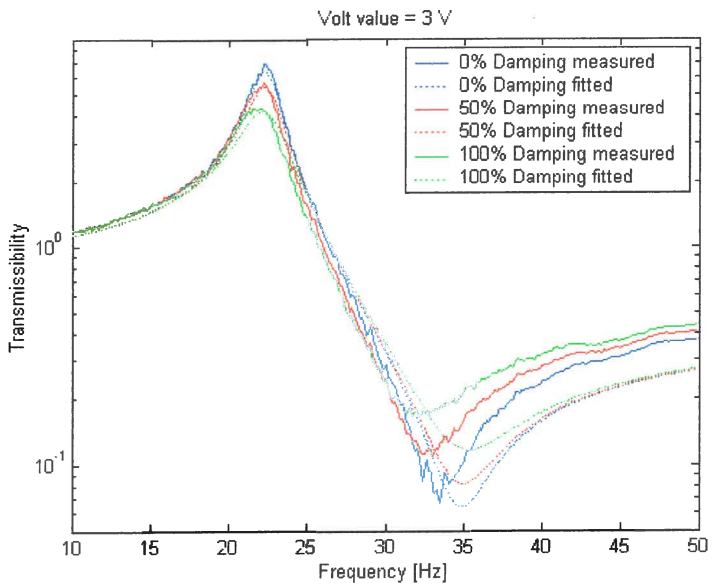

Figure D. 11 Transmissibility – 3.0 V

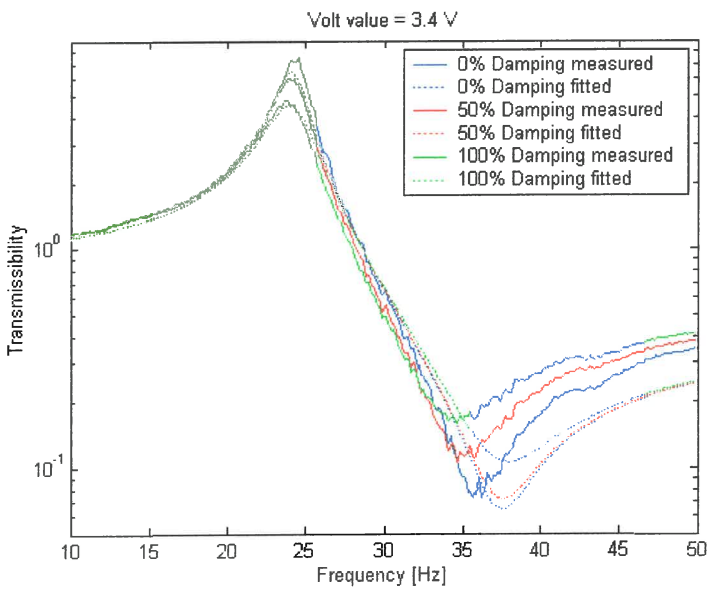

Figure D. 12 Transmissibility – 3.4 V

D.3 Effect of damping

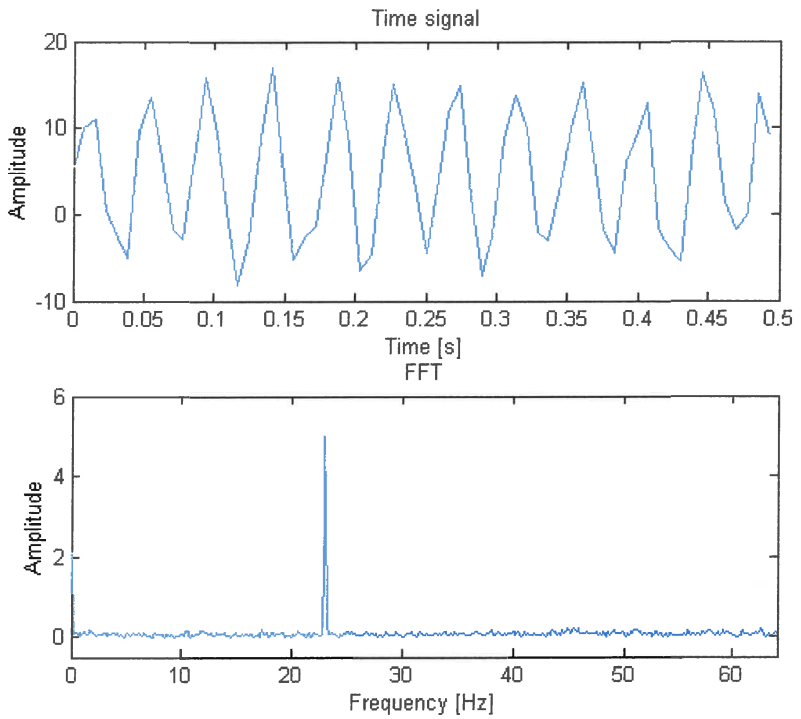

Figure D. 13 Theoretical input signal with medium noise levels

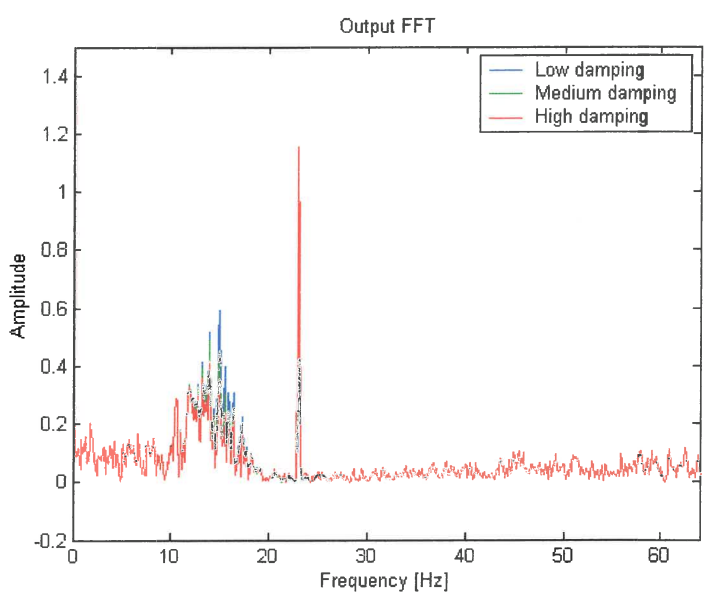

Figure D. 14 Output FFT with medium noise levels

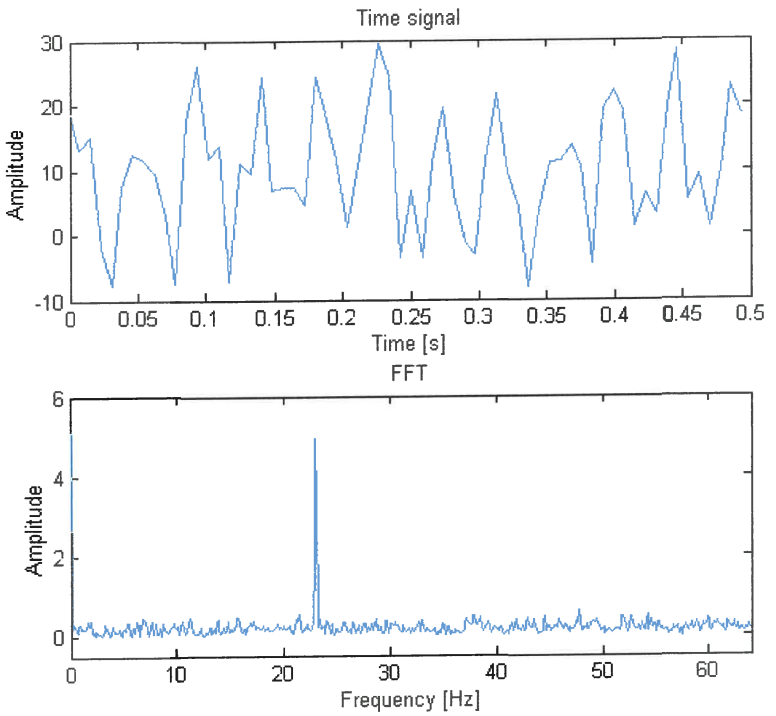

Figure D. 15 **Theoretical input signal with high noise levels**

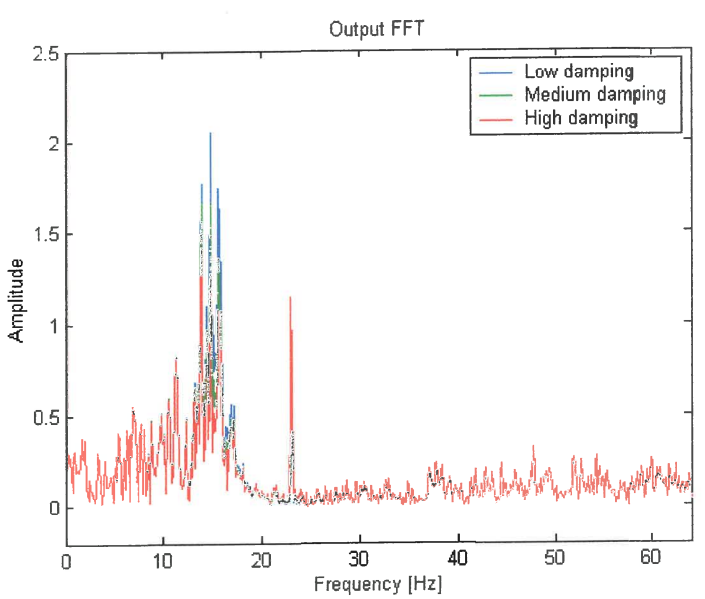

Figure D. 16 **Output FFT with high noise levels**